Spring 5-2011

Photopolymerized Thiol-ene Networks for Gas Barrier and Membrane Applications

Luke Kwisnek
University of Southern Mississippi

The University of Southern Mississippi

PHOTOPOLYMERIZED THIOL-ENE NETWORKS FOR GAS BARRIER AND MEMBRANE APPLICATIONS

by

Luke Kwisnek

Abstract of a Dissertation
Submitted to the Graduate School
of The University of Southern Mississippi
in Partial Fulfillment of the Requirements
for the Degree of Doctor of Philosophy

May 2011

ABSTRACT

PHOTOPOLYMERIZED THIOL-ENE NETWORKS

FOR GAS BARRIER AND MEMBRANE APPLICATIONS

by Luke Kwisnek

May 2011

Gas transport and free volume properties of photopolymerized thiol-ene networks for various applications are reported. For basic, commercially-available thiol-ene formulations, oxygen permeation was strictly dependent on the difference between T_{test} (room temperature for this work) and network T_g. Networks with T_g near T_{test} demonstrated the lowest values of permeability, diffusivity, and solubility. A robust, high-barrier network was selected for further modification. New networks with embedded functionality were formed using a two-step approach. Thio-Michael addition of a tetrathiol to monofunctional acrylates formed new functional thiol monomers. These functional thiols were combined with an isocyanurate-based triene and UV-cured forming robust crosslinked networks with varying functionality. For barrier applications, cyano, hydroxyl, and amide groups were introduced to the network. Primary amide groups showed the most notable decrease in oxygen permeability due to strong hydrogen bonding. Alkyl and fluoroalkyl acrylates were also introduced to the network to increase permeability toward breathable membrane applications. Oxygen permeability increased substantially as both alkyl and fluoroalkyl length increased. Both alkyl and fluoroalkyl side groups acted as pillars or spacers which prevented packing and expanded free volume. Fluoroalkyl-modified networks demonstrated higher permeability compared to

alkyl-modified networks of corresponding alkyl length. In addition to a structural effect from the bulkiness of the fluoroalkyl chains, a thermodynamic effect related to the frustration of fluorine in the network may have also contributed. Hydrophobocity also increased as alkyl and fluoroalkyl length increased. Measurement of water vapor permeation for the fluoroalkyl-derivatized series revealed the potential of these materials as UV-curable, water-repellant, breathable membranes.

Photopolymerized thiol-ene chemistry was also used to fabricate membranes for various CO_2 separation applications. An initial approach was made to improve a basic photopolymerized poly(ethyleneglycol)diacrylate (PEGDA) membrane by incorporating a small amount of various multifunctional thiols. Thiol-modified PEGDA membranes demonstrated improvements in gas permeability, tensile elongation, and processing in air all without sacrificing CO_2 selectivity. These improvements were all due to the step-growth nature of the thiol-ene reaction. Processing improvements would especially be critical for the UV-curing of gas separation membranes where the thickness of the membrane layer is on the nanometer scale. Such thin acrylate layers are extremely sensitive to oxygen inhibition.

An alternative to the brittle PEG-acrylate membranes was also developed using pure thiol-ene chemistry. Specifically, a PEG-containing diene and a PEG-containing dithiol were combined, along with a trithiol for crosslinking, to form membranes with varying crosslink density and ethylene glycol content. Permeability increased by a factor of four as crosslink density decreased. No increases in CO_2 solubility or CO_2 selectivity were observed for these materials despite nearly doubling in PEG content. Physical crosslinks, via entanglements, prevented further increases in permeability for networks

with the lowest crosslink density. Tensile testing was used to investigate the mechanical behavior of this material family. Regarding membrane applications, flexibility and elongation may be important in the development of films for modified atmosphere food packaging. The elastomeric thiol-ene materials demonstrated strain at break approaching 200%, a vast improvement over the brittle PEG-acrylate membranes.

The University of Southern Mississippi

PHOTOPOLYMERIZED THIOL-ENE NETWORKS FOR GAS BARRIER AND MEMBRANE APPLICATIONS

by

Luke Kwisnek

A Dissertation
Submitted to the Graduate School
of The University of Southern Mississippi
in Partial Fulfillment of the Requirements
for the Degree of Doctor of Philosophy

Approved:

Sergei Nazarenko
Director

Jeffrey S. Wiggins

Daniel A. Savin

James W. Rawlins

J. Paige Phillips

Susan A. Siltanen
Dean of the Graduate School

May 2011

ACKNOWLEDGMENTS

I am forever grateful to my advisors, Dr. Sergei Nazarenko and Dr. Charles E. Hoyle, for countless reasons. First, freedom. Freedom to not only take a break or vacation when I needed it but also just day-to-day freedom to try whatever I wanted in the lab just to see if it would work. Second, encouragement. Dr. Hoyle truly lived his life by an "open door policy" and was always excited to hear about the latest news, good or bad. And for both Dr. Hoyle and Dr. Nazarenko for recognizing my potential and always urging me forward even when it was difficult to do so. Third, guidance. I had not believed it possible to learn so much in such a short few years and that is all thanks to my advisors' seemingly endless wisdom – they were, at all times, eager to share knowledge and understanding and to point me in the right direction. Last, and most encompassingly, for giving me invaluable tools, both scientific and otherwise, that will be with me my entire life. At this moment I am deeply and truly excited about my future and I owe every bit of this feeling to my advisors. From the bottom of my heart: thank you.

Thanks to Fusion UV for financial support of my research and Bruno Bock for providing thiol compounds. I must also thank my parents, my brother, and my sister for their endless support. I am also extremely grateful to my friends and coworkers for helping immensely along the way. This includes, but is certainly not limited to, correcting early and mostly terrible drafts, hearing fresh and often crazy ideas, giving me a hard time so I would not hear it from my professors, driving to and from airports since my car was on its last legs, cooking meals because I cannot cook, etc. And for really just being there. I could not imagine going through graduate school without you all.

TABLE OF CONTENTS

LIST OF TABLES

LIST OF CHARTS

Chart

LIST OF SCHEMES

Scheme

LIST OF ILLUSTRATIONS

Figure

CHAPTER I

RESEARCH BACKGROUND

UV-Initiated Photopolymerization

Photopolymerization is an energy efficient, environmentally friendly, and rapid processing method. Typically, liquids containing 100% reactive components (i.e. no solvents or other VOCs) are applied to a substrate and then "cured" with UV light forming a crosslinked network, hence the industrial name for this process – UVcuring.[1-3] UV curable materials are used as coatings, adhesives, and inks in printing, packaging, wood products, electronics, and numerous other applications.[1-3] A general scheme for the UV curing process is shown in Figure I-1.

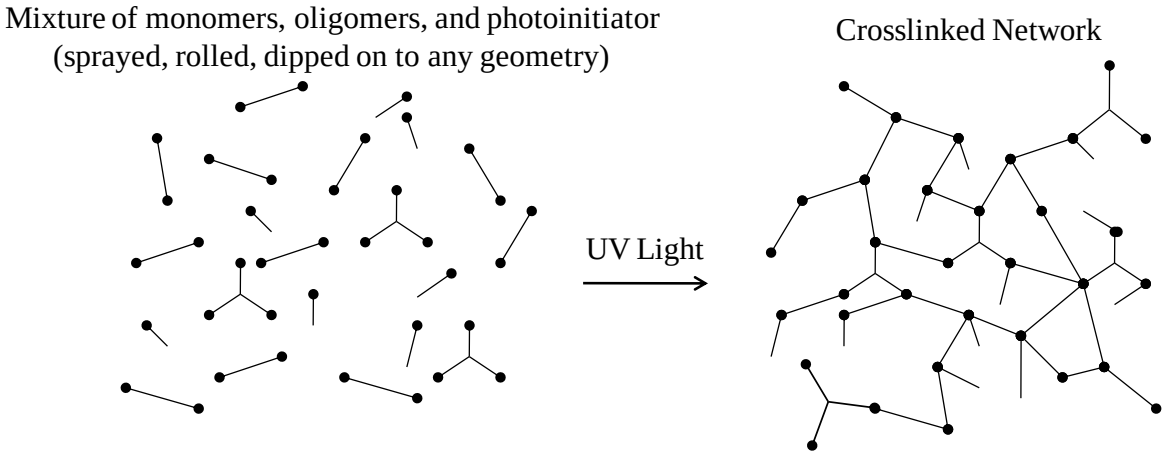

Figure I-1. General scheme for UV curable materials. Starting with a liquid mixture of various functional monomers, followed by applying this liquid to almost any substrate via spraying, rolling, or dipping, UV light exposure is used to rapidly form a crosslinked network material.

Free-radical based chemistries dominate the UV curing market. The most common of these are the acrylates and methacrylates.[1-3] A vast library of commercially available monomers, oligomers, crosslinkers, and additives with acrylate functionality are available and are used to great success. However, acrylates typically suffer from two important drawbacks: shrinkage and oxygen inhibition.[1-3] These two disadvantages stem from the nature of the acrylate polymerization method: chain growth. In contrast, free-radical thiol-ene chemistry proceeds via a unique step-growth mechanism.[4] This mechanism, shown in Figure 2, is the net addition of any thiol (-SH) to any ene (C=C). The key step in this addition is chain-transfer of the carbon-centered radical to a thiyl radical via hydrogen abstraction. As a result of the step-growth nature, thiol-enes are insensitive to oxygen and also exhibit low shrinkage.[4] Details aside, both UV-initiated acrylate and thiol-ene radical photopolymerization afford the overall advantages of UV curing.

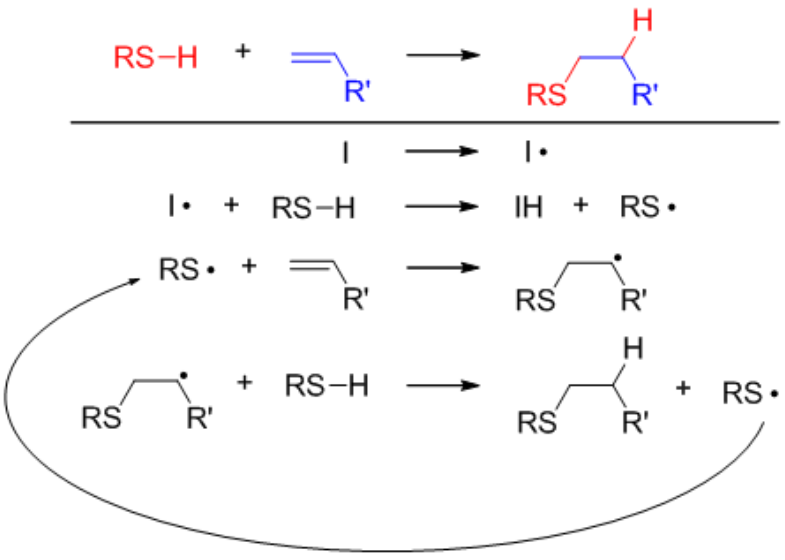

Figure I-2. Free-radical, step-growth thiol-ene mechanism. This mechanism proceeds for any thiol and any ene, initiated typically with UV light and a photoinitiator (I). Overall reaction shown in red/blue.

Thiol-Ene Chemistry

While the thiol-ene reaction has been known for nearly a century,[5] it remained dormant for decades. Only the photopolymerization community, consisting of industrial researchers and a small group of academics including Hoyle and Bowman, were aware of this reaction and its versatility in material fabrication during the last 20 to 30 years.[6-9] However, only during the last three years has thiol-ene chemistry received widespread attention. Following key papers by Hawker[10-11] and Schlaad[12-13] recognizing thiol-ene reactions as embodying all aspects of "click" chemistry as put forth by Sharpless,[14] thiol-ene took off like a rocket. The thiol-ene reaction is a member of the family of thiol-X reactions (where X = alkene, alkyne, acrylate, isocyanate, et al.) which are all now accepted as "click" chemistry, meaning the reactions rapidly achieve high yields with little to no byproducts.[15-21] Additional advantages of the "click" philosophy as demonstrated by thiol-enes are the practical reaction conditions: generally no solvents, in air, and at room temperature.[15-20]

Specifically, the thiol-ene reaction is the net addition of a thiol or mercaptan compound to a double bond (ene).[3,20] Essentially any thiol and any ene may be used. Depending on the electronic character of the ene, the reaction may proceed by either a UV-initiated free-radical mechanism (Figure 2) or a nucleophile-catalyzed anionic mechanism. The nucleophile-catalyzed (or more descriptively, nucleophile-*initiated*) anionic addition, called thio-Michael addition, proceeds with electron poor double bonds such as acrylates as shown in Figure 3.[3,20] The efficacy of these reactions is due to the ease of hydrogen abstraction for the radical reaction and the strong nucleophilicity of S- (thiolate anion) for Michael addition. Thiol chemistries of all types have been effectively

used to form a variety of well-defined structures and modifications on a monomer, oligomer, and polymer scale.[21-29]

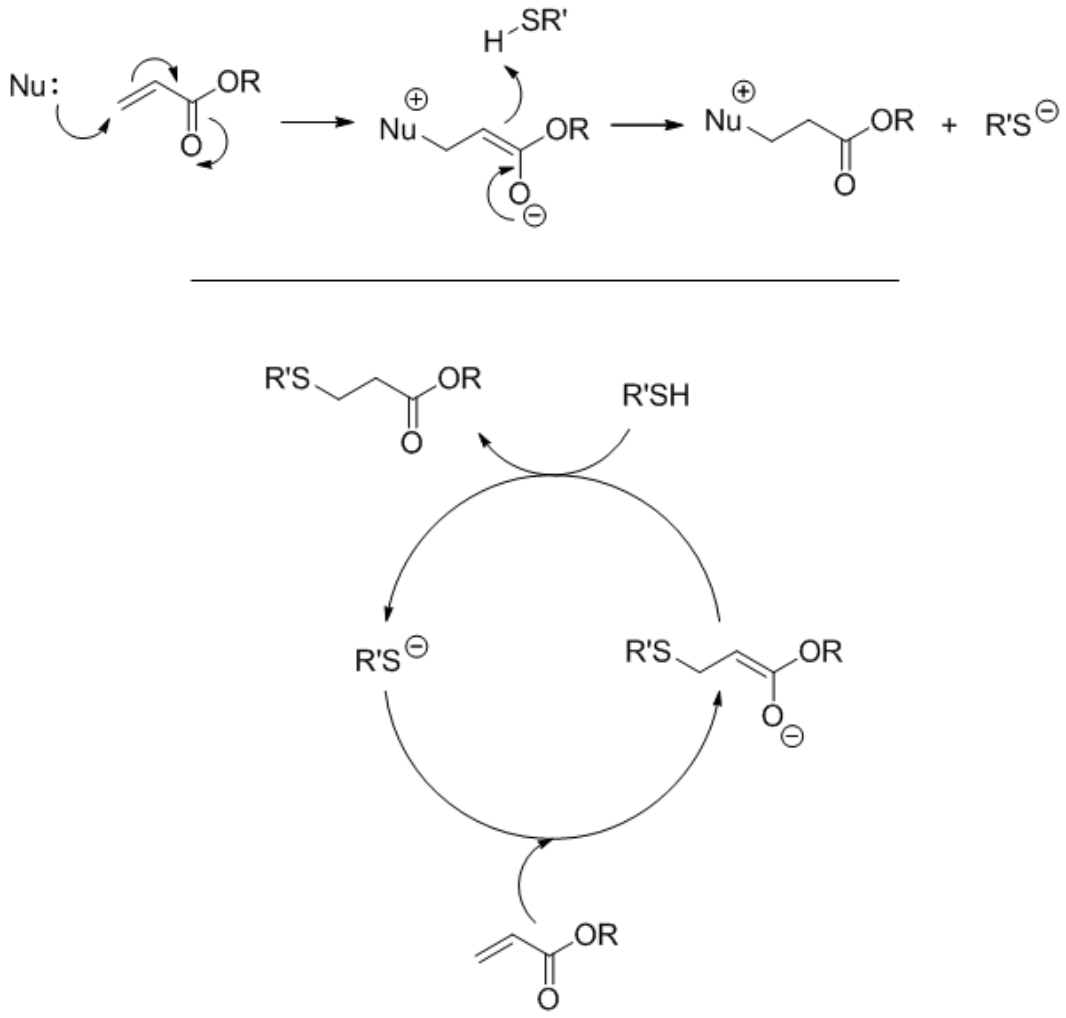

Figure I-3. Nucleophile-initiated anionic thio-Michael addition mechanism. Initiation step, which generates thiolate anion, is at top; once initiated, thiol and acrylate enter step-growth cycle shown at bottom.

While small molecule couplings require only monofunctional thiols and enes, when $f_{avg} > 2$ the result is a crosslinked thiol-ene network.[3] Thiol-ene networks have been widely studied and are known for their low shrinkage, narrow glass transitions, and overall uniformity as compared to traditional photopolymerized networks.[3,20,30-36] Modularity is another strong suit of thiol-ene networks. A variety of commercially-available thiol and ene monomers are available. By mixing and matching these components, properties can be tuned to meet specific requirements in glass transition temperature, modulus, density, degradability, elongation, etc. The synthesis of new monomers and building blocks opens up the possibilities further still.[37-42]

Gas Permeation in Polymers

Despite all of these advantages, there was a lack of investigation into the gas permeation and free volume properties of photopolymerized materials. Thiol-enes were particularly underrepresented. When this research project began, we were only able to identify one reference in the public domain regarding oxygen permeability in a thiol-ene network.[43] Oxygen is the most widely investigated permeant gas in polymeric materials.[44-47] A contaminant of foods and beverages, a detriment to medical and electronic devices, and a component in gas separations such as air enrichment, oxygen is a non-polar gas that is also used as a probe of free volume.[44-47] While oxygen permeability may be measured according to classic constant-volume, variable-pressure techniques,[48-49] commercial instruments (MOCONs) that are able to detect extremely low levels of oxygen flux are also employed.[47]

The permeability of not only oxygen but all other gases depends on two factors: diffusivity and solubility as given by the general relationship $P = DS$. Diffusivity, D, is a kinetic term related to the transport of gas molecules across a polymer film. Diffusivity controls the permeation of permanent gases. Figure 4a shows how depending on polymer structure, oxygen permeability spans seven orders of magnitude and oxygen diffusivity nearly the same.[50] Solubility, a thermodynamic term, also depends on polymer structure but in a unique way. Polymers with polar groups such as ether or nitrile exhibit high selectivity for quadrupolar gases like CO_2 and H_2S.[51] This solubility or affinity is due to specific interactions between the gas and the polymer structure. But solubility also depends on the gas itself. The inherent solubility or compressibility of a gas is given by its critical temperature, the temperature above which a gas cannot be liquefied, as seen in Figure 4b. High critical temperature means high inherent solubility.

(a)

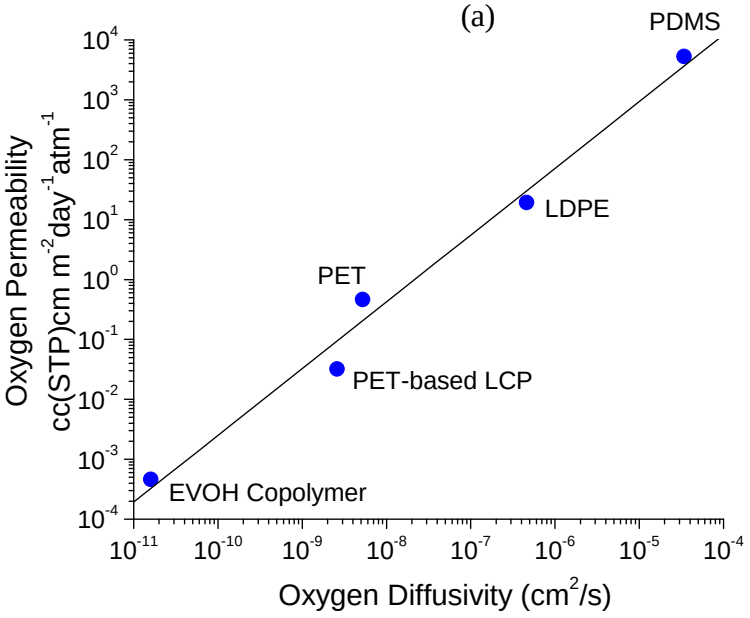

(b)

Gas	Critical Temp (°C)
H_2O	374
H_2S	100
CO_2	31
O_2	-119
N_2	-147
H_2	-240

Figure I-4. (a) Log-log plot of permeability versus diffusivity, demonstrating diffusion control of permeability for various unrelated polymers. (b) Critical temperature of various gases indicating inherent compressibility (solubility).

Often for industrial applications, only the steady-state flux is required. Steady-state gas flux depends on sample thickness and applied pressure.[46] In order to obtain the permeability, flux is treated according to the formula $J = P \cdot \Delta p / l$ where J is the flux, l the thickness, Δp the pressure driving force, and the permeability P.[46] But in order to understand controlling factors for permeability and to allow the rational design of new barrier and membrane materials, it is necessary to decouple the diffusivity and solubility terms. Traditionally, this decoupling is done via the time lag method for constant-volume variable-pressure systems.[48-49] The polymer film is degassed under high vacuum for ~24 hours, a gas of known *absolute* pressure is introduced to the upstream, and then the downstream is closed off. As gas permeates across the film, pressure builds up in the constant volume of the downstream. This pressure increase is monitored with a sensitive pressure transducer and recorded in real-time, generating data seen in Figure 5a. The extrapolation of the steady-state portion to zero pressure, i.e the x-intercept, yields the time lag which allows calculation of diffusivity via the relation shown as an inset (where t_L is the time lag and l is the sample thickness).[48-49]

A MOCON or other commercial instrument based on a *partial* pressure driving force may also be used to determine D and S. These instruments use what is known as the "sweep gas" technique where the sample is first conditioned for ~24 hrs under a nitrogen purge. Pure oxygen is then introduced to the test side of the film. While both sides of the test film are at 1 atm pressure, there is a partial pressure driving force of 1 atm oxygen which causes the permeation of oxygen across the film. The nitrogen then carries or sweeps the permeated oxygen away to the sensor for quantitative measurement.[47] Experimental data generated by this method is shown in Figure 5b. By

performing a least-square, two-parameter fit via the equation shown, the diffusivity, D, is determined.[47] In both methods, the steady-state flux determines P. Solubility is then calculated via the relationship $P = DS$.

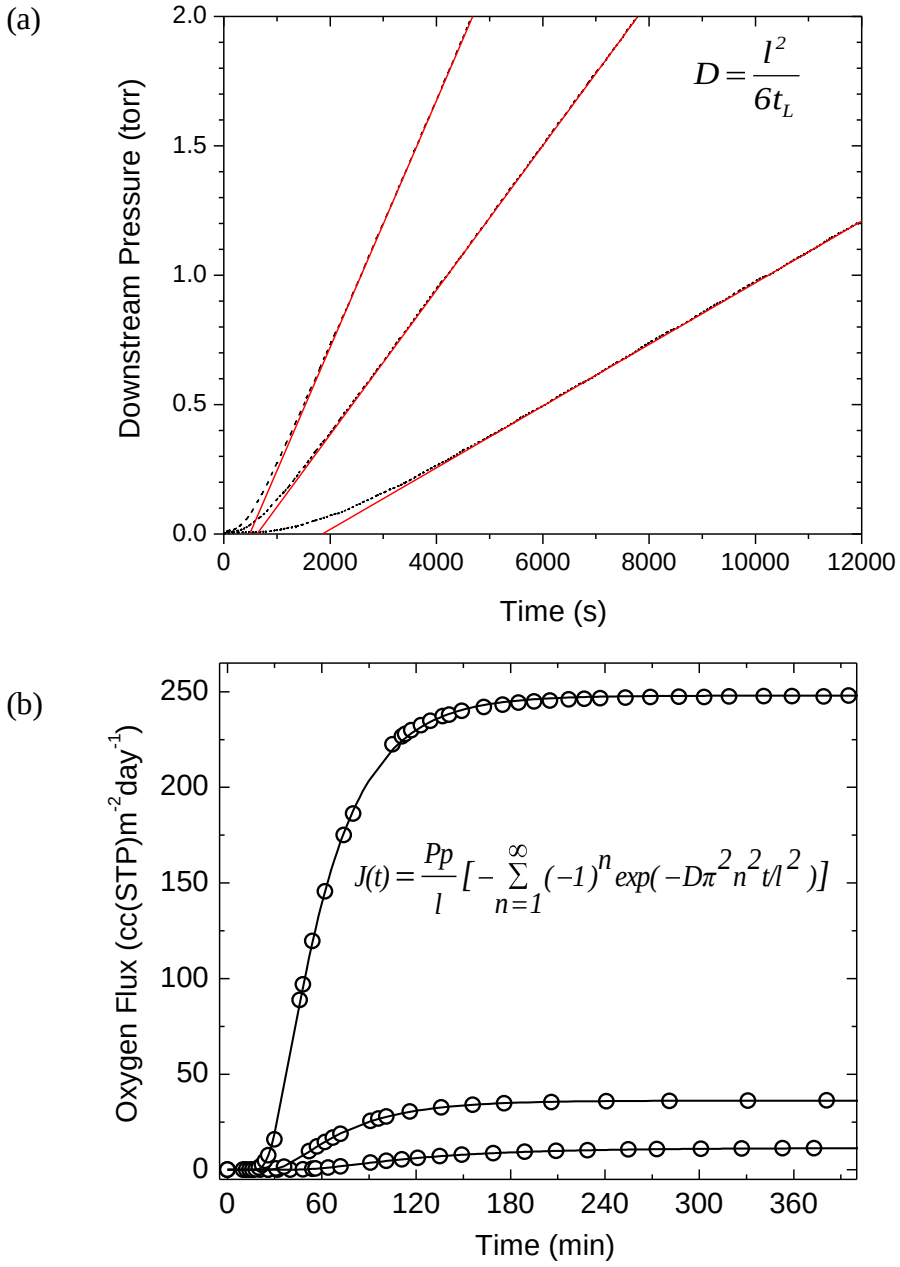

Figure I-5. (a) Typical experimental downstream pressure versus time plots for constant-volume variable-pressure technique (custom-built device). (b) Typical oxygen flux versus time plots for partial-pressure sweep gas technique (MOCON).

Applications in gas permeation are far reaching. One significant market is gas barrier, as briefly mentioned already. Food and beverage packages, electronics and pharmaceuticals, and organic electronics and photovoltaics all require a protective barrier layer or coating that reduces or completely blocks oxygen and water vapor ingress. Typical barrier polymers are those with strongly-interacting functional groups like poly(ethylene-co-vinylalcohol) (EVOH) copolymers, poly(vinylidenechloride) (PVDC) or Saran®, Nylon MXD6 an aromatic polyamide based on m-xylenediamine, and copolymers of acrylonitrile and methyl acrylate known commercially as Barex®.[44-45,50] The common thread of these materials is the presence of strongly interacting functional groups such as amide, hydroxyl, nitrile, and chloride. An empirical correlation between the molar concentration of polymer functional groups and the resulting gas permeability has been developed.[52-53] Ratings for each functional group, called the Permachor (π) parameter, were determined – amide, hydroxyl, and nitrile groups ranked highest as shown in Figure 6.[52] These parameters have aided in the design of new barrier materials including our work on thiol-ene networks. While the gas barrier field is mature, there remain unsettled challenges. Organic electronics and photovoltaics require extremely high water vapor barrier; there are currently no all-polymeric materials capable of reaching these stringent demands. Also classic thermal processing methods may be inapplicable to delicate substrates like organic electronics.

Structure	Permachor (π) value	Structure	Permachor (π) value
	-54	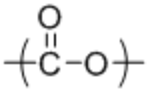	102
	-50		108
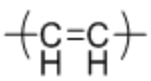	-12		205
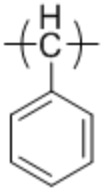	39	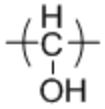	255
		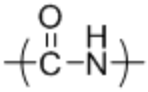	309

Figure I-6. Permachor (π) values for polymeric functional groups and repeat unit structures.[52] Polymers with higher overall permachor values (i.e. high concentration of amide, hydroxyl, nitrile, etc.) exhibit higher barrier.[52]

On the other end of the permeability spectrum, polymers with high gas permeability and selectivity are used in gas separations.[46,54-55] Gas separation membranes are energy efficient, continuously operating, small-footprint replacements for more costly and polluting separation methods like amine treatment, cryogenic distillation, and pressure swing adsorption.[54-55] Some common membrane separation processes are natural gas purification, gas drying or dehydration, hydrogen recovery, and air separation.[54-55] While certain low T_g polymers such as PDMS are used in specific separations, the majority of membrane separations are accomplished with high T_g glassy

polymers including polyimide, polysulfone, and cellulose acetate.[54] The static free volume of these non-equilibrium glasses enables them to discriminate between gases based on size or kinetic diameter. This size selectivity translates into a difference in diffusivity and these membranes are thus termed *diffusivity selective*.[54] Drawbacks to glassy polymer membranes include physical aging and processing complexity.[54]

Solubility selective membranes, however, are an emerging and promising approach to CO_2 separations in particular.[51,54-56] Unsolved challenges in this field include hydrogen purification (CO_2/H_2), a separation for which there are is currently no widely used membrane solution.[57-58] Modified atmosphere packaging of fresh produce is another under researched area. A delicate balance of CO_2 and O_2 is required to increase shelf-life of fresh foods.[55,59-60] Regarding material selection for solubility selective membranes, low T_g rubbery polymers which do not undergo physical aging and can have extremely high permeability have been explored. An excellent example is poly(ethyleneglycol) (PEG). PEG is known for its high CO_2 solubility selectivity.[51,56,61-63] Unfortunately pure PEG crystallizes to ~70 vol% resulting in low gas permeability.[63] In order to achieve high permeability membranes, the problem of crystallinity has been remedied in essentially two ways. One, PEG has been employed in phase-separated blends of block copolymers made via solution casting.[64-67] A more promising route in our eyes was the second approach: UV cured acrylate-functional crosslinked networks.[49,51,68-70] The improvement over semi-crystalline PEG is shown in Figure 7, a classic Robeson "upper bound" plot, illustrating the tradeoff between permeability and selectivity in CO_2/N_2 gas separation membranes.[71] The photopolymerized PEGDA amorphous crosslinked network increased CO_2 permeability by a factor of 10 while maintaining high selectivity.

This increase in permeability is critical because industrial application requires that membranes be highly permeable as well as highly selective – a feat that has proven quite challenging.[71] In addition to having promising separation performance, the PEG-acrylate systems also employ the inherent advantages of photopolymerization as mentioned already.

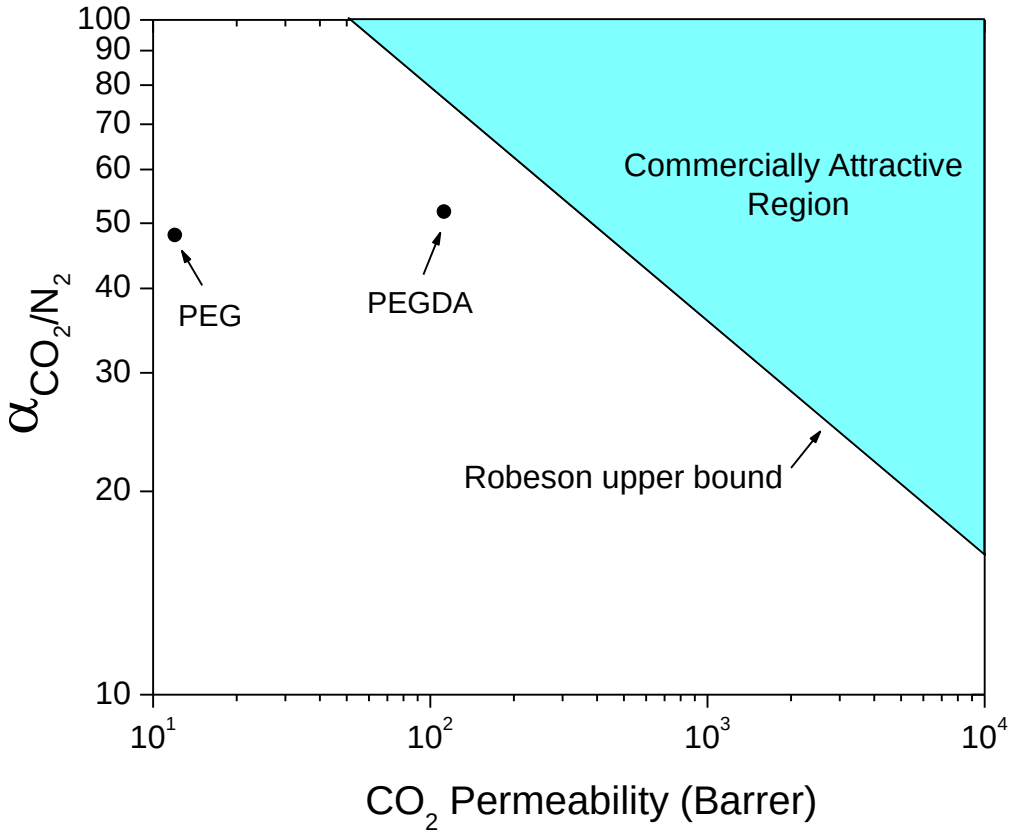

Figure I-7. Robeson "upper bound" plot for CO_2/N_2 separation, a gas pair representative of closed atmosphere regeneration or flue gas scrubbing applications. Y-axis is gas selectivity, x-axis is gas permeability. The upper bound line indicates that most polymer membranes demonstrate a tradeoff between permeability and selectivity and thus fall below the line. Performance of pure semi-crystalline PEG was improved by photopolymerizing PEG-diacrylate (PEGDA) forming amorphous, PEG-containing crosslinked networks. Both data points via the literature and measured at 35 °C.[51]

Photopolymerization in Gas Barrier and Membrane Fabrication – State of the Art

What is the state of the art regarding photopolymerization of gas barrier and membrane materials? Perhaps the most successful implementation in this area is soft contact lenses.[72-75] Contacts must be flexible, mechanically robust, and comfortable. A critical prerequisite regarding eye health, however, is extremely high oxygen permeability.[72] Interestingly, according to a recent review all modern soft contact lenses are silicone hydrogel amphiphilic conetworks, the majority of which are photopolymerized.[73] Much of what is known about this technology lies in patents[73-75] and likely trade secrets. Nevertheless, the success of UV curing in this area speaks for itself.

Gas separations also require highly permeable polymeric materials. Along with high permeability, high selectivity for specific gas pair(s) is also required. All commercial polymeric gas separation membranes are produced in one of two ways.[76] Thin sheet extrusion followed by spiral winding of various layers.[76] Or solvent-based hollow-fiber spinning of a microporous support, followed by a 100 nm selective membrane layer, and another coating layer to fill pin holes.[76] These assemblies are required in order to maximize the effective membrane surface area for the small space they occupy. We feel that due to the complexity of current assembly methods, UV curing may indeed be beneficial to the assembly process.

As mentioned already, the Freeman research group has published heavily on UV cured, solubility-selective, PEG-based acrylate membranes for various CO_2 separations. These UV cured membranes showed remarkable promise especially for hydrogen purification.[51,68-70] In fact, Membrane Technology and Research (MTR) Inc.'s new

Polaris™ membrane system shown in Figure 8 employs this exact photopolymerized PEG-acrylate technology.[77] Polaris membranes are ten times more efficient than cellulose acetate, the previous standard in CO_2 removal.[77] Much less promising are limited reports on UV curing of glassy membranes for diffusivity-selective membrane separations.[78-79]

Figure I-8. MTR Inc.'s new Polaris™ membrane system. This skid-mounted, small-footprint membrane employs the photopolymerized PEG-acrylate membrane technology developed in Freeman's labs.[77] According to MTR's website: *"Polaris is an important new innovation: for the first time, membranes can achieve practical separation of carbon dioxide from hydrogen."*

As far as we are aware, only a small number of patents exist in this area. Microporous supports have been coated with acrylate mixtures and photopolymerized.[80-81] The approach is elegant and could simplify membrane fabrication but the separation performance was lacking.[80-81] Highly breathable, waterproof microporous (GORE-TEX®) membranes have also been coated with photopolymerized materials. A PEG-based thiol-ene formulation, specifically, was successfully employed as a hydrophilic

inner coating for a GORE-TEX® membrane.[82] The liquid thiol-ene formulation was applied to the membrane, penetrating into the pores of the membrane, and UV cured as a permanent layer. This crosslinked PEG-based network provided a hydrophilic interface between the hydrophobic GORE-TEX® and the humid atmosphere, increasing water vapor permeability of the composite membrane under various conditions.[82]

UV cured materials for gas barrier have also been attempted. UV cured α-hydroxymethylacrylate dip coatings improved the oxygen barrier of PET bottles.[83] Thiol-ene networks were also explored for water vapor barrier in a recent patent application.[84] However, it is generally recognized that so far no polymer exhibits the barrier required by high tech organic electronic and photovoltaic applications. Inorganic coatings such as silicon oxide (SiO_x) or silicon aluminum oxide ($SiAlO_x$) and indium tin oxide (ITO) offer the transparency and barrier properties required but not without drawbacks.[44,85-88] Inorganics suffer from pinhole defects especially when applied as thin layers. For this reason, multilayer barrier assemblies or sandwiches as shown in Figure 9 are the current state of the art in gas and water vapor barrier coatings.[85-88] By alternating layers of inorganic and organic (polymeric) material, the polymer layers seal pinholes preventing convective gas flow. It is for this reason that the polymer layer must have good adhesion to the inorganic layer as well as providing high barrier. In a recent patent, the importance of the oxygen and water vapor permeability of the acrylate layer was clearly demonstrated.[85] Water vapor permeability in particular varied by over an order of magnitude depending on the acrylate structure.[85] This work raises fundamental questions regarding the role of interfacial adhesion and gas permeability of the organic layer in a

multilayer assembly. Also note that UV curing of the polymer layer is straightforward although appears to be an uncommon approach.

Figure I-9. Schematic diagram of a typical multilayer barrier assembly. Layer thickness (of both organic and inorganic) is generally 100 nm or less.

It is evident that useful and challenging applications exist for not only high barrier materials but also highly permeable membranes. With rapid and robust processing, ease of application, and versatility as its advantages, thiol-ene chemistry was explored as a potential method of forming gas barrier and membrane materials. The following chapter reiterates some of this background material in the context of work that was done over the course of the research project. The scope and aims of the project will be presented.

References

1. Hoyle, C.E.; *Photocurable Coatings*, in: C.E. Hoyle, J.F. Kinstle (Eds.), Radiation Curing of Polymeric Materials, ACS, Washington D.C., **1990**, pp. 1-16.
2. Fouassier, J. P.; *An Introduction to the Basic Principles in UV Curing*, in: Fouassier, J. P. and Rabed, J. F. (Eds.), Radiation Curing in Polymer Science and Technology – Volume I, Elsevier Applied Science, New York, **1993**, pp. 49-117.
3. Yagci, Y.; Jockusch, S.; Turro, N. J. *Macromolecules* **2010**, 43, 6245.
4. Lee, T. Y.; Roper, T.; Hoyle, C. E. *J. Polym. Sci., Part A: Polym. Chem.* **2004**, *42*, 5301-5338.
5. Kharasch, M. S.; Read, J.; Mayo, F. R. *Chem. Ind. (London)* **1938**, *57*, 752.
6. Morgan, C. R.; Magnotta, F.; Ketley, A. D. *J. Polym. Sci.: Polym. Chem. Ed.* **1977**, *15*, 627.
7. Hoyle, C. E.; Hensel, R. D.; Grubb, M. B. *J. Polym. Sci.: Polym. Chem. Ed.* **1984**, *22*, 1865-1873.
8. Hoyle, C. E.; Hensel, R. D.; Grubb, M. B. *Polymer Photochemistry* **1984**, *4*, 69-80.
9. Cramer, N. B.; Bowman, C. N. *J. Polym. Sci., Part A: Polym. Chem.* **2001**, *39*, 3311-3319.
10. Hagberg, E. C.; Malkoch, M.; Ling, Y.; Hawker, C. J.; Carter, K. R. *NanoLett.* **2007**, *7*, 233–237.
11. Killops, K. L.; Campos, L. M.; Hawker, C. J. *J. Am. Chem. Soc.* **2008**, *130*, 5062-5064.
12. Gress, A.; Volkel, A.; Schlaad, H. *Macromolecules* **2007**, *40*, 7928-7933.
13. Brummelhuis, N. t.; Diehl, C.; Schlaad, H. *Macromolecules* **2008**, *41*, 9946-9947.

14. Kolb, H. C.; Finn, M. G.; Sharpless, K. B. *Angew. Chem., Int. Ed.* **2001**, *40*, 2004–2021.

15. Becer, C. R.; Hoogenboom, R.; Schubert, U. S.; *Angew. Chem., Int. Ed.* **2009**, *48*, 2.

16. Iha, R. K.; Wooley, K. L.; Nystrom, A. M.; Burke, D. J.; Kade, M. J.; Hawker, C. J. Chem. Rev. **2009**, *109*, 5620.

17. Sumerlin, B. S.; Vogt, A. P. *Macromolecules*, **2010**, *43*, 1.

18. Kade, M.; Burke, D. J.; Hawker, C. J.; Journal *J. Polym. Sci., Part A: Polym. Chem.* **2010**, *48*, 743-750.

19. Hoyle, C. E.; Lowe, A. B.; Bowman, C. N. *Chem. Soc. Rev*. **2010**, *39*, 1355-1387.

20. Hoyle, C. E.; Bowman, C. N. *Angew. Chem., Int. Ed.* **2010**, *49*, 1540-1573.

21. Khire, V. S.; Benoit, D. S. W.; Anset, K. S.; Bowman, C. N. *J. Polym. Sci., Part A: Polym. Chem*. **2006**, 44, 7027.

22. Khire, V. S.; Lee, T. Y.; Bowman, C. N. *Macromolecules* **2007**, *40*, 5669–5677.

23. Clark, T.; Kwisnek, L.; Hoyle, C. E.; Nazarenko, S. *J. Polym. Sci., Part A: Polym. Chem*. **2009**, *47*, 14.

24. Chan, J.W.; Yu, B.; Hoyle,C. E.; Lowe, A. B. *Polymer*, **2009**, 50, 3158.

25. Chan, J. W.; Hoyle, C. E.; Lowe, A. B. *J. Am. Chem. Soc.* **2009**, *131*, 5751.

26. Dondoni, A.; *Angew. Chem., Int. Ed.* **2008**, *47*, 8995-8997.

27. Hensarling, R. M.; Doughty, V. A.; Chan, J. W.; Patton, D. L.; *J. Am. Chem. Soc.* **2009**, *131*, 14673-14675.

28. Antoni, P.; Robb, M. J.; Campos, L.; Montanez, M.; Hult, A.; Malmstrm, E.; Malkoch, M.; Hawker, C. J. *Macromolecules*, **2010**, *43*, 6625-6631.

29. Mazzolini, J.; Mokthari, I.; Briquel, R.; Boyron, O.; Delolme, F.; Monteil, V.; Bertin, D.; Gigmes, D.; D'Agosto, F.; Boisson, C. *Macromolecules*, **2010**, *43*, 7495-7503.

30. Chan, J. W.; Zhou, H.; Hoyle, C. E.; Lowe, A. B. *Chem. Mater.* **2009**, *21*, 1579–1585.

31. Senyurt, A. F.; Hoyle, C. E.; Wei, H.; Piland, S. G.; Gould, T. E. *Macromolecules* **2007**, *40*, 3174–3182.

32. Shin, J.; Matsushima, H.; Chan, J. W.; Hoyle, C. E. *Macromolecules* **2009**, *42*, 3294-3301.

33. Salinas, C. N.; Anseth, K. S. *Macromolecules* **2008**, *41*, 6019-6026

34. Lu, H.; Carioscia, J. A.; Stansbury, J. W.; Bowman, C. N. *Dental Materials* **2005**, *21*, 1129-1136.

35. Campos, L. M.; Meinel, I.; Guino, R. G.; Schierhorn, M.; Gupta, N.; Stucky, G. D.; Hawker, C. J. *Adv. Mater.* **2008**, *20*, 3728-3733.

36. Campos, L. M.; Truong, T. T.; Shim, D. E.; Dimitriou, M. D.; Shir, D.; Meinel, I.; Gerbec, J. A.; Hahn, H. T.; Rogers, J. A.; Hawker, C. J. *Chem. Mater.* **2009**, *21*, 5319-5326.

37. Shin, J.; Nazarenko, S.; Hoyle, C. E. *Macromolecules* **2009**, *42*, 6549.

38. Carioscia, J. A.; Lu, H.; Stanbury, J. W.; Bowman, C. N. *Dental Materials* **2005**, *21*, 1137-1143.

39. Clark, T.; Kwisnek, L.; Hoyle, C. E.; Nazarenko, S. *J. Polym. Sci., Part A: Polym. Chem.* **2009**, *47*, 14.

40. Kwisnek, L.; Nazarenko, S.; Hoyle, C. E. *Macromolecules* **2009**, *42*, 7031.

41. Kwisnek, L.; Kaushik, M.; Hoyle, C. E.; Nazarenko, S. *Macromolecules* **2010**, *43*, 3859-3867.

42. Kim, S. K.; Guymon, C. A. *J. Polym. Sci., Part A: Polym. Chem.* **2011**, *49*, 465-475.

43. Choi, J.; Lee, K. M.; Wycisk, R.; Pintauro, P. N.; Mather, P. T. *Macromolecules* **2008**, *41*, 4569.

44. Lang, J.; Wyser, Y. *Packaging Technology and Science* **2003**, *16*, 149.

45. Lagaron, J. M.; Catala, R.; Gavara, R. *Mater. Sci. Technol.* **2004**, *20*, 1-7.

46. Koros, W. J.; Coleman, M. R.; Walker, D. R. B. *Annu. Rev. Mater. Sci.* **1992**, *22*, 47-89.

47. Sekelik, D. J.; Stepanov, E. V.; Nazarenko, S.; Schiraldi, D.; Hiltner, A.; Baer, E. *J. Polym. Sci. Part B: Polym. Phys.* **1999**, *37*, 847.

48. Barrer, R. M.; Rideal, E. K. *Trans. Faraday Soc.* **1939**, *35*, 628-643.

49. Lin, H.; Freeman, B. D.; *Macromolecules* **2006**, *39*, 3568-3580.

50. Pauly, S. "Permeability and Diffusion Data," in *Polymer Handbook*, Eds. J. Brandrup et al., John Wiley & Sons, **1999**.

51. Lin, H.; Freeman, B. D. *J. Mol. Struct.* **2005**, *739*, 57.

52. Salame, M. *Polymer Engineering and Science* **1986**, *26*, 1543.

53. Lee, W. M. *Polymer Engineering and Science* **1980**, *20*, 65.

54. Bernardo, P.; Drioli, E.; Golemme, G. *Ind. Eng. Chem. Res.* **2009**, *48*, 4638.

55. T.M. Murphy, G.T. Offord, D.R. Paul, *Fundamentals of Membrane Gas Separation*, in: E. Drioli ,L. Giorno (Eds.), *Membrane Operations: Innovative Separations and Transformations*, Wiley, Weinheim Germany, **2009**, pp. 63-82.

56. Brunetti, A.; Scura, F.; Barbieri, G.; Drioli, E. *J. Membr. Sci.* **2010**, *359*, 115-125.

57. Ockwig, N. W.; Nenoff, T. M. *Chem. Rev.* **2007**, *107*, 4078-4110.

58. Shao, L.; Low, B. T.; Chung, T-S.; Greenberg, A. R. *J. Membr. Sci.* **2009**, *327*, 18-31.

59. Zagory, D.; Kader, A. A. *Food Technology* **1988**, *42*, 70-77.

60. Church, I. J.; Parsons, A. L. *J. Sci. Food Agric.* **1995**, *67*, 143-152.

61. Kawakami, M.; Yamashita, Y.; Yamasaki, M.; Iwamoto, M.; Kagawa, S. *J. Polym. Sci. Polym. Lett. Ed.* **1982**, *20*, 251-257.

62. Okamoto, K.; Fuji, M.; Okamyo, S.; Suzuki, H.; Tanaka, K.; Kita, H. *Macromolecules* **1995**, 28, 6950-6956.

63. Lin, H.; Freeman, B. D. *J. Membr. Sci.* **2004**, *239*, 105-117

64. Bondar, V. I.; Freeman, B. D.; Pinnau, I. *J. Polym. Sci., Part B: Polym. Phys.* **2000**, *38*, 2051-2062.

65. Yave, W.; Car, A.; Peinemann, K-V.; Shaikh, M. Q.; Ratzke, K.; Faupel, F. *J. Membr. Sci.* **2009**, *339*, 177-183.

66. Yave, W.; Car, A.; Funari, S. S.; Nunes, S. P.; Peinemann, K-V. *Macromolecules* **2010**, *43*, 326-333.

67. Reijerkerk, S. R.; Knoef, M. H.; Nijmeijer, K.; Wessling, M. *J. Membr. Sci.* **2010**, *352*, 126-135.

68. Lin, H.; Van Wagner, E.; Freeman, B. D.; Toy, L.G.; Gupta, R. P. *Science* **2006**, *311*, 639-642.

69. Richards, J. J.; Danquah, M. K.; Kalakkunnath, S.; Kalika, D. S.; Kusuma, V. A.; Matteucci, S. T.; Freeman, B. D. *Chem. Eng. Sci.* **2009**, *64*, 4707-4718.

70. Kusuma, V. A.; Freeman, B. D.; Borns, M. A.; Kalika, D. S. *J. Membr. Sci.* **2009**, *327*, 195-207.

71. Robeson, L. M. *J. Membr. Sci.* **2008**, *320*, 390-400.

72. Nicolson, P. C.; Vogt, J. *Biomaterials* **2001**, *22*, 3273-3283.

73. Erdodi, G.; Kennedy, J. P. *Prog. Polym. Sci.* **2006**, *31*, 1-18.

74. Bausch & Lomb, Inc., U.S. patent 6359024, March **2002**.

75. Bausch & Lomb, Inc., U.S. patent 6776934, August **2004**.

76. Baker, R. W.; *Ind. Eng. Chem. Res.* **2002,** *41,* 1393-1411.

77. (a) NSF Award Number 0515425, "Reverse-Selective Membrane Materials for the Purification of Hydrogen and Other Light Gases."

(b) http://www.ftc.gov/be/workshops/microeconomics/2009/docs/peterson.pdf

(c) http://www.mtrinc.com/co2_removal_from_syngas.html

78. Tiemblo, P.; Guzman, J.; Riande, E.; Salvador, E. F. ; Peinado, C. *J. Polym. Sci., Part B: Polym. Phys.* **2001**, *39*, 786-795.

79. Tiemblo, P.; Fernandez-Arizpe, A.; Riande, E.; Guzman, J. *Polymer* **2003**, *44*, 635-641.

80. Hoechst Celanese Corp., U.S. patent 4976897, December **1990**.

81. Hoechst Celanese Corp., U.S. patent 5102552, April **1992**.

82. W. L. Gore & Associates, Inc., U.S. patent 4969998, November **1990**.

83. Kaya, E.; Smith, T.; Nayak, B.; Mathias, L. J. *Polymer Preprints: American Chemical Society, Division of Polymer Chemistry* **2005**, *46*, 857.

84. National Starch and Chemical Company, U.S. patent application 11/474772, June **2006**.

85. Erlat, A. G.; Spontak, R. J.; Clarke, R. P.; Robinson, T. C.; Haaland, P. D.; Tropsha, Y.; Harvey, N. G.; Vogler, E. A. *J. Phys. Chem. B* **1999,** *103,* 6047-6055.

86. 3M Innovative Properties Company, U.S. patent 7018713, March **2006**.

87. Hoechst Celanese Corp., U.S. patent application 12/400431, March **2009**.

CHAPTER II

RESEARCH OVERVIEW

Despite success in its current applications and the numerous advantages discussed in the previous chapter, UV curing is not widely employed in the barrier and membrane fields. The most probable reason for this divide was apparent upon surveying the literature: there was a general lack of understanding of transport in photopolymerized materials as Chapter I showed. A significant portion of the state of the art lies in patents as well as isolated yet promising reports. There thus exists an opportunity for fundamental contributions to this field especially given the obvious potential.

Combining the processing simplicity of UV curing and the well-defined and robust thiol-ene modification reactions, this research project reports the first steps toward understanding controlling factors for gas transport in photopolymerized thiol-ene networks. We first wished to establish a baseline of gas transport properties for commercially-available UV curable thiol-ene networks. A starting point window of gas permeation in thiol-ene networks was identified. This window is best explained by Figure II-1. From the low permeability barrier materials all the way to highly breathable membranes, useful applications and challenges exist for not only oxygen and water vapor permeability (shown) but a number of other gases and vapors. After this initial scouting work presented in Chapter I,[1] efforts were made to expand the window through materials science employing the thiol-acrylate Michael addition reaction. Chapter I demonstrates network modification for high barrier[1] while Chapters II and III employ the same reaction with bulky functional groups aimed at increasing permeability towards highly breathable

materials.[2-3] Lastly, photopolymerized thiol-ene membranes containing polyethyleneglycol for various CO_2 separations are presented in Chapters IV and V.[4-5]

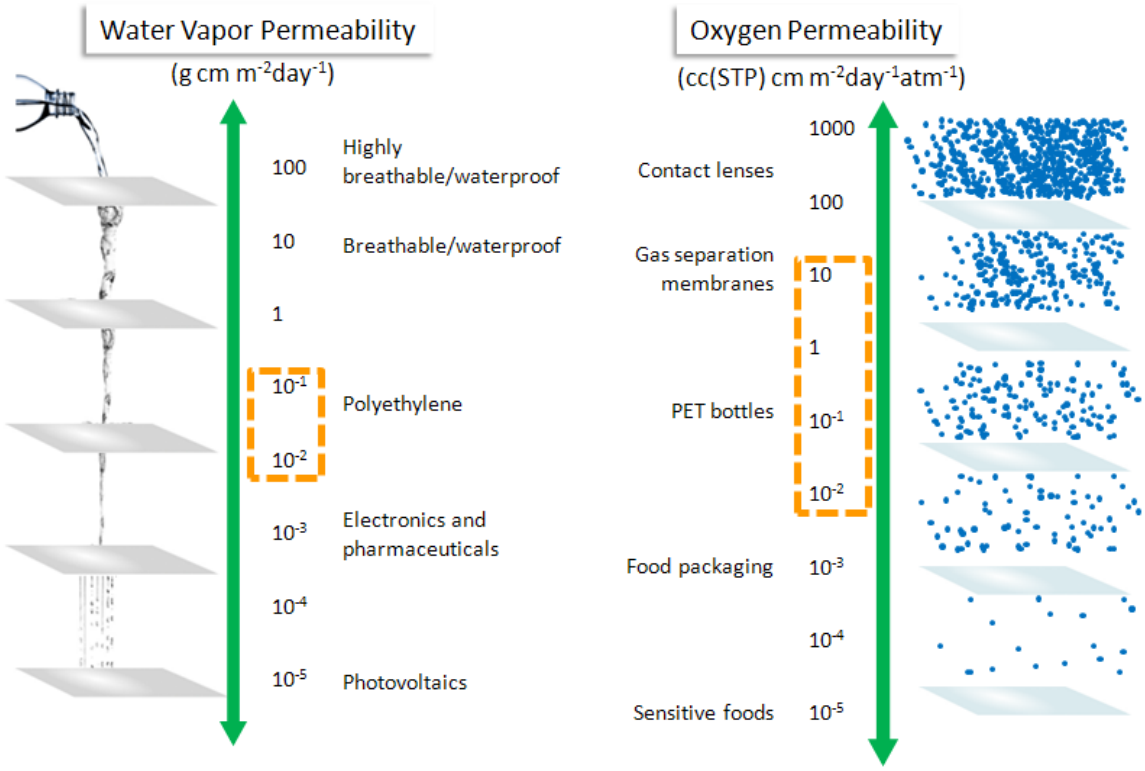

Figure II-1. General ranges of permeability for both water vapor and oxygen with industrially relevant benchmarks noted. Orange boxes represent approximate range for commercially-available UV cured thiol-ene networks.

References

1. Kwisnek, L.; Nazarenko, S.; Hoyle, C. E.; *Macromolecules*, 42, **2009**, 7031-7041.
2. Kwisnek, L.; Kaushik, M.; Hoyle, C. E.; Nazarenko, S.; *Macromolecules*, 43, **2010**, 3859-3867.
3. Kwisnek, L.; Goetz, J.; Greenhoe, B. M.; Kaushik, M.; Nazarenko, S.; *Manuscript in preparation*.
4. L. Kwisnek, et al., Multifunctional thiols as additives in UV-cured PEG-diacrylate membranes for CO_2 separation, *J. Membr. Sci.*, 369, **2011**, 429-436.
5. Kwisnek, L.; Heinz, S.; Wiggins, J. S.; Nazarenko, S.; *Manuscript in preparation*.

CHAPTER III

OXYGEN TRANSPORT PROPERTIES OF THIOL-ENE NETWORKS

*Luke Kwisnek, Sergei Nazarenko, and Charles E. Hoyle**

Abstract

Oxygen transport characteristics, i.e. permeability, diffusivity, and solubility, have been determined for a variety of photopolymerized thiol-ene networks. Despite the abundance of thiol-ene research and the importance of such information, it is until now absent from the literature. One model network, which showed high oxygen barrier properties, was selected for further modification. Covalent bonding of functional groups to the network was enabled by an interesting approach: thio-Michael addition of various functionalized acrylates to a tetrathiol monomer. Cyano, hydroxyl, amide, and alkyl functional groups were explored. These new modified thiols were subsequently copolymerized with an isocyanurate-based multifunctional ene. This modification technique enabled a study on how different functional groups embedded in a uniform network affect T_g and oxygen barrier properties. All studied networks exhibited oxygen diffusivity and permeability which both spanned nearly three orders of magnitude. Correlation of both oxygen permeability and oxygen diffusivity with T_g was observed. This correlation allows the prediction of oxygen barrier properties of thiol-ene networks using T_g.

Introduction

The use of polymers in gas barrier applications is well-documented, especially in the case of oxygen transport.[1-3] Oxygen uptake is of key concern with food, beverage, and other packaging applications.[3] While the polymer must be easily processed and often in high volumes, the key property for selection of such materials is gas permeability. The rate of gas transport through polymer films, while improvable through factors such as orientation, crystallinity, and addition of high-aspect ratio particulates,[4] is primarily determined by the chemical natures of the penetrant and the polymer.[1] Polymers with strong secondary forces obtained through dipole-dipole interactions and hydrogen bonds that lead to tight packing and low free volumes have naturally high barriers to non-polar gases like oxygen and nitrogen: examples include polyacrylonitrile, poly(styrene-co-acrylonitrile), poly(vinylidene chloride), poly(vinyl alcohol), and some polyamides.[3] Using the functional groups of these high-barrier polymers as models, White devised a plethora of high-barrier thermoplastics based on epoxy chemistry including poly(hydroxyl ether sulfonamides)[5] and poly(hydroxy amide ethers).[6] The common thread among these materials is an enhancement in intermolecular cohesion via the inclusion of amide, sulfone, and hydroxyl groups which subsequently improves the barrier to oxygen.

While the high-barrier field may be well surveyed, improvement of the oxygen barrier of polymers is a perpetual task; recent technologies include new liquid crystalline polymers, multilayered systems and blends, and both organic and inorganic coatings.[3] Coatings are a common solution to barrier problems, and photocurable films offer potentially attractive benefits when used as coatings since they are eco-friendly, generally

comprise 100% reactive components, and cure rapidly when exposed to UV-light.[7] With regards to barrier properties of photopolymerized materials, oxygen transport properties of a UV-cured acrylate coating have been reported: Mathias et al. reported barrier improvement of PET beverage bottles coated with a UV-curable liquid methacrylate followed by UV-photopolymerization.[8] In contrast to acrylates, photopolymerized thiol-ene networks gel at high conversion leading to low shrinkage, homogenous network density, and uniform glass transitions.[9] Thiol-ene photopolymerization also occurs readily in the presence of oxygen. The polymerization of a thiol-ene network follows a free-radical process, not a typical chain-growth reaction, that proceeds via a step-growth free-radical chain mechanism with two propagation steps.[9]

The unprecedented uniformity of thiol-ene networks, coupled with the ability to bind specific functional groups to the network without altering the basic network structure, provides an outstanding opportunity for evaluating structural effects on gas transport properties. In addition, there is a need for assessment of gas transport in thiol-enes. The only published data on barrier properties of UV-cured thiol-ene materials is by Mather and Pintauro: a neat NOA63 film was reported to have an oxygen permeability comparable to PET, indicating potential for thiol-enes in oxygen barrier or membrane applications.[10] And with decades of published oxygen transport research on a multitude of polymeric materials, it is important to note that sulfur-containing polymers and coatings are underrepresented even while other coatings like SiO_x are currently used and well-documented.[3] Herein, we report in detail the oxygen transport properties of free-standing thiol-ene films that have strongly-interacting functional groups incorporated into the network. The expectation is that such groups, inferable by the work of Salame[1] and

White et al.[5,6] in linear polymer systems, when incorporated into a highly uniform network will provide a conclusive description of how the transport properties of highly-uniform structured networks can be tuned.

Experimental

Materials

Thiol monomers trimethylolpropane tris(3-mercaptopropionate) (3T) and pentaerythritol tetrakis(3-mercaptopropionate) (4T) were supplied by Bruno Bock Thiol-Chemical-S; thiol monomer tris[2-(3-mercaptopropionyloxy)ethyl] isocyanurate (3TI) was obtained from Yodo Chemical Co. Ltd. Ene monomers tri(ethylene glycol) divinyl ether (TEGDVE), pentaerythritol allyl ether (TAE), 2,4,6-triallyloxy-1,3,5-triazine (TOT) were obtained from Aldrich. Ene monomer triallyl-1,3,5-triazine-2,4,6(1*H*,3*H*,5*H*)-trione (TTT) was supplied by Sartomer. Thiol and ene structures are shown in Chart III-1. Ethyl acrylate (EA), acrylamide (Am), acrylonitrile (AN), 2-hydroxyethyl acrylate (HEA), N-isopropylacrylamide (NIPAM), diethylamine, and tributylamine were obtained from Aldrich (see Chart III-2). Isophorone diisocyanate (IPDI) was provided by Bayer Material Science. The cleavage-type photoinitiator alpha,alpha-dimethoxy-alpha-phenylacetophenone (Irgacure 651) was supplied by Ciba Specialty Chemicals. Acetone-D6, obtained from Aldrich, was used to conduct NMR measurements. All chemicals were used as received.

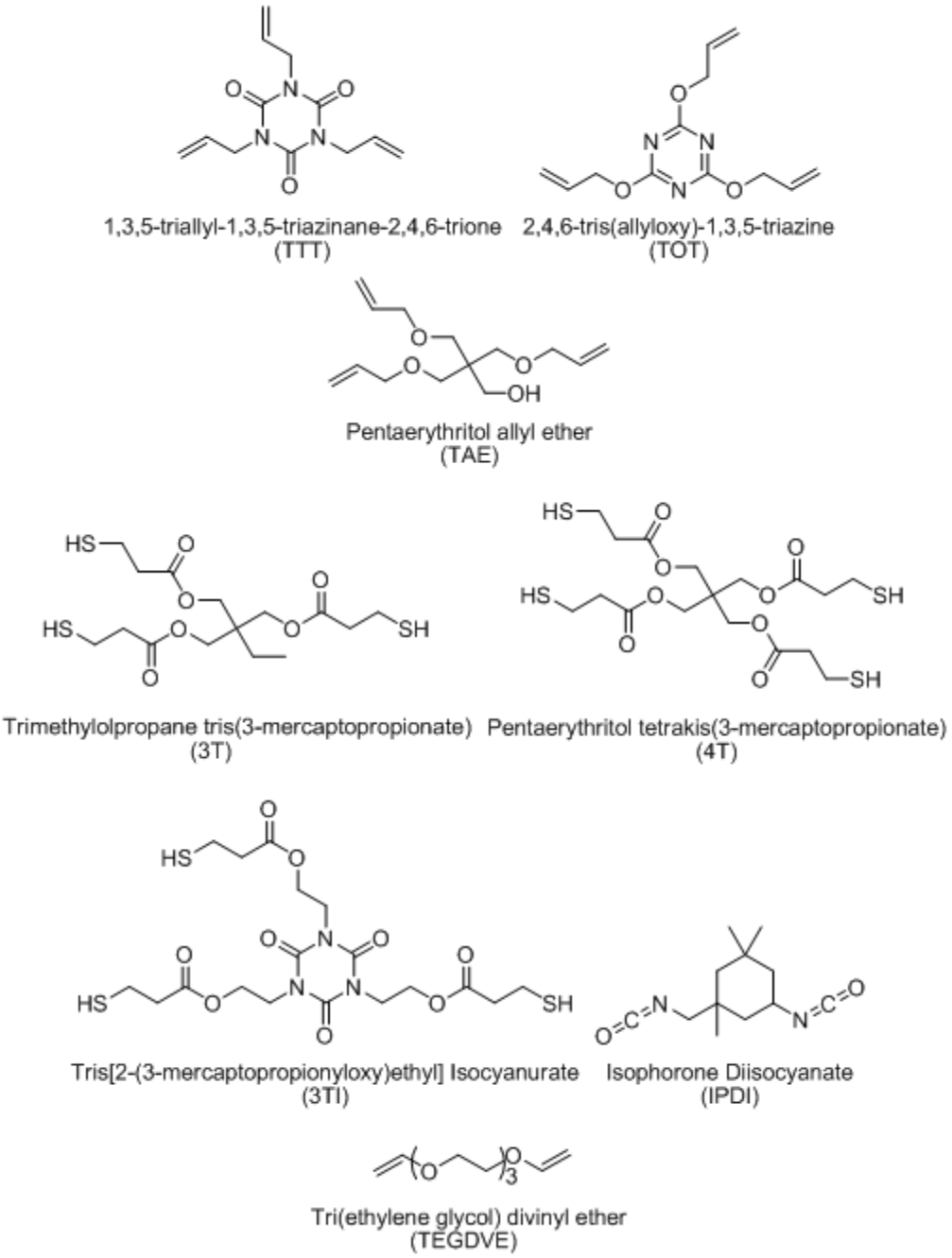

Chart III-1. Thiols, enes, and isocyanate.

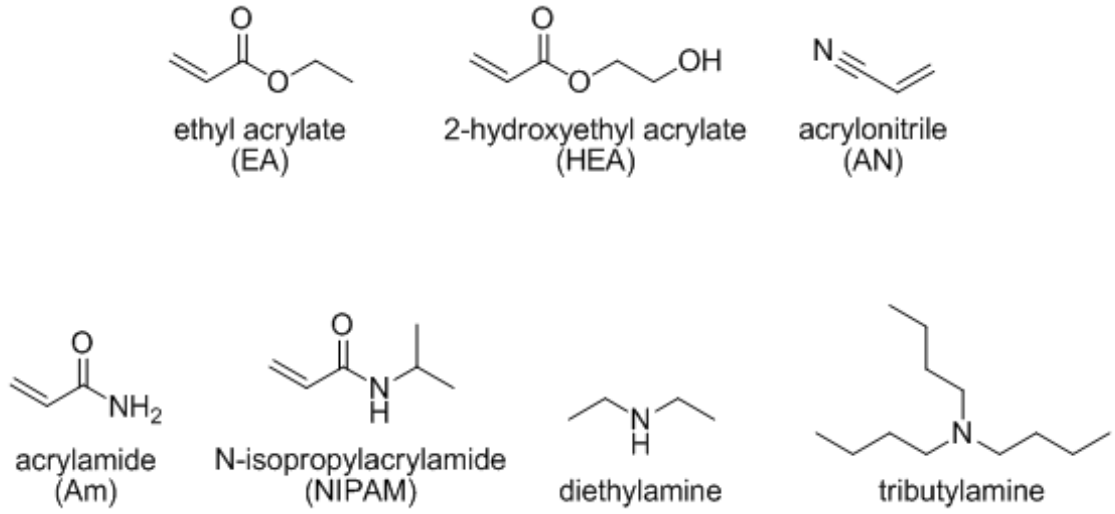

Chart III-2. Small molecules and amine catalysts.

Synthesis of Modified Thiol Monomers

Modified tri-functional thiol monomer mixtures were synthesized using an amine-catalyzed thio-Michael addition reaction between 4T and EA, Am, AN, HEA, and NIPAM at a 1:1 molar ratio so as to cap an average of one of the four thiol groups. Synthesis of products 4T-EA, 4T-AN, 4T-HEA was accomplished by first adding a quantity of 4T and 1 wt% diethylamine to a round-bottom flask. An equal molar quantity of the appropriate small molecule was then weighed in a separate vial and then added dropwise to the 4T/catalyst mixture at approximately 1 mL/min while stirring. The flask was then sealed and allowed to stir overnight. Synthesis of products 4T-Am and 4T-NIPAM require that acrylamide and N-isopropylacrylamide first be dissolved in acetone and then added dropwise at 1 mL/min while stirring. The flask was then sealed and allowed to stir overnight at which point the mixture is placed in a rotovap at 60 °C for 2 hrs to remove acetone and leave either a 4T-Am or 4T-NIPAM liquid product. A third procedure was used to synthesized 4T-Am:EA monomer mixtures. First, 4T and 1 wt%

diethylamine were mixed in a round-bottom flask. Am and EA at appropriate molar ratios were combined and dissolved in acetone. This mixture was then added dropwise to the 4T/catalyst mixture at 1 mL/min while stirring and the reaction was allowed to proceed overnight. These mixtures are rotovapped for 2 hrs at 60 °C as above to remove acetone. The final monomers are a distribution of structures with the trifunctional monomer being predominant. It is noted that the distribution could result in small changes in the macroscopic physical properties of the final networks versus networks formed from a purely trifunctional system.

Characterization of Products and Polymerization Kinetics

Modified thiol monomer products were characterized by ^{1}H NMR using a Varian Mercury 200 MHz NMR spectrometer in acetone-D6. Polymerization kinetics of selected control films and modified thiol-ene films were monitored using a Bruker 88 FTIR spectrometer modified with a fiber-optic cable to irradiate samples sandwiched between two salt plates. The conversion of thiol –SH groups at 2570 cm^{-1} (S-H stretch) and ene C=C groups at 3100 cm^{-1} (vinyl C-H stretch) were monitored as a function of irradiation time. An Oriel 200 W high pressure mercury−xenon lamp with light intensity of 6.16 mW/cm^2 at 365 nm was used to irradiate the samples and invoke photopolymerization.

Film Formation

Free-standing thin films of all thiol-ene formulations were made by dissolving 1 wt% 1,1-dimethoxy-1-phenylacetophenone (Irgacure 651) photoinitiator into the thiol-

ene mixture by sonication for approximately 10 minutes. This homogoneous mixture was then drawn down onto glass substrates using drawdown bars. Initial scouting work determined optimal thickness: materials with oxygen permeability less than 0.2 cc(STP) cm $m^{-2}day^{-1}atm^{-1}$ were cast using a .13 mm drawdown bar while those with higher permeability were drawn-down anywhere from 0.51 to 1.3 mm thickness depending on the permeability value. This procedure was done to ensure an adequate amount of experimental data points in the non-steady state region of the flux curves for proper fitting. Films were cured using 10 passes under a Fusion UV curing line system with a D bulb (400 W/cm^2 with belt speed of 3 m/min and 3.1 W/cm^2 irradiance). All films were normalized in air for 3-5 days prior to testing. Annealing of films was investigated using an annealing procedure of 100 °C for 4 hrs in air – this was done to verify if the UV-curing process was sufficient for full conversion of films and to complement the oxygen permeation results for unannealed films to show reproducibility.

Oxygen Permeation Testing

Oxygen permeation tests were conducted on Mocon OX-TRAN® 2/21 instruments using a continuous-flow testing cell method approved by the ASTM (D3985). All measurements were conducted at 23 °C and 0% RH. In this method, oxygen is the test gas and inert nitrogen is the carrier gas. The samples of 50 cm^2 testing area were loaded into the testing cell and flushed with nitrogen gas to purge out excess gases and to develop a zero point. Afterward, pure oxygen gas was introduced to one side of the test cell; the driving force for permeation is a difference in partial pressure of oxygen since the concentration of oxygen on the carrier side of the cell is maintained at

essentially zero. Oxygen was carried away from the downstream surface of the film by the nitrogen carrier gas to a coulometric sensor.

Permeability *P* and diffusivity *D* were obtained by performing a two-parameter least-square fit of the experimental oxygen flux *J*(*t*) data to Fick's second law solution (Equation 1):[11]

$$J(t) = \frac{Pp}{l}\left[-\sum_{n=1}^{\infty}(-1)^n \exp(-D\pi^2 n^2 t / l^2)\right] \quad (1)$$

where *p* is the applied pressure and *l* is the film thickness. Using the solution-diffusion equation (Equation 2),[12] the solubility *S* was then calculated.

$$P = D \cdot S \quad (2)$$

Instrumentation error using this method in the range of oxygen fluxes studied is +/- 5% for permeability values and +/- 10% for diffusivity values. The remaining experimental error in obtaining *P*, *D*, and *S* values is largely derived from film thickness variations. For this reason, special care was taken to evaluate films of approximately uniform thickness; thickness averages were obtained by measuring at multiple locations.

Thermal and Mechanical Analysis

A TA Instruments Q1000 DSC with heating rate of 10 ^{o}C/min was used to investigate the glass transition temperature of film samples between 8 and 12 mg. Mechanical properties were evaluated using a Rheometric Scientific DMTA V with a frequency of 1 Hz, strain rate of 0.05%, and heating rate of 5 °C/min. T_g values were

taken as the mid-point of the inflection from DSC scans and as the peak maximum in tan delta plots from DMTA.

Results and Discussion

Basic Thiol-ene Networks

In order to establish a baseline in properties, the oxygen transport characteristics of basic thiol-ene films were evaluated. These basic networks feature the 3T trifunctional thiol monomer copolymerized with four different ene monomers of varying functionality and rigidity: TEGDVE, TAE, TOT, TTT. TEGDVE, the least rigid monomer, is difunctional, while TAE, also a flexible monomer, is trifunctional. TOT and TTT have basic triazine and isocyanurate structures and are more rigid trifuctional ene monomers. The trifunctional thiol 3TI and tetrafunctional 4T were also copolymerized with TTT to increase the network rigidity and the glass transition temperature. All thiol-ene networks were obtained by exposing 1:1 molar functional group mixtures with 1 wt% photoinitiator to 10 passes under a medium pressure D bulb as detailed in the Experimental section. A high-T_g thiol-isocyanate-ene film for comparison was prepared from a one-pot mixture of 6 mmol 4T, 4 mmol IPDI, 5.3 mmol TTT, 1 wt% Irgacure 651, and 0.05 wt% tributylamine. The liquid mixture was drawn-down and cured in the same fashion as the basic thiol-enes. A portion of thiols reacted with the isocyanates via the tributylamine catalyst and the remaining thiols reacted with the TTT enes via photopolymerization. This film was then post-cured for 12 hrs at 110 °C; the result is a high-T_g crosslinked network with carbamate groups present that enhance hydrogen bonding. Note that this three component film was not considered a basic thiol-ene film and is included only for comparison with a high T_g, highly-crosslinked network.

Figure III-1 shows DSC 2nd heating scans for each of the resulting thiol-ene networks. T_g values are listed in Table III-1. As has been reported for photocured thiol-ene networks,[8,9] the DSC curves exhibit well-defined, narrow glass transition regions indicative of their high uniformity. It is important to note that simply by changing the ene component, the glass transition temperature of the film changes dramatically; this series of six thiol-ene films spans over 80 °C in glass transition temperatures. The T_g values are directly related to the thiol and ene functionalities as well as their rigidity as detailed in references 14, 15, and 16. The 4T-IPDI-TTT film has a T_g of 65 °C which is well above room temperature, thus making it a decidedly glassy network for the oxygen transport measurement.

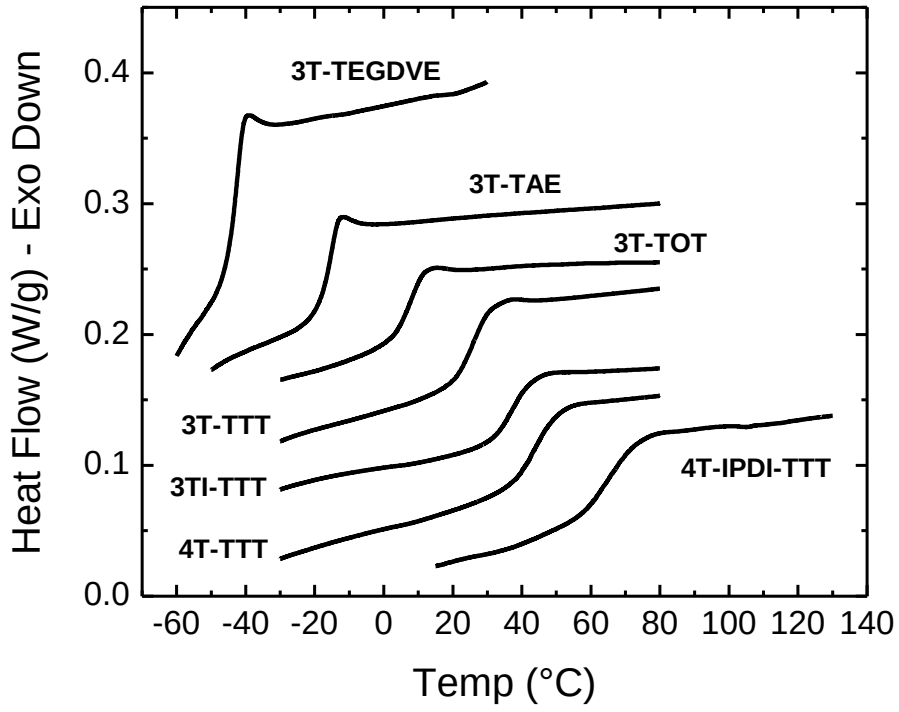

Figure III-1. DSC 2nd heating scans for basic thiol-ene films and thiol-isocyanate-ene film.

Oxygen transport measurements of the basic thiol-ene films were next conducted using a continuous-flow testing system described in the Experimental section. Figure III-2 shows a representative experimental oxygen flux data (opened symbols) obtained at room temperature for a 3T-TAE film of 0.42 mm thickness with the two-parameter fit to Equation 1 (solid line). The fit was excellent. The experimental oxygen flux curves for all samples exhibited the same type of Fickian behavior shown in Figure III-2. Equation 1 was used to fit flux data and calculate permeability (*P*) and diffusivity (*D*). Using Equation 2 the solubility (*S*) was calculated. The individual *P*, *D*, and *S* values of the six basic, two-component thiol-ene films are given in Table III-2. These data are also plotted as a function of T_g in Figures III-3 and III-4.

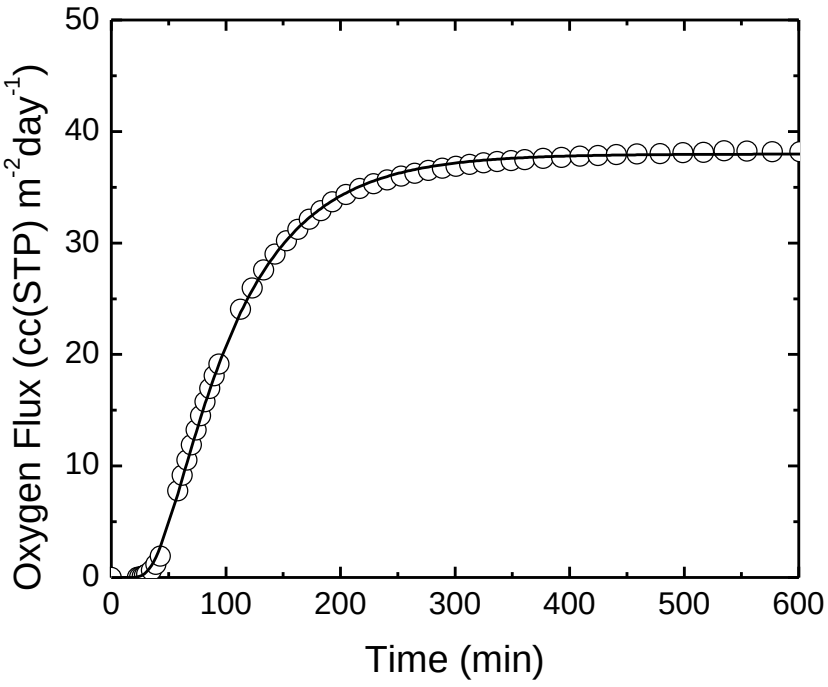

Figure III-2. Representative oxygen flux fit curve for 3T-TAE film of 0.42 mm thickness.

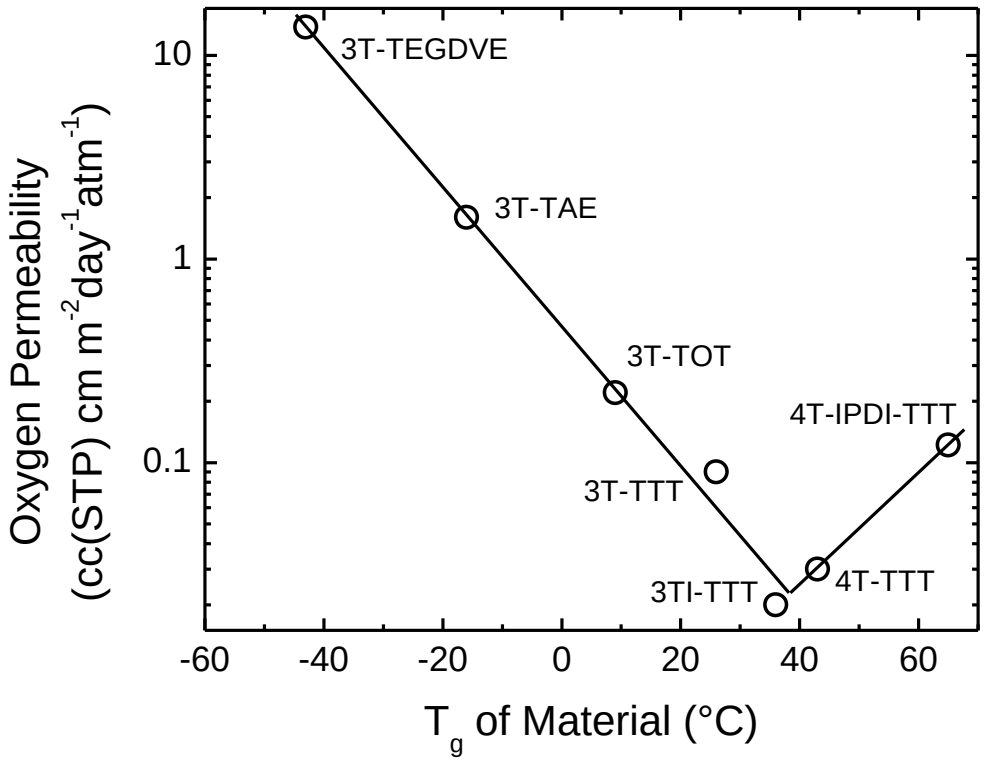

Figure III-3. Relationship between oxygen permeability and the T_g of basic thiol-ene materials.

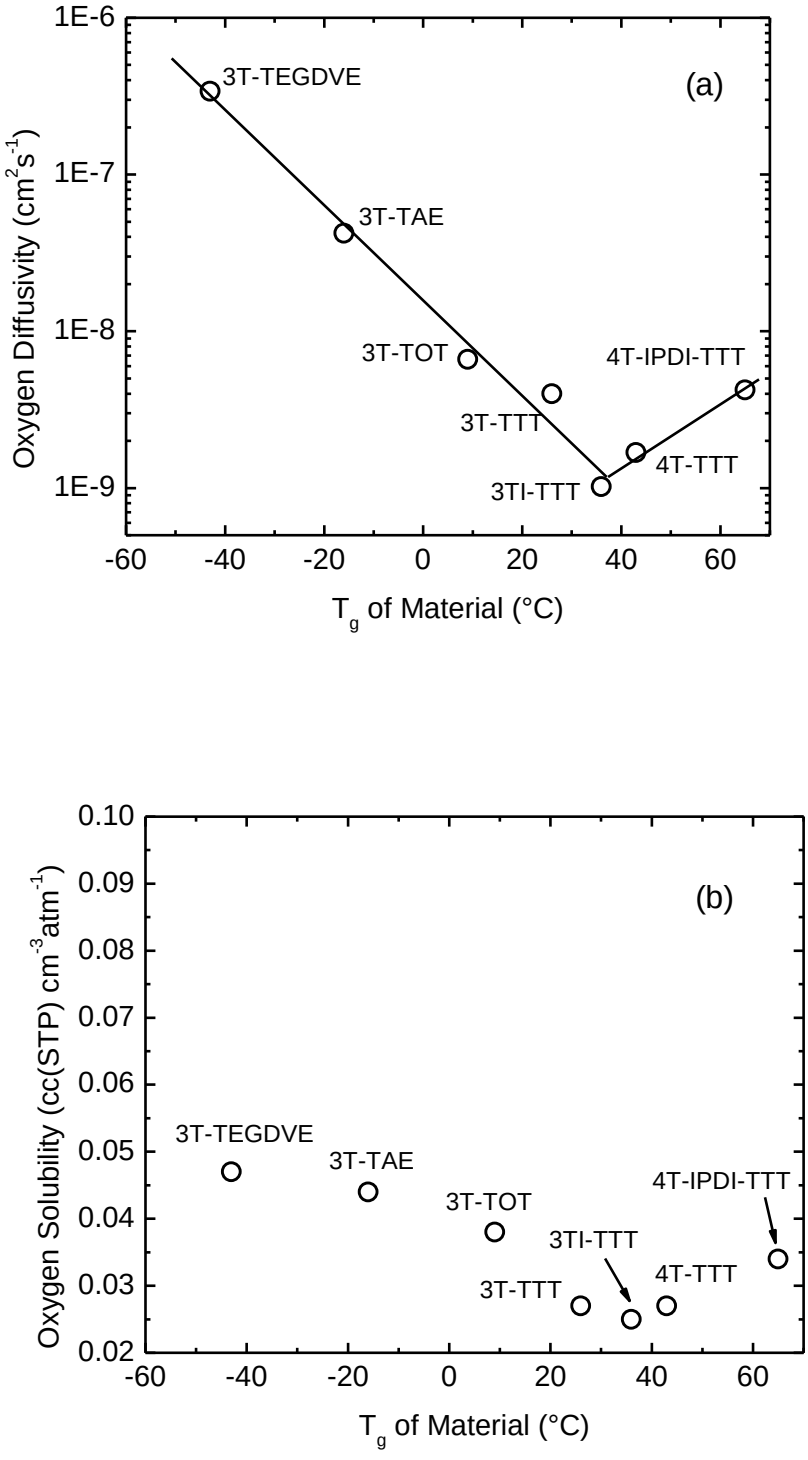

Figure III-4. Relationship between (a) oxygen diffusivity and T_g and (b) oxygen solubility and T_g of basic thiol-ene materials.

For rubbery networks exhibiting glass transition temperatures below room temperature, the temperature (23 °C) at which all transport measurements were conducted, P and D exponentially decreased as T_g increased. In turn for glassy networks exhibiting T_g above room temperature, in particular for 4T-TTT and 4T-IPDI-TTT, P and D exponentially increased with T_g. A minimum in both oxygen permeability and diffusivity is thus observed near the testing temperature (23 °C). These two dependencies in semi-log coordinates displayed an almost perfect V-shape trend as one can see in Figures 3 and 4a.

The V-shape trend of *P*, *D* and *S* with T_g has been interpreted in this article by means of a free volume concept broadly used in the literature to interpret gas barrier data. It is widely accepted that *P*, *D*, and *S* of a polymer increase with the free volume. While solubility changes somewhat in proportion to the amount of free volume, diffusivity and subsequently permeability exhibit an exponential dependence on free volume.[17]

In general, *rubbery* polymers exhibit a correlation between free volume and the difference between T_g and T_{test} (T_{test} is the temperature at which the measurement was made). The results of free volume and gas transport measurements conducted at a specific T_{test} on different polymers with a broad range of T_g are as follows. Beginning with the lowest T_g polymer and advancing to polymers of higher T_g, the difference between T_g and T_{test} decreases, and both the free volume and gas diffusivity are reduced.[18,19] Once the T_g of the material surpasses T_{test}, the polymer is in the glassy state during the measurement. For *glassy* polymers with increasing T_g the free volume and gas diffusion coefficient at T_{test} both increase[18] since transport is enhanced by the presence of hole-free volume that is frozen into the glassy, non-equilibrium state.[20] It is noted that

such static hole-free volumes do not exist in the rubbery state.[20] As the difference between T_g and T_{test} increases for glasses, the amount of frozen hole-free volume also increases. In summary, there is a clear minimum for both free volume and gas diffusivity where $T_{test} = T_g$. This is precisely the result seen with the basic thiol-enes when combining the results for both rubbery and glassy networks: exponential dependencies of permeability and diffusivity vs. T_g, with minimums near T_{test}.

As expected, oxygen solubility for thiol-enes in Figure 4b also shows a minimum. Similar behavior was shown for the relationship between oxygen solubility and the T_g for PET – a minimum in oxygen solubility appears at $T_{test} = T_g$.[11] The TTT-based films in particular display low oxygen solubility; in fact, solubility that is almost three times lower than PET. This results from the scarcity of free-volume in the highly-dense crosslinked thiol-ene networks as compared to linear, amorpohous PET[13] which is glassy at room temperature. As well, the sulfur present in the networks may also contribute to the low solubility of oxygen.

It can be concluded that the basic thiol-enes, while having different T_g, different functionalities, different ene groups, and different monomer rigidities, belong to the same *family* in terms of oxygen transport properties. The permeability and diffusivity values correlate well with the difference between T_g and T_{test} and form a minimum, allowing prediction of these characteristics from this semilog relationship. While these results are consistent with well-known observations, they represent to the best of our knowledge the first report of the correlation of T_g and transport properties for a family of highly-crosslinked thiol-ene networks that obeys a prototypical fit.

Modified Thiol-ene Networks

Having established benchmark oxygen transport properties for commercially-available thiol and ene monomers, the tunability of the thiol-ene networks was explored. In the past, the effect of a plethora of functional groups and repeat units on the gas barrier properties of linear polymers has been evaluated phenomenologically.[1,2] The three most effective structural units for decreasing oxygen permeability were the cyano group, the hydroxyl group, and the amide repeat unit. The primary amine catalyzed thiol-acrylate Michael addition reaction in Figure III-5 was used to develop a platform to assess the effect of a wide range of functional groups including alkyl, hydroxyl, cyano, primary amides, and secondary amides on T_g and oxygen barrier properties.

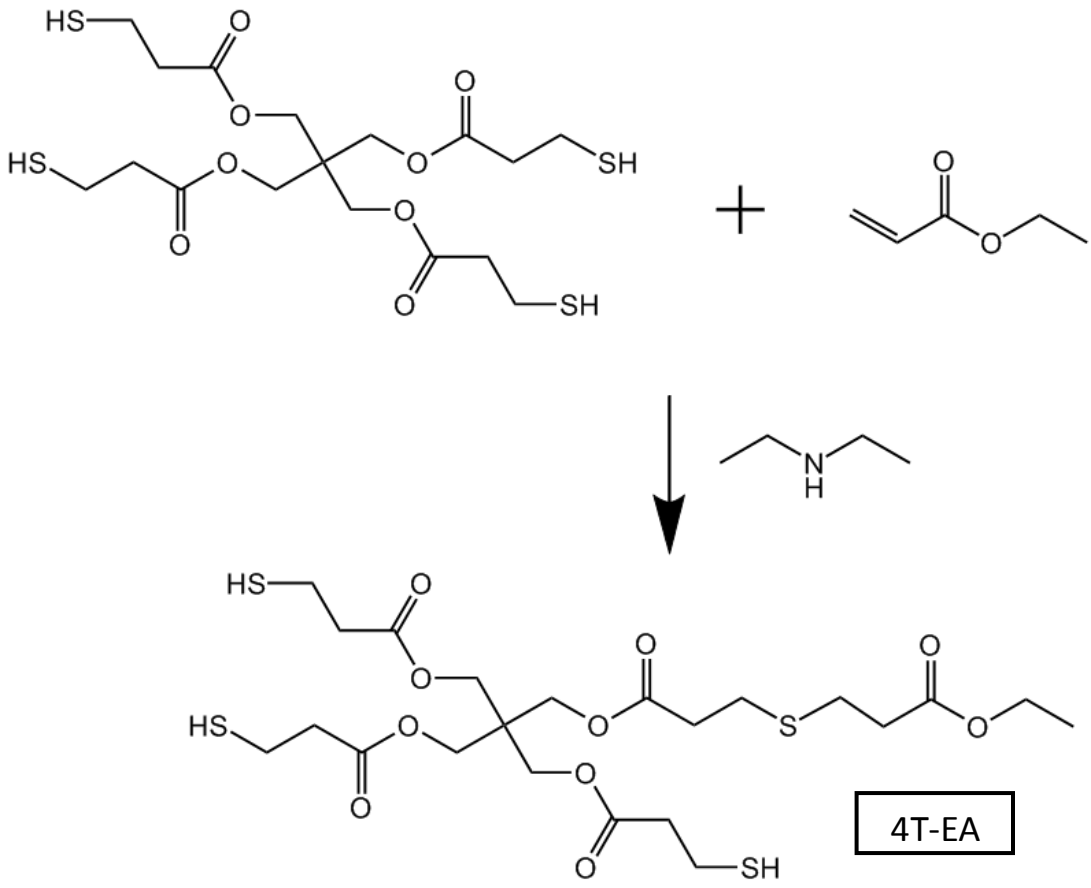

Figure III-5. Thio-Michael addition reaction mechanism of 4T and EA with diethylamine catalyst. Product shown is representative of predominant structure in mixture. Other products were formed by reacting 4T with the other enes in Chart III-2 (i.e. 4T-AN, 4T-HEA, 4T-NIPAM, 4T-AM).

In order to verify that all of the respective electron deficient ene effectively reacted via the thiol-acrylate Michael reaction, each of the products were characterized by ^{1}H NMR. Figure III-6 shows ^{1}H NMR spectra of the precursor 4T and products 4T-EA, 4T-AN, 4T-HEA, 4T-NIPAM, and 4T-Am. The near-complete loss of the double bond protons at ~6 ppm indicated that the thiol-acrylate Michael reaction was successful.

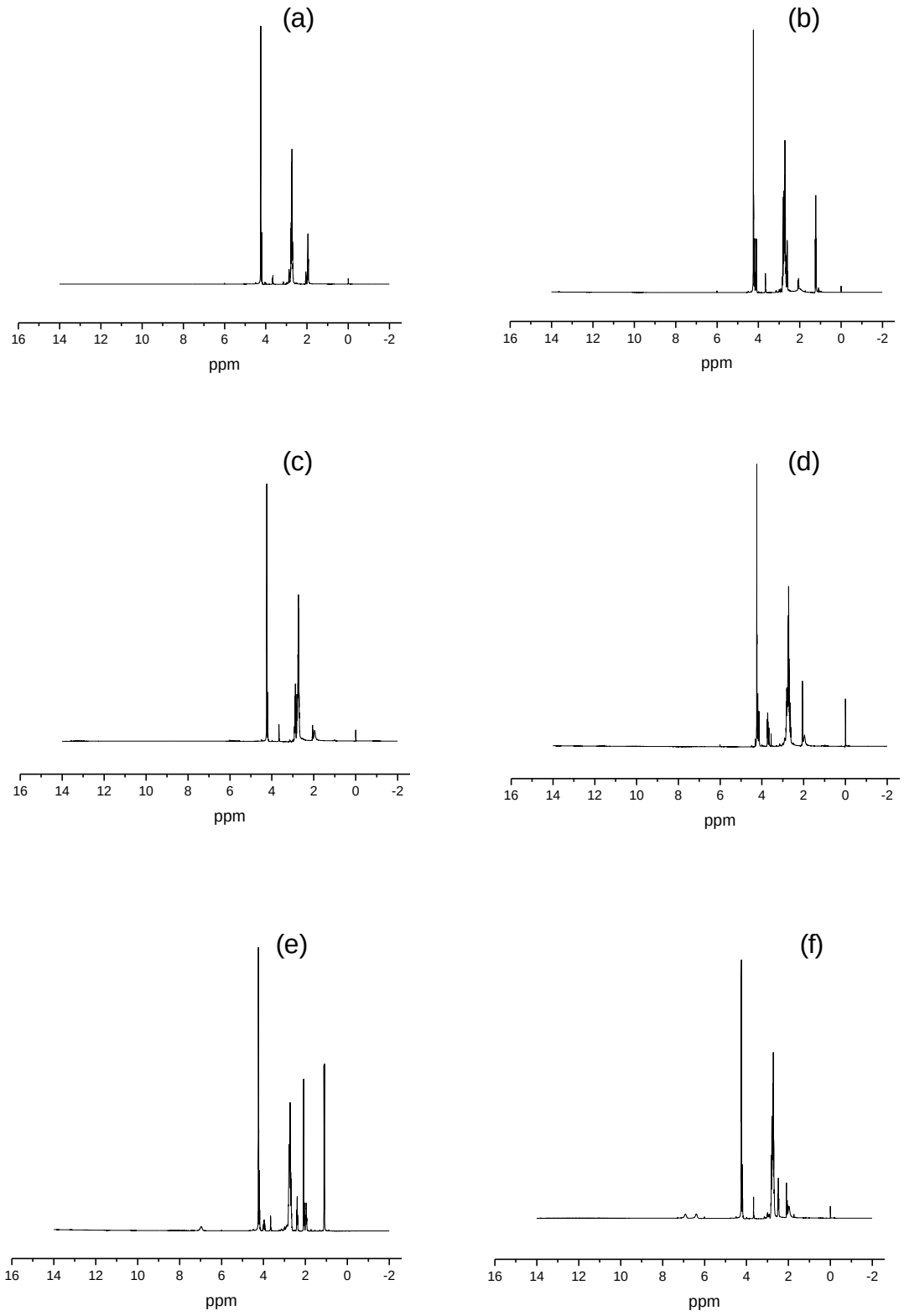

Figure III-6. ^{1}H NMR spectra for (a) 4T, (b) 4T-EA, (c) 4T-AN, (d) 4T-HEA, (e) 4T-NIPAM, and (f) 4T-Am.

The modified trifunctional thiol monomers were photopolymerized with the TTT ene monomer to form a set of thiol-ene networks for systematic evaluation of chemical structural effects on *D* and *S*. Results can be readily compared with the 4T-TTT (4:3) network with a *dangling* thiol group, the 3T-TTT network, and the 4T-EA-TTT network which has a non-polar ethyl group that is also incapable of hydrogen bonding. This series of films serves as a convenient model for establishing the effect of different dangling functional groups on *D* and *S* in a highly uniform crosslinked network. The thiol-ene system is in general well-suited for such a study because it is highly uniform, it is characterized by high functional group conversions, it has no crystallinity, and the molecular weight variation between crosslinks is essentially identical for all of the systems investigated. How a particular functional group incorporated into a uniform network affects glass transition temperature and oxygen transport properties will be realized.

Real-time IR photopolymerization kinetics for the modified thiol-ene systems are shown in Figure III-7. The thiol and ene functional groups proceed rapidly to high conversion at room temperature. The 4T-EA-TTT and 4T-HEA-TTT systems attained the highest conversion, i.e., 90% for both the thiol and ene functional groups. The 4T-AN-TTT system and 4T-NIPAM-TTT systems reached approximately 80% and 85% conversion, respectively, under the polymerization conditions used. Lastly the 4T-Am-TTT system reached the lowest conversions of 75%. The thiol and ene conversions in all cases are essentially identical indicating that the free-radical thiol-ene reaction proceeds rapidly with no indication of ene homopolymerization. This conformity also reinforces ^{1}H NMR results that the 4T-modified monomers are stoichiometrically trifunctional on

average. Note that the light intensity used in monitoring these polymerization kinetics is smaller that that of the light used to cure films for evaluation where conversions reach nearly 100%.

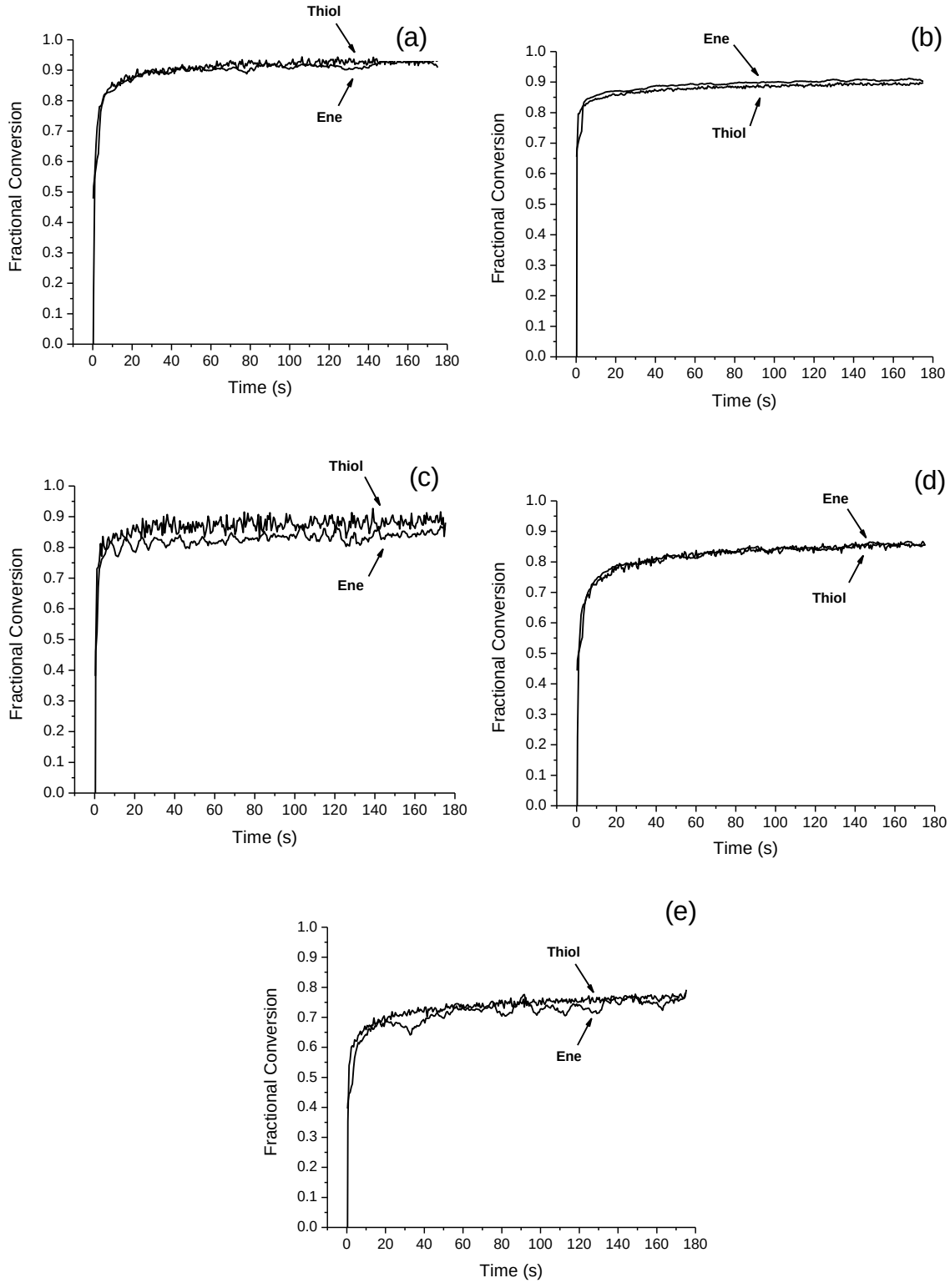

Figure III-7. RT:FTIR conversion versus time plots for (a) 4T-EA-TTT, (b) 4T-HEA-TTT, (c) 4T-NIPAM-TTT, (d) 4T-AN-TTT, (e) 4T-Am-TTT.

IR measurements at various temperatures were conducted to verify the presence of hydrogen bonding in the O-H stretching region of 4T-HEA-TTT in accordance with prior IR temperature measurements on poly(HEA).[21] A liquid mixture of 4T-HEA, TTT, and 1 wt% Irgacure 651 was sandwiched between two salt plates and compressed to form a thin layer followed by photopolymerization using the procedure described previously. Spectra were recorded at 23 (room temperature), 60, 100, 140, and 180 °C. As Figure III-8 shows, as temperature increased the spectrum shifts to higher wavenumbers, the associated proton shoulder/peak at ~3450 cm^{-1} decreases in intensity, and the entire O-H stretching region decreases in intensity. This is in agreement with results on poly(HEA) films when subjected to higher temperatures and indicates that both associated and free protons are present at room temperature, with reduction in the associated protons with increasing temperature.[21]

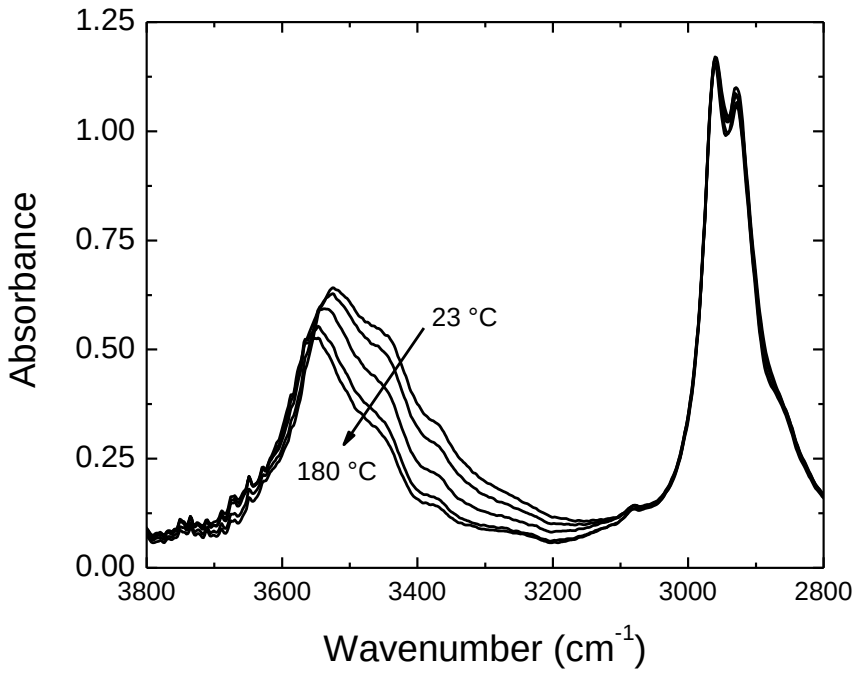

Figure III-8. Effect of temperature on IR spectra of 4T-HEA-TTT film in the O-H stretching region demonstrating the presence of hydrogen bonding.

The second DSC heating scans for all the cured networks in Figure III-9a have narrow glass transitions which are characteristic of thiol-ene films and indicate highly uniform networks. In each case, the networks containing the hydroxyl, primary and secondary amides, and cyano groups show an increase in T_g when compared to the 4T-EA-TTT based network, which only has a hydrocarbon side group with no possibility for polar interaction or hydrogen bonding. This suggests that in each case either dipole-dipole or hydrogen-bonding interactions result in an increase in the glass transition temperature and rigidity of the film. The 3T-TTT control film has a T_g equal to or higher than any of the modified films presumably due to the absence of any *dangling* side groups attached to the network. A free thiol group in the network of the 4T-TTT(4:3)

film results in a glass transition between that of the 3T-TTT and 4T-TTT(1:1) films. This clearly shows that a free thiol-functional arm in the network increases the glass transition of the film compared to any of the modified thiol-ene films. This may well be due to a chemical based structural effect or to the distribution of thiol functional species that actually comprise the modified trifunctional thiols, i.e., the thiol functionality for the 4T-modified systems only represents a nominal average functionality. In order to further evaluate the thiol-ene networks, DMTA measurements were made on each film. As seen in Figure III-9b, the basic trends for the peak maximum in the tan delta versus temperature plots are essentially the same except that in each case the DMTA based glass transition temperatures (see Table III-1) are higher. This results from the time-scale differences in DSC versus DMTA runs.

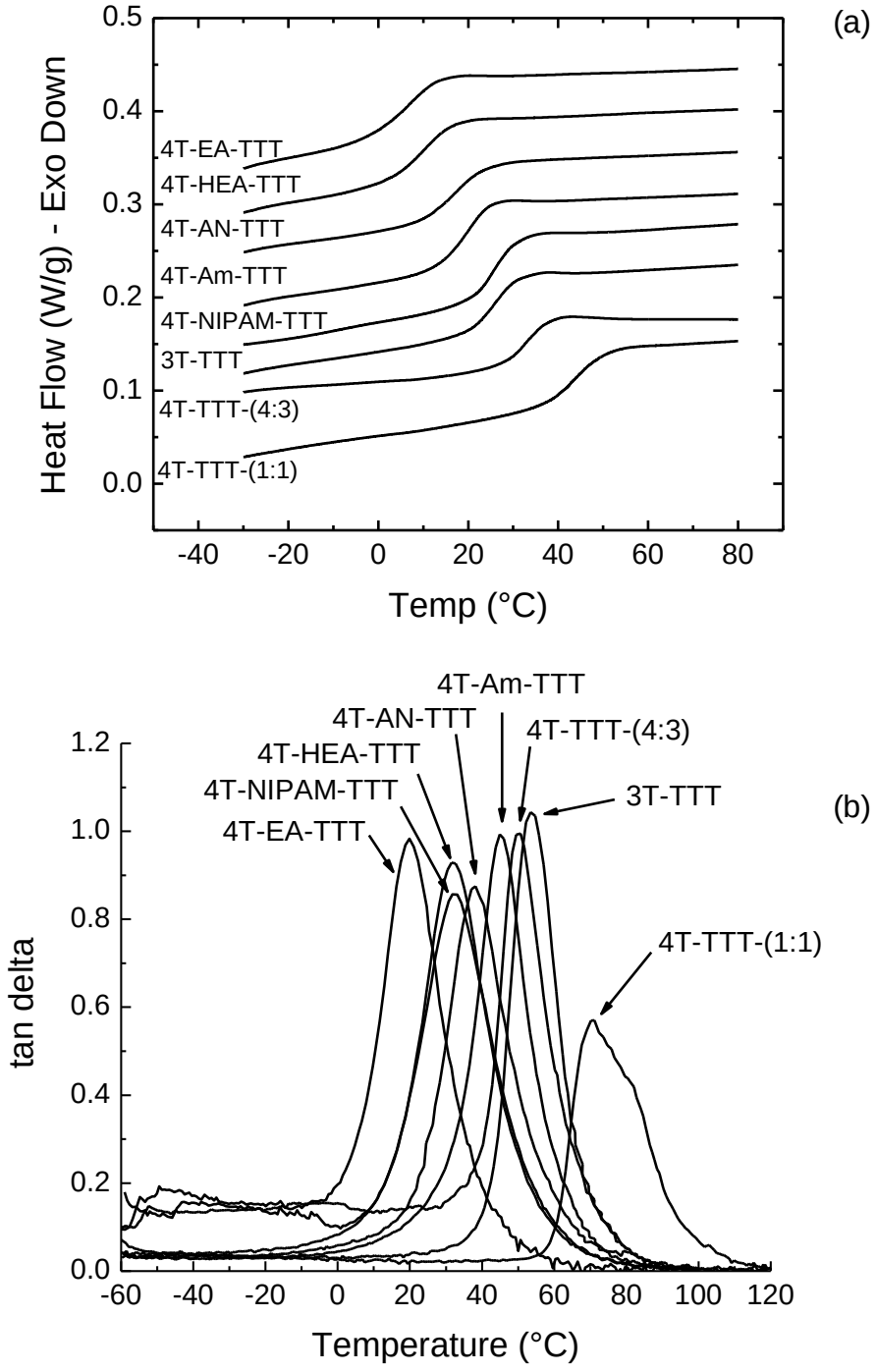

Figure III-9. (a) DSC 2nd heating scans and (b) tan δ vs. temperature plots for modified thiol-ene films and controls.

Simulated oxygen flux *J(t)* curves generated for the networks (assuming 0.10 mm thick films) using their corresponding P and D values are shown in Figure III-10 for comparison. The highest permeability was observed for the 4T-EA-TTT network with a value of 0.39 cc(STP) cm m^{-2} day^{-1} atm^{-1}. As mentioned previously, this film is a relevant control for the modified thiol-enes. The permeabilities of the other modified films are all lower demonstrating the effect of strongly-interacting functional groups in increasing oxygen barrier properties at room temperature. The oxygen solubility data exhibit in particular remarkable behavior: with the exception of the 4T-HEA and 4T-NIPAM systems, each of the modified films show solubilities lower than that of any of the other basic thiol-ene networks. Secondary interactive forces, dipole-dipole interactions from the cyano group of acrylonitrile and hydrogen bonding from the amide group of acrylamide,[22] hinder oxygen transport in the network.

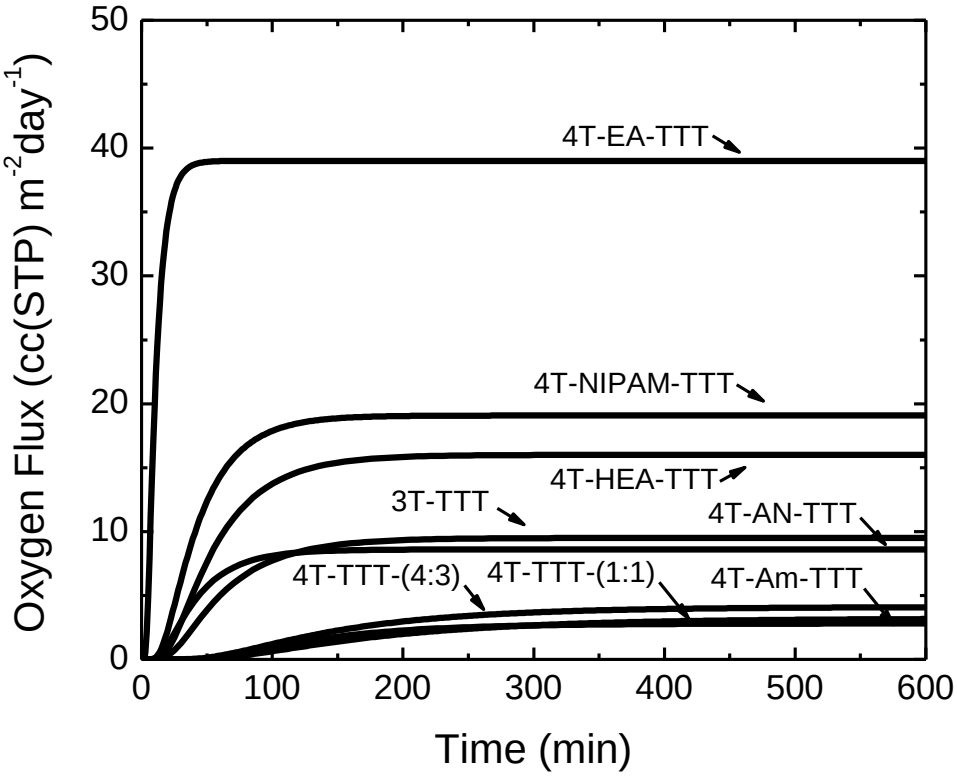

Figure III-10. Simulated oxygen flux curves for modified thiol-enes and controls of 0.10 mm thickness.

Figure III-11 shows semilog dependencies of oxygen permeability and diffusivity versus T_g for the modified films. The corresponding values for the basic thiol-ene networks from Tables III-1 and III-2 are also added to this plot. As one may see the data for all modified networks roughly followed the same trend as the family of basic networks showing noticeable variation.

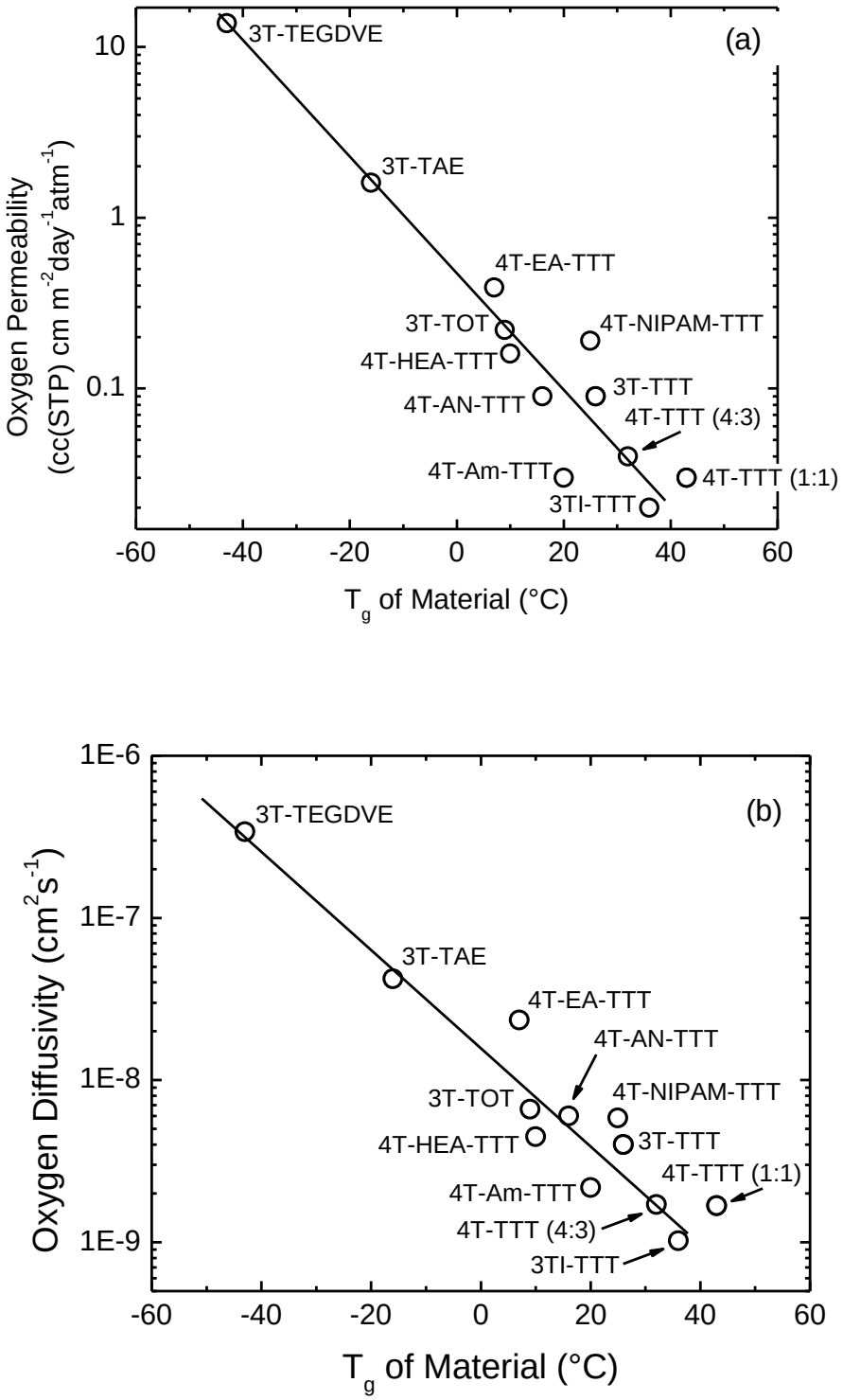

Figure III-11. (a) Oxygen permeability vs. T_g and (b) oxygen diffusivity vs. T_g for modified and control thiol-enes.

As seen in Figure III-11b, the thiol-ene films with accessible hydrogen bonding species, 4T-HEA-TTT and 4T-Am-TTT, exhibited permeability and diffusivity values that fall below the corresponding trend established for the basic networks. This was attributed to the accessibility of the hydrogen bonded functional groups in the modified networks implying improved cohesion and thus lower oxygen permeability and diffusivity.

To further evaluate the effect of the amide functional group on T_g and gas transport properties, a series of modified trifunctional thiol monomers was synthesized by using the thio-Michael addition of a combination of ethyl acrylate and acrylamide at different concentrations. An average of one out of every four groups on the 4T thiol monomer was capped by either an ethyl acrylate or acrylamide unit at varying relative concentrations: 0:100 (the pure ethylacrylate 4T-EA), 25:75, 50:50, 75:25, and 100:0 (the pure acrylamide 4T-Am). Networks cured from these mixtures are referred to by the molar fraction of acrylamide in the Michael reaction feed: 0.00, 0.25, 0.50, 0.75, and 1.00. Real-time IR kinetics for both thiol and ene functional group conversion are shown in Figure III-12. Both the thiol and ene conversion decreases as acrylamide fraction increases; the highest and lowest conversions were obtained by the pure 4T-EA-TTT and pure 4T-Am-TTT samples, respectively. It appears that an increase in hydrogen bonding of the amide group, derived from increased acrylamide fraction, lowers final conversion due to restriction in mobility of monomer species during polymerization. As previously discussed, the light intensity used to photocure films for glass transition and oxygen permeability measurements was much higher to ensure high conversions in all cases.

According to Figure III-13 which shows DSC 2nd heating scans for fully cured films, the T_g (see Table III-1) also increases as a function of increasing acrylamide content due to enhanced hydrogen bonding and resulting network mobility restrictions.

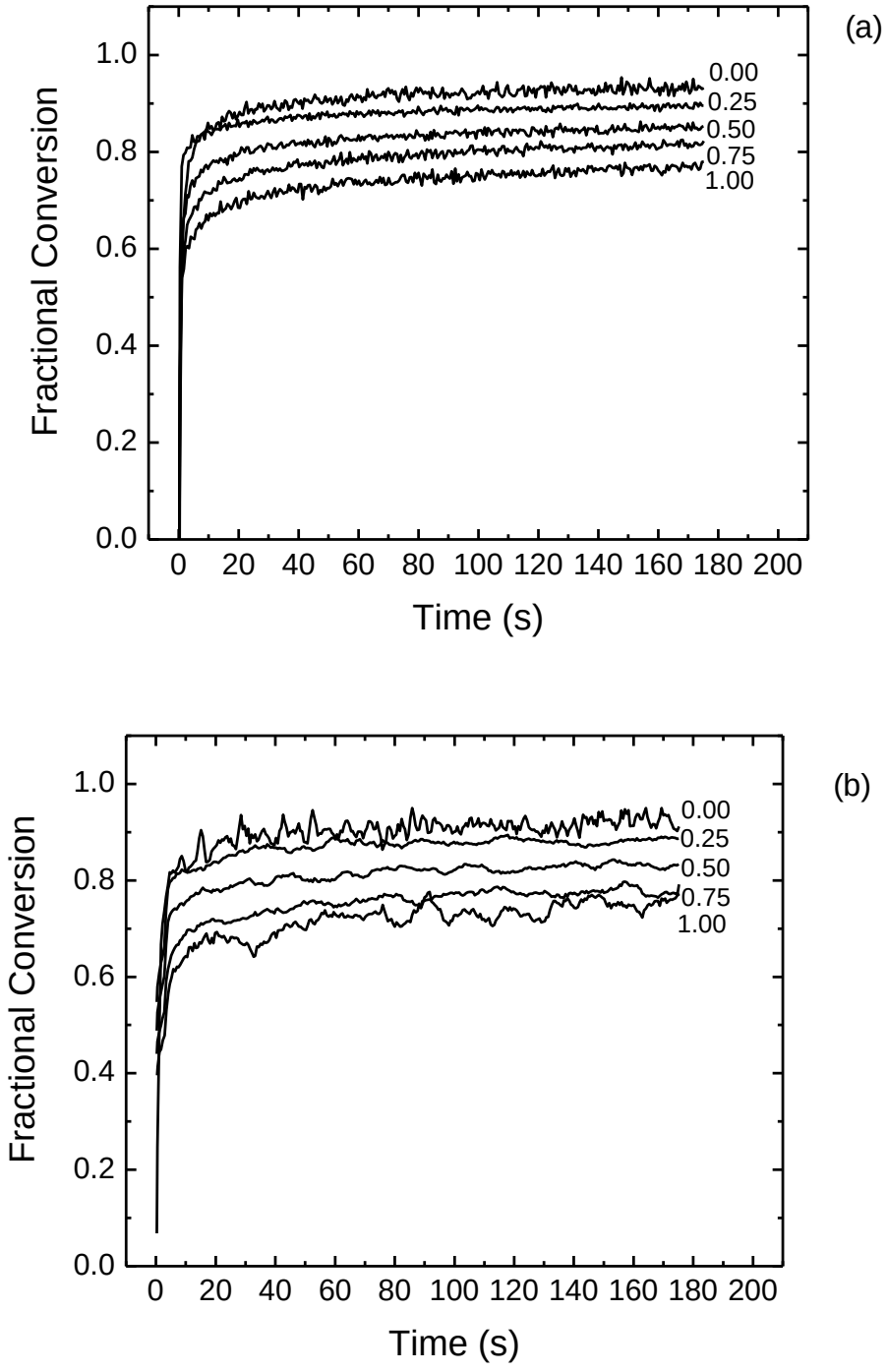

Figure III-12. RT:FTIR group conversion versus time for 4T-Am:EA-TTT systems: (a) thiol conversion, (b) ene conversion. Labels denote acrylamide molar fraction in Michael reaction feed used to make the respective modified thiols.

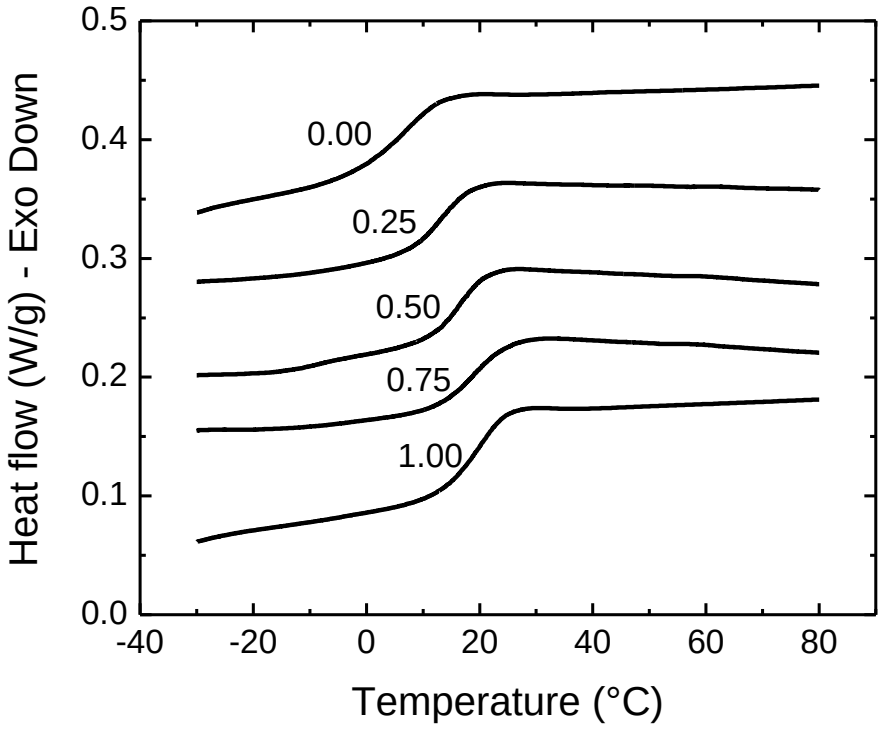

Figure III-13. DSC 2nd heating scans for series of 4T-Am:EA-TTT modified thiol-ene films. Labels denote acrylamide molar fraction for Michael reaction feed used to make the respective trifunctional thiols.

The oxygen transport results for the series of modified films given in Table III-2 indicate a decrease in oxygen permeability with an increase in acrylamide molar fraction. Figure III-14a shows that an increase of the acrylamide fraction results in an exponential decrease in oxygen permeability. This decrease is a direct consequence of restriction in mobility in the thiol-ene network due to hydrogen bonding. Interestingly, somewhat similar behavior was previously observed in the case of linear copolymers.[1] Exponential changes in permeability are established as a function of co-monomer molar fraction leading to development of the Permachor concept.[1] Interestingly, thiol-ene network T_g

also increases with increasing amide molar fraction but only linearly as shown in Figure III-14b thus resulting in an exponential decrease of oxygen permeability of acrylamide modified networks with corresponding T_g, i.e. the difference between T_g and T_{test}.

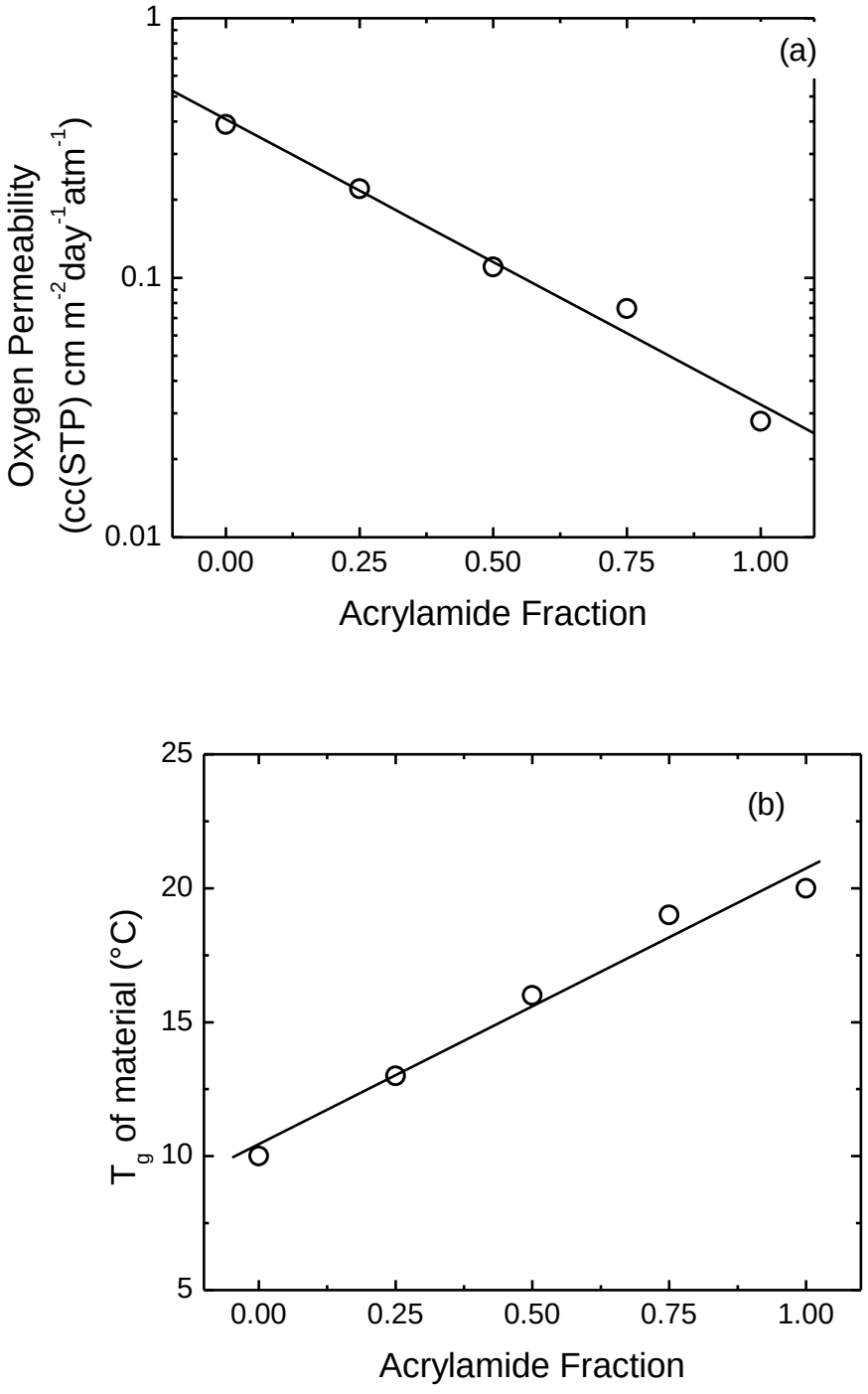

Figure III-14. (a) Semilog plot of oxygen permeability and acrylamide fraction substituted onto thiol group of 4T, (b) linear plot of T_g and acrylamide fraction, and (c) semilog plot of oxygen permeability and T_g for the 4T-Am:EA-TTT networks.

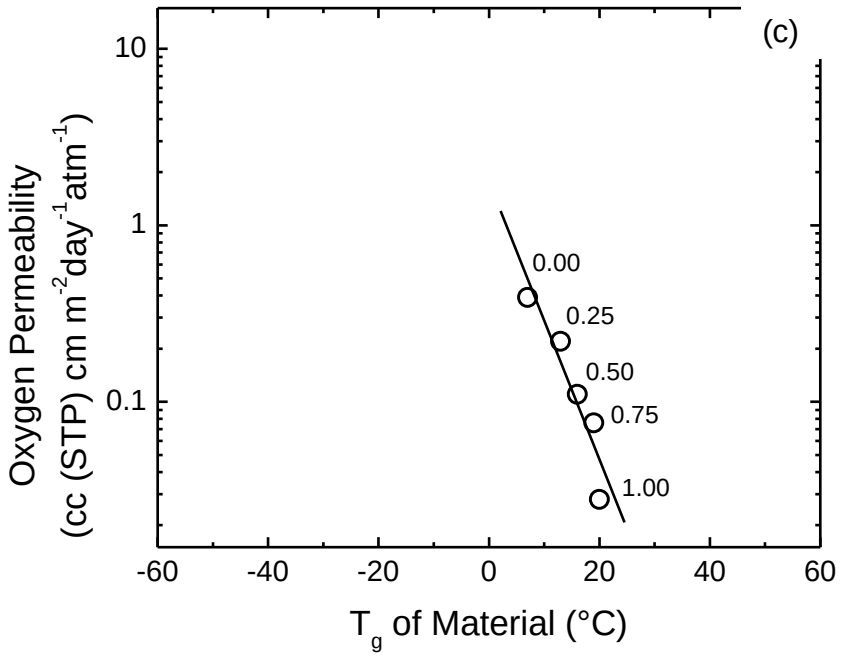

Figure III-14 (continued).

It is important to notice that the plot in Figure III-14c is similar to those in Figures III-3 and III-11, further illustrating the general correlation of log(*P*) and the difference between T_{test} and T_g for both the base thiol-ene networks (Figure III-3), the modified thiol-ene networks (Figure III-11) and the thiol-amide-ethyl-ene networks (Figure III-14). However the slope of the semilog plot in Figure 14c for the 4T-Am:EA-TTT based networks is greater than that of the corresponding plots in Figures III-3 and III-11. This deviation can be seen in Figure III-15 which includes all of the basic thiol-ene systems along with all of the 4T-Am:EA-TTT systems. Therefore amide modified thiol-ene networks form a different kind of family with regards to oxygen barrier properties versus T_g as compared to basic thiol-ene networks.

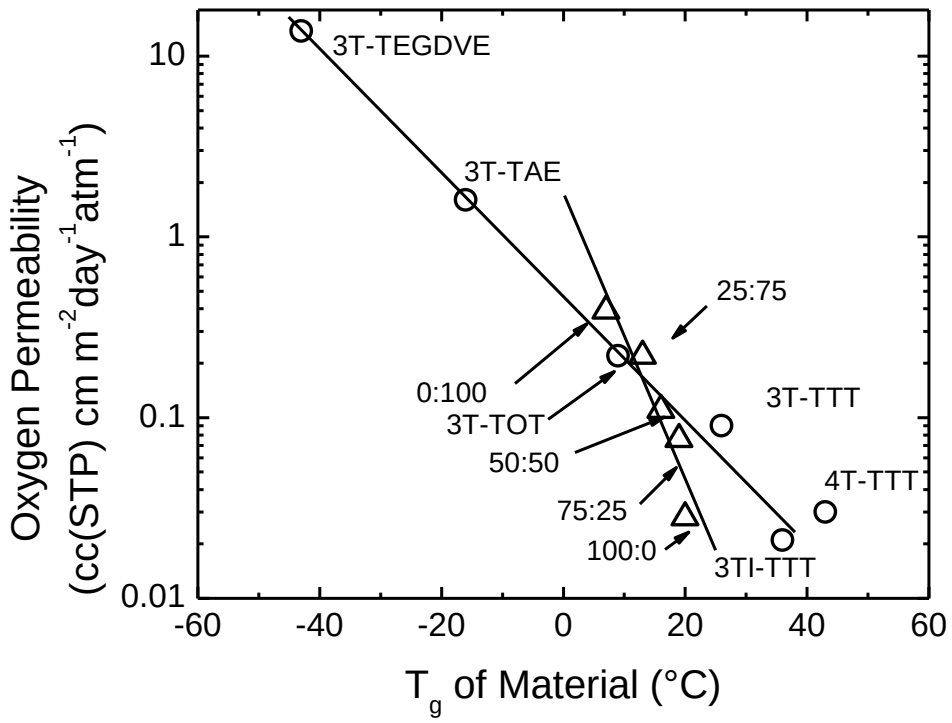

Figure III-15. Relationship between oxygen permeability and the T_g of 4T-Am:EA-TTT modified thiol-ene films compared to that of basic thiol-ene films.

Finally, annealing of selected films for 4 hrs at 100 °C in air was conducted to demonstrate that sufficient film curing was provided by the Fusion lamp in order to optimize conversion. Oxygen permeability values given in Table III-2 for the annealed films are similar with oxygen permeability values for non-annealed films. This implies that the maximum of chemical conversion has been reached upon UV curing at room temperature leading to ultimate oxygen barrier properties and no further post curing is required.

Table III-1. Glass Transition Temperatures Determined by DSC and DMTA.

Material	T_g (°C) (DSC)	T_g (°C) (Tan δ peak)
3T-TEGDVE	-48	--
3T-APE	-15	--
3T-TOT	9	--
3T-TTT	26	54
4T-TTT (1:1)	43	71
4T-TTT (4:3) (dangling thiol)	32	50
3TI-TTT	36	--
4T-IPDI-TTT	65	--
4T-EA-TTT	10	20
4T-AN-TTT	20	38
4T-HEA-TTT	16	32
4T-NIPAM-TTT	25	32
4T-Am-TTT	20	45
25:75 Am:EA	13	--
50:50 Am:EA	16	--
75:25 Am:EA	19	--

Table III-2. Oxygen Transport Data for Thiol-Ene Networks and PET for Comparison.

Material	Oxygen Permeability (cc(STP) cm $m^{-2}day^{-1}atm^{-1}$) Normal	Annealed	Oxygen Diffusivity (cm^2s^{-1})	Oxygen Solubility (cc(STP) $cm^{-3}atm^{-1}$)
3T-TEGDVE	13.8	--	3.40E-07	0.047
3T-APE	1.6	--	4.20E-08	0.044
3T-TOT	0.22	--	6.60E-09	0.038
3T-TTT	0.09	0.1	4.00E-09	0.027
4T-TTT (1:1)	0.032	0.032	1.40E-09	0.027
4T-TTT (4:3)	0.041	0.042	1.70E-09	0.026
3TI-TTT	0.021	0.024	1.00E-09	0.025
4T-IPDI-TTT	0.12	--	4.20E-09	0.034
4T-EA-TTT	0.39	0.45	2.40E-08	0.019
4T-AN-TTT	0.09	--	6.00E-09	0.017
4T-HEA-TTT	0.16	0.16	4.50E-09	0.041
4T-NIPAM-TTT	0.19	--	5.80E-09	0.038
4T-Am-TTT	0.03	0.03	2.20E-09	0.015
25:75 Am:EA	0.22	--	6.50E-09	0.039
50:50 Am:EA	0.11	--	4.50E-09	0.028
75:25 Am:EA	0.076	--	4.20E-09	0.021
PET	0.36	--	5.00E-09	0.083

Conclusions

The oxygen transport characteristics, specifically permeability, diffusivity, and solubility, were studied for a variety of thiol-ene networks. Using commercially available monomers, the functionality, rigidity, and type of ene group were varied, allowing the photopolymerization of networks spanning 100 °C in T_g. One network which showed high oxygen barrier properties was selected for further chemical modification. New thiol monomers were synthesized by a thio-Michael addition reaction of a tetrathiol to functionalized acrylates. These modified thiols were copolymerized with an isocyanurate-based ene monomer. The modified networks allowed an exploration into the effects of appendage groups with varied chemical structure (hydroxyl, amide, cyano, and alkyl) on T_g and oxygen barrier properties.

Both oxygen permeability and oxygen diffusivity, measured at room temperature, correlated remarkably well with T_g for both the rubbery and glassy networks, in agreement with classic behavior. Minimums in oxygen permeability, diffusivity, and solubility were found for samples whose glass transitions were near room temperature where the oxygen permeation measurements were conducted. Thus V-shaped correlations of both permeability and diffusivity with T_g were drawn. These relationships can allow prediction of the room-temperature oxygen transport properties of any basic thiol-ene network simply by knowing its glass transition temperature.

Using the network modification platform, the T_g and oxygen barrier properties were tuned by changing the nature and concentration of the functional group in the network. Of particular interest was the introduction of primary amides as dangling appendages which resulted in especially low oxygen permeability. As the result of a

hydrogen bonding effect from the primary amide group, a deviation from the trend seen with basic thiol-enes was observed. The use of thiol-ene networks as a platform to investigate the systematic effect of functional groups on network properties has far reaching implications. This method allows for the general assessment of how chemical structure can affect physical, mechanical, transport, and even optical properties of polymer networks.

References

1. Salame, M. *Polymer Engineering and Science* **1986**, *26*, 1543.
2. Lee, W. M. *Polymer Engineering and Science* **1980**, *20*, 65.
3. Lang, J.; Wyser, Y. *Packaging Technology and Science* **2003**, *16*, 149.
4. Sekelik, D. J.; Stepanov, E. V.; Nazarenko, S.; Schiraldi, D.; Hiltner, A.; Baer, E. *Journal of Polymer Science Part B: Polymer Physics* **1999**, *37*, 847.
5. White, J. E.; Haag, A. P.; Garth, P. R.; et al. *Journal of Polymer Science Part A: Polymer Chemistry* **1996**, *34*, 2967.
6. Brennan, D. J.; Silvis, H. C.; White, J. E.; Brown, C. N. *Macromolecules* **1995**, *28*, 6694.
7. Kloosterboer, J.G. *Advances in Polymer Science* **1988**, *84*, 8.
8. Kaya, E.; Smith, T.; Nayak, B.; Mathias, L. J. *Polymer Preprints: American Chemical Society, Division of Polymer Chemistry* **2005**, *46*, 857.
9. Hoyle, C. E.; Lee, T.Y.; Roper, T. *Journal of Polymer Science Part A: Polymer Chemistry* **2004**, *42*, 5301.
10. Choi, J.; Lee, K. M.; Wycisk, R.; Pintauro, P. N.; Mather, P. T. *Macromolecules* **2008**, *41*, 4569.
11. Hiltner, A.; Liu, R. Y. F.; Baer, E. *Journal of Polymer Science Part B: Polymer Physics* **2005**, *43*, 1047.
12. Crank, J. *The Mathematics of Diffusion*, Oxford University Press, **1975**.
13. Pauly, S. "Permeability and Diffusion Data," in *Polymer Handbook*, Eds. J. Brandrup et al., John Wiley & Sons, **1999**.
14. Shin, J.; Nazarenko, S. Hoyle, C. E. *Macromolecules* **2008**, *41*, 6741.

15. Cook, W. D.; Chausson, S. et al. *Polymer International* **2008**, *57*, 469.

16. Cook, W. D.; Chen, F. et al. *Polymer International* **2007**, *56*, 1572.

17. Cohen, M. H.; Turnbull, D. *Journal of Chemical Physics* **1959**, 31, 1164.

18. Yampol'skii, Y. P.; Volkov, V. V. *Journal of Membrane Science* **1991**, *64*, 191.

19. Lin, H.; Freeman, B. D. *Journal of Molecular Structure* **2005**, *739*, 57–74.

20. Vrentas, J. S.; Duda, J. L. *Journal of Applied Polymer Science* **1978**, 22, 2325.

21. Lee, T. Y.; Roper, T. M. et al. *Macromolecules* **2004**, *37*, 3659.

22. Galetich, I.; Stepanian, S. G. et al. *J. Phys. Chem*. A. **2000**, *39*, 104.

CHAPTER IV

FREE VOLUME, TRANSPORT, AND PHYSICAL PROPERTIES OF N-ALKYL DERIVATIZED THIOL-ENE NETWORKS: CHAIN LENGTH EFFECT

*Luke Kwisnek, Mukul Kaushik, Charles E. Hoyle, and Sergei Nazarenko**

Abstract

The free volume, transport, and physical properties of a series of n-alkyl derivatized thiol-ene networks are reported. Derivatized thiol monomers were prepared via a nucleophile-catalyzed thio-Michael addition reaction of multifunctional thiols to n-alkyl acrylates ranging from n = 1 to n = 16 in length. Using UV-initiated photopolymerization, crosslinked networks were fabricated from these systematically modified thiol monomers. Each network consisted of the same molar concentration of alkyl chains. Both the thio-Michael reactions and the network photopolymerizations reached high conversion regardless of n-alkyl length which is typical of the thiol-ene click reaction. The incorporation of alkyl chains led to the formation of new networks with markedly loose packing as probed by density measurements. The density decreased by 11% as n increased from 1 to 16. It is believed that the alkyl chains acted as spacers or pillars which expanded the crosslinked network scaffold increasing the free volume. The free volume behavior of these expanded networks was probed by positron annihilation lifetime spectroscopy (PALS). The hole volume size as measured by PALS doubled with an increase in alkyl chain length from 1 to 16. Oxygen transport measurements indicated an exponential increase in oxygen permeability across two orders of magnitude which was related to the increase in free volume. Glass transition

temperatures were interestingly comparable for all derivatized networks regardless of n-alkyl length. Water contact angle was additionally evaluated for these derivatized networks. As expected, contact angle increased with increasing n-alkyl length, demonstrating that the surfaces were altered (becoming more hydrophobic) due to an increased concentration of methylene groups in the bulk.

Introduction

The incorporation of n-alkyl side chains of various length (up to n = 18) has been a common approach to polymer modification for some time. Various applications for these modified systems have been explored, such as lubricant oil and fuel viscosity modifiers,[1] modifiers to improve processing characteristics,[2-4] and temperature responsive permeation valves or barriers.[5-6] The effect of alkyl side chains has been studied almost exclusively for linear polymers.[1-6] It is interesting to discuss herein some property changes relevant to this paper and associated with the incorporation of alkyl chains of different lengths (length effect) such as T_g, contact angle, gas transport, and free volume. In general, it was observed for nearly all modified polymers (both glassy and rubbery) that T_g decreased gradually with an increase in alkyl side chain length which was attributed to increased mobility and perhaps less favorable packing associated with the presence of alkyl side chains.[7-10] Less commonly, T_g exhibited a U-shaped behavior over a similar range of alkyl side chain lengths i.e. a decrease for shorter alkyl chains followed by an increase for longer alkyl chains.[11-12] It was generally shown that gas permeability gradually increased with increasing alkyl side chain length[5,8,10,13] as long as the side chains did not crystallize in which case the permeability decreased due to the presence of

impermeable crystallites.[5-6] Because permeability has been often related to free volume, the increase in permeability may be indicative of looser packing for alkyl side chain containing polymers although this effect has not been explored in great detail and free volume was not directly probed.[5,8,10,13] Finally, water contact angle was shown to increase with an increase in alkyl side chain length implying that hydrophobicity was increased as a result of a higher concentration of methylene groups to the system.[14]

In addition to linear polymer modification, attempts have been made to incorporate n-alkyl chains into crosslinked networks. However, only a small number of reports have been found to the best of our knowledge and they indeed caught our attention.[15-17] In two cases, n-alkenes up to n = 17 in length were incorporated (grafted) directly into flexible polymethylhydrosiloxane (PMHS) crosslinked networks.[15-16] Interestingly it was observed that the alkyl chain modified networks exhibited a noticeable increase in volume indicative of looser packing and higher free volume.[16] This effect was not explored in great detail.[16] Also crosslinked networks of chitosan were modified with n-alkyl chains from n = 4 to n = 10 in length.[17] An increase in protein transport was observed as alkyl chain length increased at high pH. This effect was attributed to a loose stacking of the network due to the bulky alkyl chains.[17] Lastly, we were not able to identify water contact angle measurements conducted on alkyl chain modified networks.

UV-photopolymerization is an efficient and eco-friendly method of generating crosslinked networks. UV-photopolymerized thiol-ene networks in particular are known for their narrow glass transitions, low shrinkage, and 90%+ functional group conversion.[18-19] The UV-photoinitiated thiol-ene reaction, recognized as a “click”

reaction,[20-22] proceeds via a step-growth free-radical process in which thiols add across double bonds (enes) in a 1:1 manner; this mechanism is reported in detail in Reference 11. The thiol-ene reaction is generally conducted in the bulk and is uninhibited by oxygen making it a practical method for material fabrication.[18] Multifunctional thiols are reacted with multifunctional enes to yield a crosslinked network; films are generally optically clear, flexible, and robust.[18] In addition to the photoinitiated free-radical addition of a thiol to any ene, thiols also add to electron deficient enes (acrylates) via a nucleophilic catalyst, again in a 1:1 manner. This thio-Michael addition reaction has been utilized to modify surfaces,[23-24] to synthesize dendimers, stars, and oligomeric macromolecules,[25-27] and also to modify thiol monomers with different functionalities[28] including short n-alkyl chains up to n = 6 in length.[29] This reaction platform, coupled with the photopolymerization of thiol-ene networks, enabled us to conduct the current study with a focus on free volume and oxygen transport in n-alkyl derivatized, highly crosslinked networks.

In previous work, we reported on a series of densely-crosslinked thiol-ene networks with oxygen transport properties that correlated well with T_g.[28] Oxygen permeability values spanning three orders of magnitude were governed by a free volume effect based on the difference between T_{test} (23 °C) and network T_g. A high barrier network was further modified with strongly interacting functional groups to demonstrate barrier improvement.[28] In this report, the same network is modified with n-alkyl chains from n = 1 to n = 16 in length, at constant molar concentration, with the expectation that this modification will result in a free volume increase and a decrease in barrier properties. Therefore, our intent in this work was to expand the upper range of permeabilities in

basic UV-curable thiol-ene networks which can be controlled through simple chemical derivatization of a thiol monomer.

Experimental

Materials

Tetrafunctional thiol monomer pentaerythritol tetrakis(3-mercaptopropionate) (4T) was supplied by Bruno Bock Thiol-Chemical-S. Trifunctional ene monomer triallyl-1,3,5-triazine-2,4,6(1*H*,3*H*,5*H*)-trione (TTT) was supplied by Sartomer. Photoinitiator alpha,alpha-dimethoxy-alpha-phenylacetophenone (Irgacure 651) was supplied by Ciba Specialty Chemicals. Nucleophilic catalysts diethylamine and dipropylamine were obtained from Aldrich. N-alkyl acrylates, from n = 1 to n = 16, were obtained as follows: methyl acrylate, ethyl acrylate, butyl acrylate, hexyl acrylate, and lauryl acrylate (n = 1, 2, 4, 6, 12) were obtained from Aldrich. Octyl acrylate and decyl acrylate (n = 8, 10) were obtained from Monomer-Polymer and Dajac Labs. Tetradecyl acrylate and hexadecyl acrylate (n = 14, 16) were obtained from TCI America. All materials, shown in Chart IV-1, were used as received.

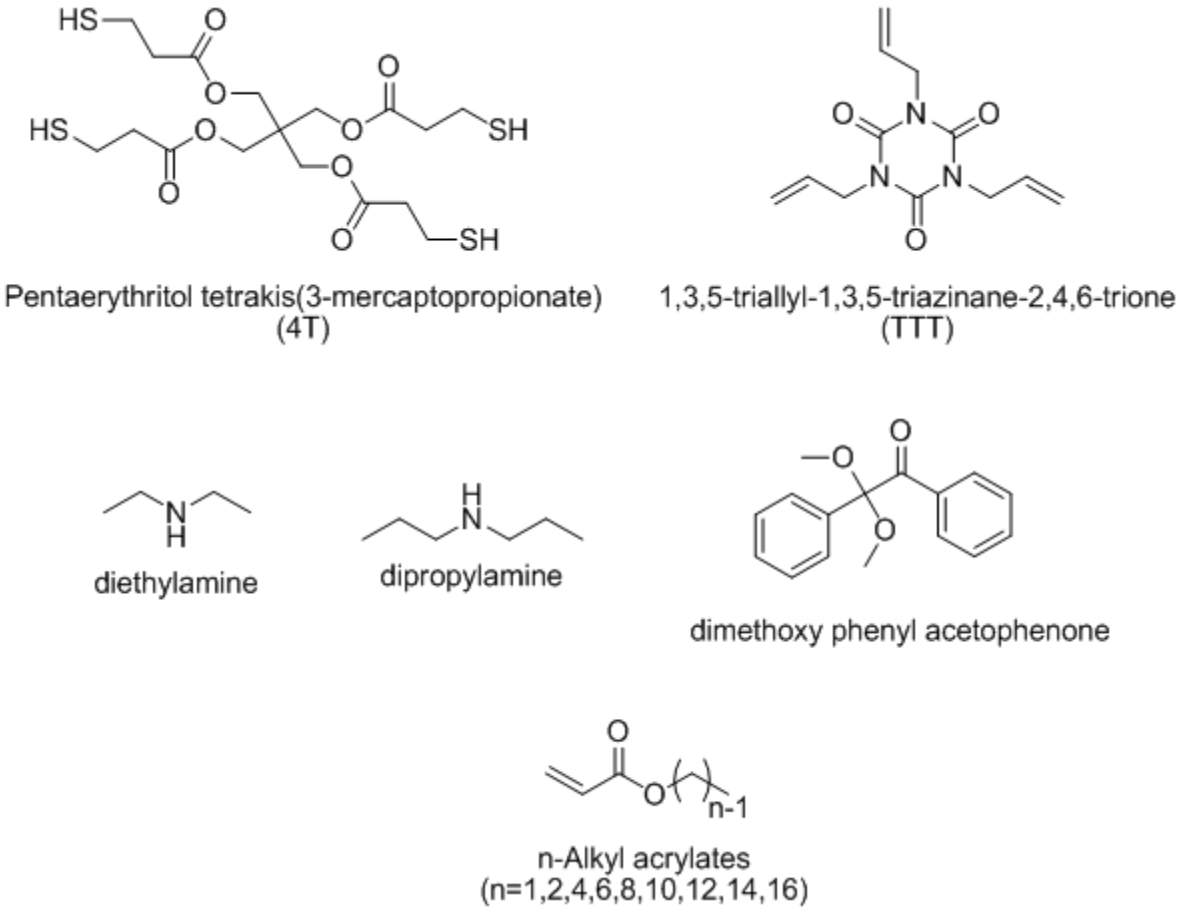

Chart IV-1. Chemical structures of thiol and ene monomers, amine catalysts, photoinitiator, and n-alkyl acrylate monomers used for derivatization. n = 1 indicates methyl acrylate, n = 2 indicates ethyl acrylate, and so on.

Synthesis of n-Alkyl Derivatized Thiol Monomers

N-alkyl derivatized trifunctional thiol monomers were synthesized using a nucleophile-catalyzed thio-Michael reaction represented in Scheme IV-1. An example synthesis procedure for 4T derivatized with ethyl acrylate (n = 2) is given as follows. An amount of 4T was introduced to a round bottom flask along with 2 mol% diethylamine. In a separate vial, an equal molar quantity of ethyl acrylate was weighed out and then added dropwise to the 4T/catalyst mixture at approximately 1 mL/min under mild

stirring. The flask was then sealed and allowed to stir overnight. The resulting product, a distribution of structures which is on average a trifunctional thiol with an attached ethyl acrylate group, was not purified and used as-synthesized. This same procedure was used to synthesize modified thiol monomers with alkyl groups from n = 1 through n = 14. Hexadecyl acrylate, n = 16, is solid at room temperature and was melted prior to dropwise addition. Furthermore the vessel containing the 4T/catalyst mixture was heated to 40 °C during the addition of acrylate to prevent vitrification of the 4T-16 product. Dipropylamine, at 2 mol%, was used as the nucleophilic catalyst since it is a higher-boiling amine. As in the previous procedure, the flask was sealed and allowed to stir overnight with no further purification steps.

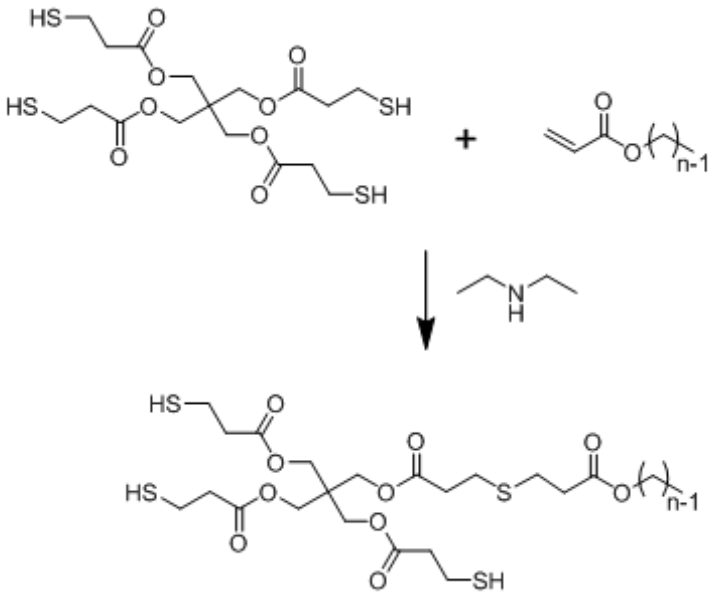

Scheme IV-1. Nucleophile-catalyzed thio-Michael derivatization reaction of multifunctional thiol with n-alkyl acrylates. Product shown is ideal trifunctional thiol with one attached alkyl chain which represents the average product. Actual product is a distribution of structures.

Characterization of Products and Network Conversion

Derivatized thiol monomers were characterized by ^{1}H NMR using a Varian Mercury 200 MHz NMR spectrometer in acetone-D6. Network conversions were characterized for samples sandwiched between two salt plates before and after UV-photopolymerization using 10 passes under a Fusion UV curing line system with a D bulb (400 W/cm^2 with belt speed of 3 m/min and 3.1 W/cm^2 irradiance). Sample thickness for IR measurements was approximately 20 microns. Change in peak area of thiol –SH groups at 2570 cm^{-1} (S-H stretch) and ene C=C groups at 3080 cm^{-1} (vinyl C-H stretch) were measured using a Bruker Tensor 37 FT-IR.

Film Formation

All of the n-alkyl derivatized thiol monomers were readily miscible in TTT ene monomer (1:1 molar ratio) at room temperature with only mild sonication, resulting in optically clear, homogeneous liquid mixtures. Free-standing thin films of all thiol-ene formulations were made by dissolving 1 wt% 1,1-dimethoxy-1-phenylacetophenone (Irgacure 651) photoinitiator into the thiol-ene mixture by sonication for approximately 10 minutes. These mixtures were then drawn down onto glass substrates using drawdown bars. The networks formed by copolymerization of the derivatized thiols with TTT are subsequently referred to by the number, n, of the carbons attached to the acrylate group: for example n = 1 describes a network of 4T derivatized with methyl acrylate and copolymerized with TTT, n = 2 describes a network of 4T derivatized with ethyl acrylate and copolymerized with TTT, and so on. In this recipe, stoichiometry of thiol, ene, and n-alkyl acrylate are equivalent (0.33 M each) in the final films. The basic unmodified

thiol-ene network, 4T-TTT (4:3 functional group ratio meaning dangling thiol functional arms in the network), was drawn down to a thickness of approximately 0.080 mm. Remaining films were drawn-down at thicknesses ranging from 0.2 mm to 1.3 mm. This was done to ensure an adequate amount of experimental data points in the non-steady state region of each oxygen flux curve for proper fitting. Films were cured using 10 passes under a Fusion UV curing line system with a D bulb (400 W/cm^2 with belt speed of 3 m/min and 3.1 W/cm^2 irradiance). All films were normalized in air for 3-5 days prior to testing.

Oxygen Permeation Testing

Oxygen permeation tests were conducted on Mocon OX-TRAN® 2/21 instruments using a continuous-flow testing cell method approved by the ASTM (D3985). All measurements were conducted at 23 °C and 0% RH. Further details on this method were reported elsewhere.[28]

Permeability P and diffusivity D were obtained by performing a two-parameter least-square fit of the experimental oxygen flux $J(t)$ data to Fick's second law solution (Equation 1):[30]

$$J(t) = \frac{Pp}{l}\left[-\sum_{n=1}^{\infty}(-1)^n \exp(-D\pi^2 n^2 t / l^2)\right] \quad (1)$$

where p is the applied pressure and l is the film thickness. Using the solution-diffusion equation (Equation 2), the solubility S was then calculated.

$$P = D \cdot S \tag{2}$$

Instrumentation error using this method in the range of oxygen fluxes studied is +/- 5% for permeability values and +/- 10% for diffusivity and solubility values. The remaining experimental error in obtaining *P*, *D*, and *S* values is largely derived from film thickness variations. For this reason, special care was taken to evaluate films of approximately uniform thickness; thickness averages were obtained by measuring at multiple locations.

Free Volume Analysis

Positron annihilation lifetime spectroscopy (PALS) is widely used in the characterization of free volume of polymers.[31-32] PALS involves measurements of the lifetime of positrons injected into a polymer sample from a positron-emitting nucleus, generally Na^{22}. The lifetime (τ_3) and decay intensity (I_3) in % of the long-lived orthopositronium (positron/electron pair) o-Ps species were used to extract information about the average size of holes and general amount of free volume. The o-Ps lifetime can be related to the radius of a spherical cavity according to Equation 3:[33]

$$\tau_3 = \frac{1}{2}\left[1 - \frac{R}{R+d} + \frac{1}{2\pi}\sin\left(\frac{2\pi R}{R+d}\right)\right]^{-1} (ns). \tag{3}$$

Where R is the average hole radius, and d = 0.1656 nm is the empirically determined electron layer thickness.[33] The average free volume of a hole (V_h) can then be calculated as $V_h = 4/3\pi R^3$.

Positron annihilation lifetime spectroscopy (PALS) experiments were conducted with a fast−fast coincidence system which is described elsewhere.[34-36] The spectrometer

held two samples of approximately 1 mm thickness and 1 cm diameter with the Na^{22} positron source sandwiched between. All measurements were taken over an hour, for a total of 1×10^6 counts in each PALS spectrum. The PALS spectra were processed using PATFIT-88 software.[37] Error associated with determining τ_3 values using this software was approximately +/- 2%.

Miscellaneous Physical Properties

A TA Instruments Q1000 DSC with heating rate of 10 ^oC/min was used to investigate the glass transition temperature of film samples between 8 and 12 mg. Dynamic mechanical properties were evaluated using a Rheometric Scientific DMTA V with a frequency of 1 Hz, strain rate of 0.05%, and heating rate of 5 °C/min. T_g values were taken as the mid-point of the inflection from DSC scans and as the peak maximum in tan delta plots from DMTA. Density measurements were conducted at room temperature via the Archimedes method with a modified analytical balance and water as the buoyant fluid. Samples were film squares of approximately 1 g and masses were recorded to the third decimal place. Ambient atmosphere water contact angle measurements were conducted using a Ramé-Hart model 200-00 standard goniometer. Deionized water droplets of approximately 5 mm in diameter were applied to thin films via a 0.6 mm diameter syringe; three droplets for each film, with 5 measurements per drop, were recorded.

Results and Discussion

Derivatization and Network Conversion

Derivatization of thiol monomers was verified via ^{1}H NMR after reaction completion. Figure IV-1 shows ^{1}H NMR spectra for each modified monomer mixture. Success of the thio-Michael reaction was verified by the disappearance of the acrylate double bond proton shifts at ~6 ppm. For comparison, the ^{1}H NMR spectrum of an unreacted mixture of 4T and ethyl acrylate sans amine catalyst is shown (labeled as "Unreacted"). Following NMR verification, the monomer mixtures were not purified and used as-synthesized as mentioned in the Experimental section.

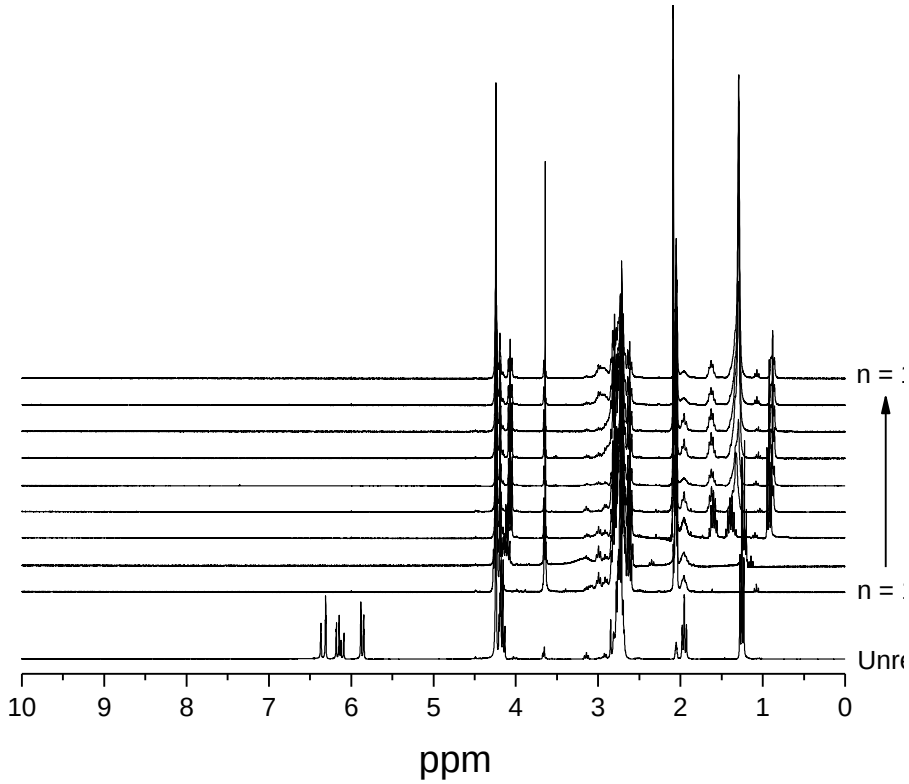

Figure IV-1. ^{1}H NMR spectra for n-alkyl derivatized thiol monomers synthesized via Scheme 1; monomers denoted by length of alkyl chain, n, where n = 1 is 4T + methyl acrylate, n = 16 is 4T + hexadecyl acrylate, etc. Disappearance of acrylate double bond proton shifts at ~6ppm indicated successful thio-Michael derivatization. Unreacted spectrum is a mixture of 4T and ethyl acrylate without amine catalyst for comparison.

The issue of the n-alkyl chains interfering with functional group conversion during polymerization is a valid one, especially given that increasing n-alkene lengths led to decreased conversions for n-alkene grafting-to reactions in siloxane networks.[15-16] To address this concern, IR measurements were conducted on liquid monomer mixtures (before curing) and cured networks (after curing) as detailed in the Experimental section. Figure IV-2 shows the peak areas for thiol (~2570 cm^{-1}) and ene (~3080 cm^{-1}) functional groups before and after UV curing for three networks. These three spectra are

representative of the entire series of n-alkyl derivatized thiol-ene networks. It is evident that high conversions are reached for each network; n-alkyl chain length has no measurable effect on the ultimate conversion of thiol and ene groups during photoinitiated polymerization. Note that the pre-polymerization monomer derivatization technique used in this work is advantageous especially in the case of forming a crosslinked network – the network conversions are near or above 90% and the n-alkyl derivatization reaction is quantitative.

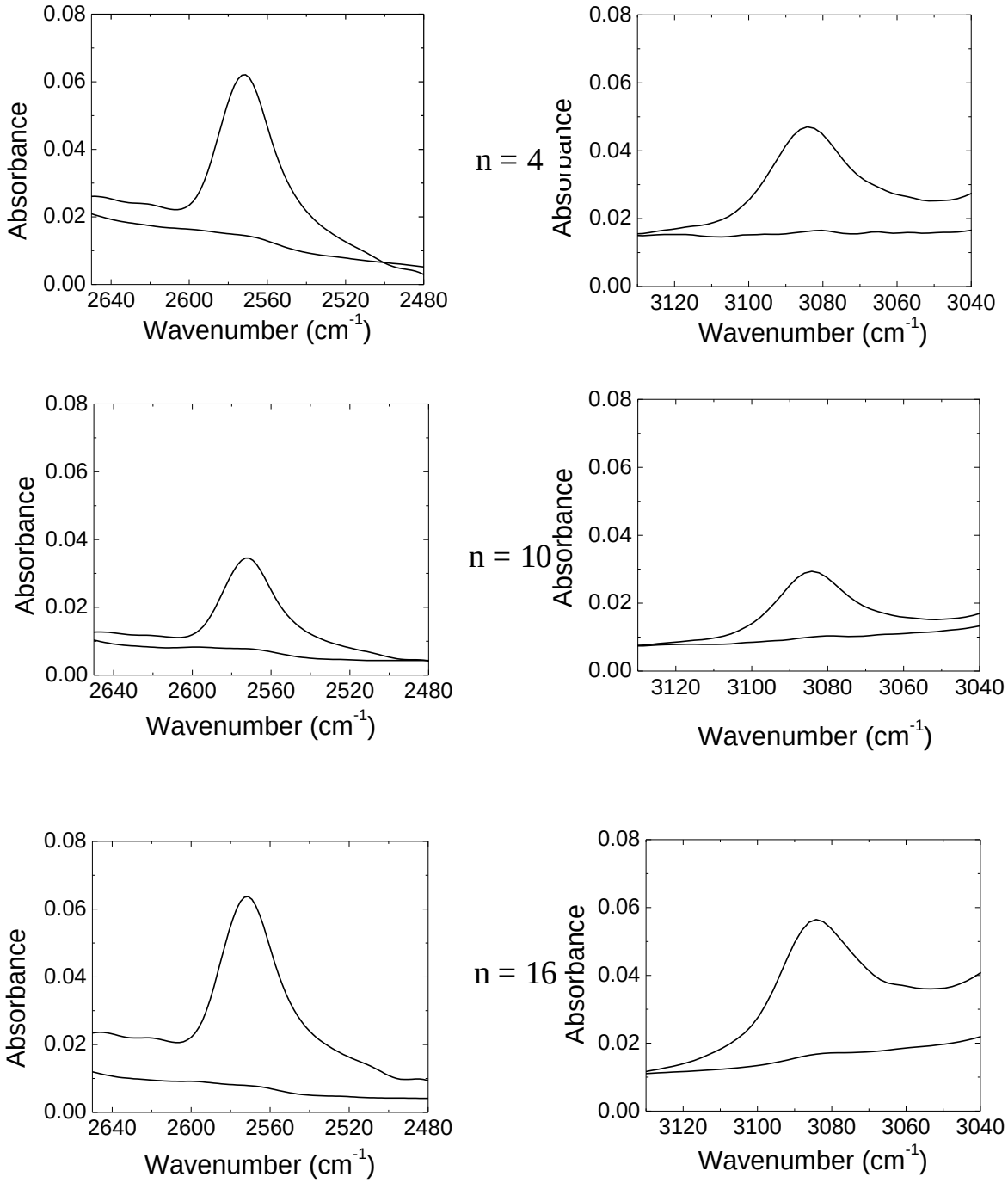

Figure IV-2. FTIR spectra of the thiol (2570 cm^{-1}) peaks and ene (3080 cm^{-1}) peaks before and after UV-initiated polymerization for three representative n-alkyl derivatized thiol-ene networks. Labels indicate length of alkyl chain in the network. High conversions are obtained for each network including those not shown.

Transport, Free Volume, and Density

Figure IV-3 shows experimental oxygen flux data (open circles) versus time for three representative n-alkyl derivatized networks – with lengths n = 1, 4, and 16. All dependencies exhibited non-steady state and steady-state portions of permeation, suggestive of complete sample degassing prior to testing as mentioned in the Experimental section. Solid lines are the fits to Equation 1. The fit was excellent in each case, indicative of Fickian behavior. The sample with n = 1 showed the smallest steady-state flux while the sample with n = 16 the largest steady-state flux, despite that it had a much greater thickness. The excellent fits allowed the accurate decoupling of the diffusivity *D*, and solubility, *S*, terms of the permeability, *P*, for all networks. Individual P, D, and S values for all modified networks are shown in Table 1. In addition, we report data for the unmodified thiol-ene network which was prepared using unmodified 4T and TTT monomers as described in the Experimental section. The basic, unmodified thiol-ene network exhibited the smallest average hole free volume size, lowest oxygen permeability, and lowest oxygen diffusivity as reported in Table 1 as well as the highest T_g as seen in Figures IV-11 through IV-13. From this point onward, we will analyze and compare materials within the n-alkyl derivatized family of networks. However, the values for unmodified network are included on each corresponding figure.

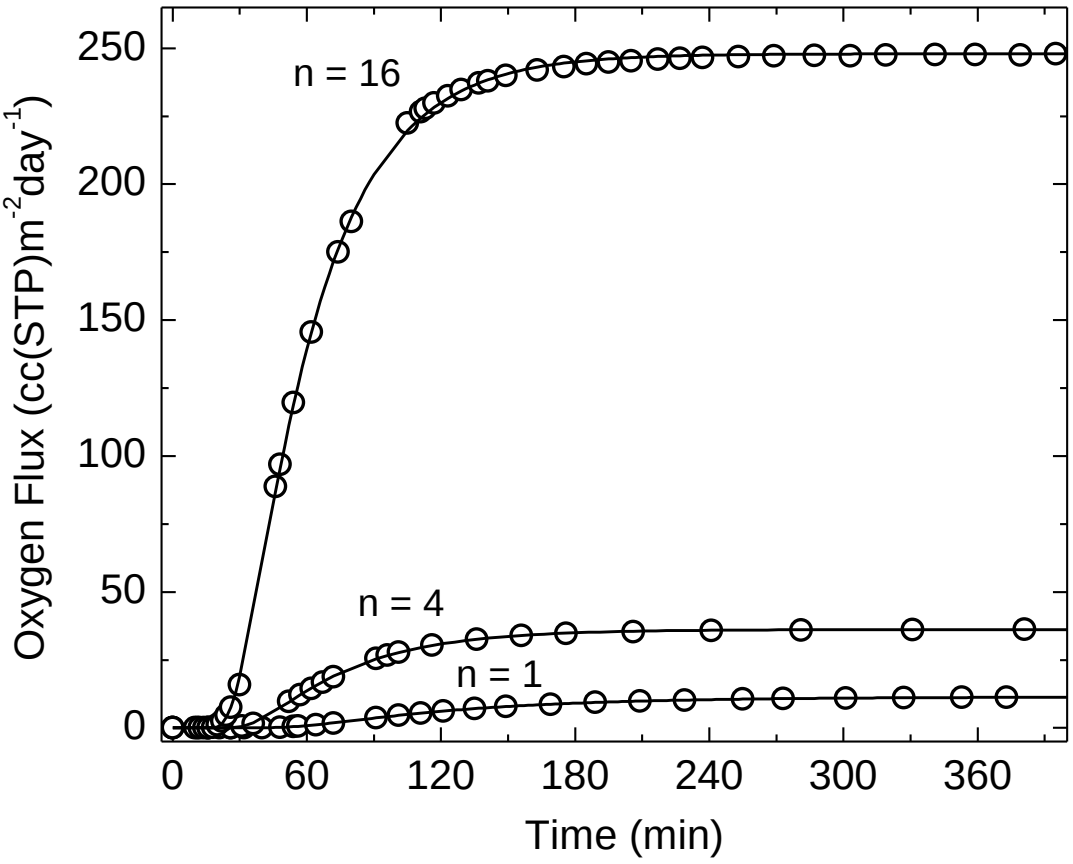

Figure IV-3. Representative experimental oxygen flux data (circles) and fit to Equation 1 (lines) for n-alkyl derivatized thiol-ene networks where n = 1 (thickness = 0.22 mm), n = 4 (thickness = 0.30 mm), and n = 16 (thickness = 0.80 mm).

Table IV-1. Oxygen Transport Data, Recorded at 23 °C, and Free Volume Data, Recorded at Ambient Room Temperature. First column, n, denotes length of alkyl chain in network; 0 represents unmodified thiol-ene network. Units for permeability: (cc(STP) cm $m^{-2}day^{-1}atm^{-1}$)

n	Oxygen Permeability	Oxygen Diffusivity (cm^2s^{-1})	Oxygen Solubility (cc(STP) $cm^{-3}atm^{-1}$)	V_h ($Å^3$)	I_3 (%)
0	0.041	1.70E-09	0.026	63	14.7
1	0.25	1.20E-08	0.025	83	15.1
2	0.39	1.80E-08	0.024	84	15.8
4	1.1	3.80E-08	0.033	101	15.3
6	2.1	6.30E-08	0.038	113	16.1
8	2.9	7.10E-08	0.047	125	16.5
10	4.7	9.50E-08	0.057	139	15.1
12	7.3	1.40E-07	0.06	154	16.2
14	14.3	2.90E-07	0.057	161	15.7
16	19.7	3.30E-07	0.07	164	15.5

For convenience, oxygen permeability and diffusivity for the n-alkyl derivatized networks are plotted logarithmically as a function of n, the alkyl chain length, in Figure IV-4. From n = 1 to n = 16, there is a gradual increase in both *P* and *D*. Particularly, permeability increases by two orders of magnitude while diffusivity increases by approximately one order of magnitude. However there appears to be a tendency for both *P* and *D* to level off across the series approaching a plateau at n = 16.

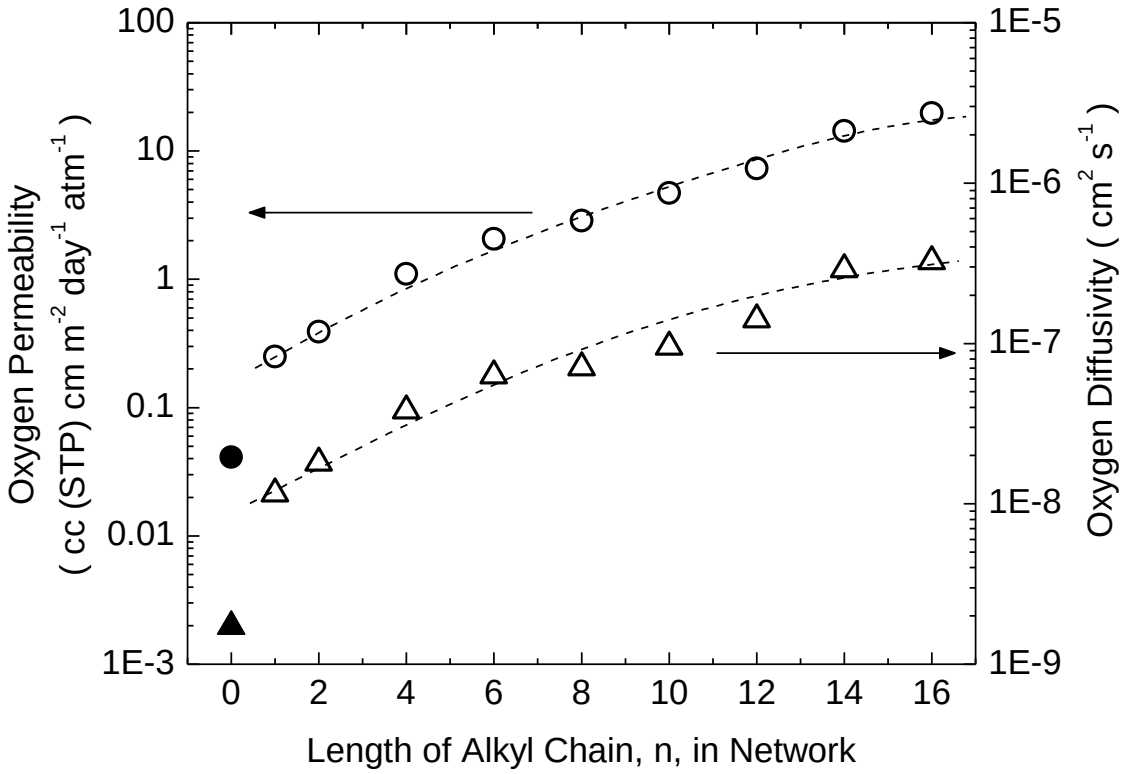

Figure IV-4. Oxygen permeability (circles) and diffusivity (triangles) as a function of n, the length of alkyl chain in the thiol-ene network. Filled symbols are data for unmodified thiol-ene network.

Oxygen solubility values also show a strong increase with increasing length of the alkyl chain as plotted linearly in Figure IV-5. Solubility values nearly quadrupled across the series of n-alkyl derivatized networks and also appear to level off in a fashion similar to P and D. Therefore both D and S make a comparable contribution to the increases in permeability, P. To further substantiate these transport results and because both D and S are often related to free volume, hole free volume was investigated via PALS.

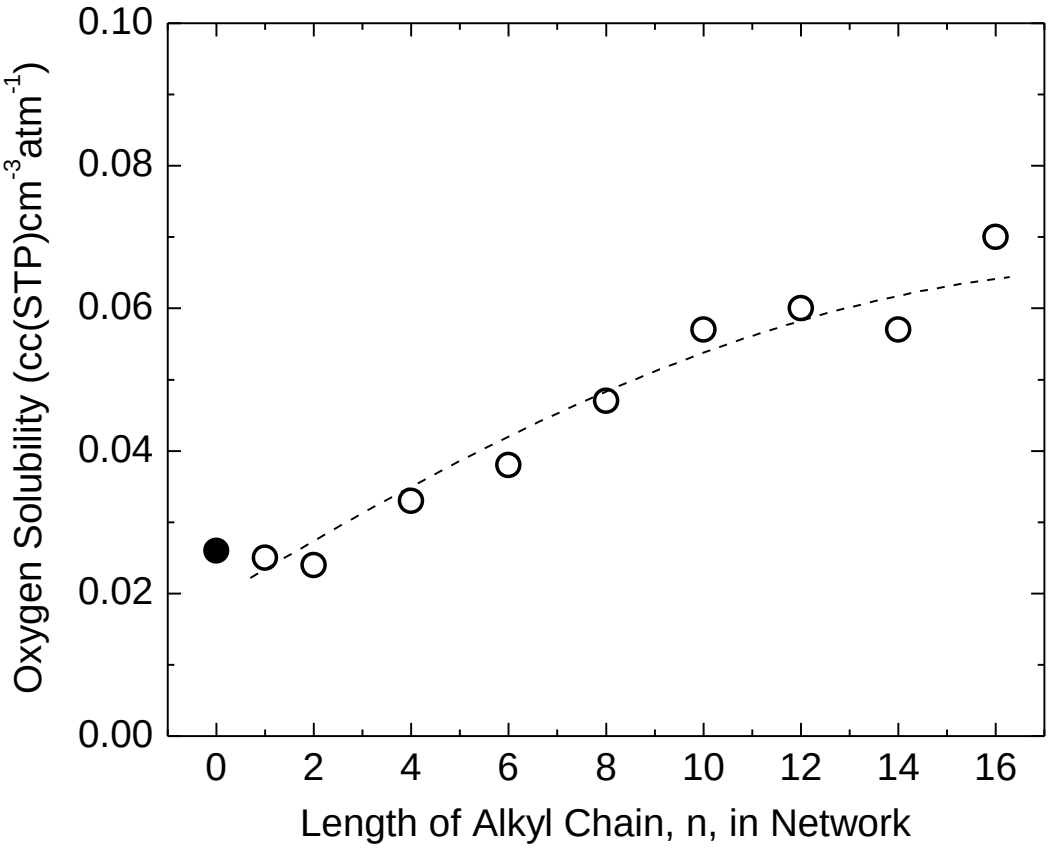

Figure IV-5. Oxygen solubility as a function of alkyl chain length. Unmodified thiol-ene network shown as filled symbol.

Free volume models are broadly used to interpret gas transport data especially in the rubbery state. Mean hole free volume, $<V_h>$, is shown as a function of the alkyl chain length in Figure IV-6 with actual values listed in Table 1. An increase in hole free volume size across the series was apparent. From n = 1 to n = 16, the extremes, V_h doubled. This increase in free volume also manifests as sizable bulk dedensification shown as a separate plot in Figure IV-6 (right axis). Over the range of alkyl chain lengths

studied, the density of the networks decreased by about 11%. This decrease in density is particularly interesting since the increased bulkiness overcomes the increase in mass associated with alkyl chains of increasing length (longer chain has more methylene groups, i.e. more mass). A small unit of network is thus increased in volume more than is indicated by the density measurements alone.

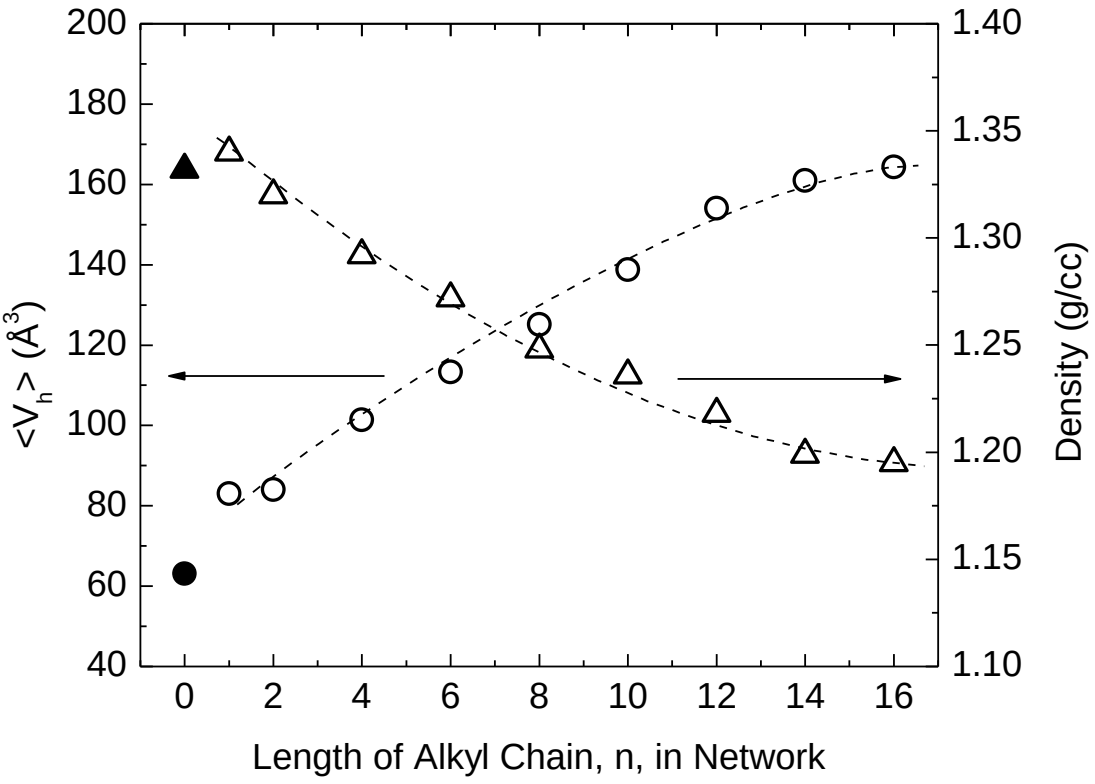

Figure IV-6. Mean hole free volume, $<V_h>$ (circles), and film density (triangles) as a function of alkyl chain length. Unmodified thiol-ene network shown as filled symbols.

Often an increase in free volume especially in the rubbery state is attributed to a chain end effect. Considering the same unit as defined in the previous paragraph, the

number of chain ends would be the same per unit however the volume concentration naturally would be reduced implying that a chain end effect cannot be responsible for this free volume behavior.

Instead it is believed that the alkyl chains act as spacers or pillars which expand the crosslinked network scaffold increasing free volume. This possibility has been considered elsewhere for linear polymers.[2-4] The rigidity or bulkiness of fairly short alkyl chains can be somewhat understood from the fact that short chains may not follow Gaussian chain statistics and this may lead to an overall chain configuration enriched with trans conformations. It is anticipated that this effect will be less dramatic as n increases further beyond a certain limit leading to a leveling off of this expansion effect. Figure IV-7 represents graphically the explanation related to our system where free volume increase is associated with the separation of the network scaffold by alkyl chains. Thus the expansion of the network scaffold due to the bulkiness of alkyl chains is a plausible explanation for the free volume increase and concomitant dedensification in the derivatized thiol-ene networks reported here.

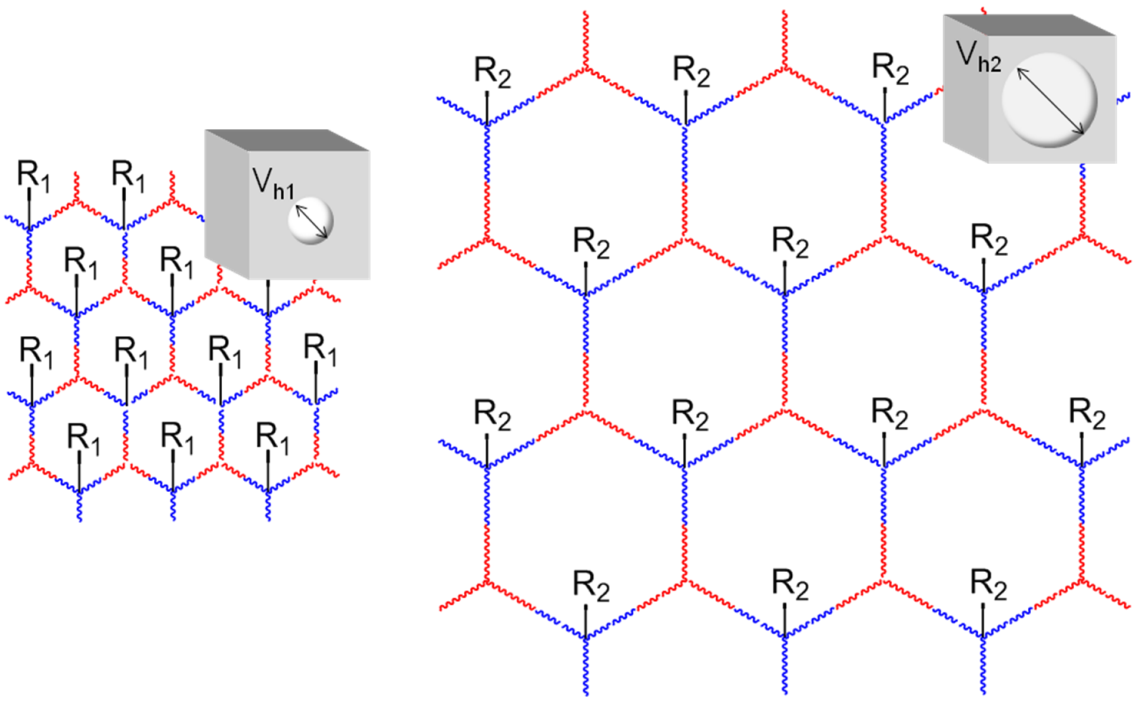

Figure IV-7. Idealized, two-dimensional lattice-like schematic illustrating expansion of network scaffold with increasing alkyl chain length ($R_2 > R_1$). Also shown are representative three-dimensional network sections demonstrating increased free volume hole size ($V_{h2} > V_{h1}$) corresponding to this network expansion.

A question can be raised regarding nanophase separation (aggregation) of hydrophobic alkyl chains. This effect was previously identified for linear polymers with flexible backbones,[7] however we believe that this scenario is unlikely due to topological restrictions imposed by the crosslinked network assuming that alkyl chains are incorporated randomly. Nanophase separation may occur prior to network formation and this possibility cannot be completely ruled out although it is not exactly clear to what extent this behavior could be related to dedensification.

It is worthwhile to discuss a more quantitative correlation between free volume and transport. The general relationship between hole free volume and gas diffusivity can be explicitly expressed using the generalized Equation 4 as follows:

$$D = Ae^{\left(\frac{-B}{V_h}\right)} \quad (4)$$

where D is the diffusion coefficient, A and B are constants, and V_h is the hole free volume.[38] This relationship was shown to be valid when the free volume term is either hole free volume[39-43] or fractional free volume.[44-47] The intensity, I_3, has been related to the concentration of holes[39] however this intensity is constant for all derivatized networks as shown in Figure IV-8. This result shows that the number of holes is equivalent for each network.[39] Thus mean hole free volume, $<V_h>$, corresponds to fractional free volume, V_f,[39] and so a plot of log(D) vs. $1/<V_h>$ should elucidate the general free volume dependency of gas diffusivity for the n-alkyl derivatized thiol-ene networks as shown in Figure IV-9. There appears to be a satisfactory correlation between log(D) and $1/<V_h>$ in this case. This correlation, likely due to the homologous nature of this series of materials and in agreement with the oxygen transport results, is indicated by the dashed line. It is evident that hole free volume is one of the governing factors for oxygen transport in this series of networks.

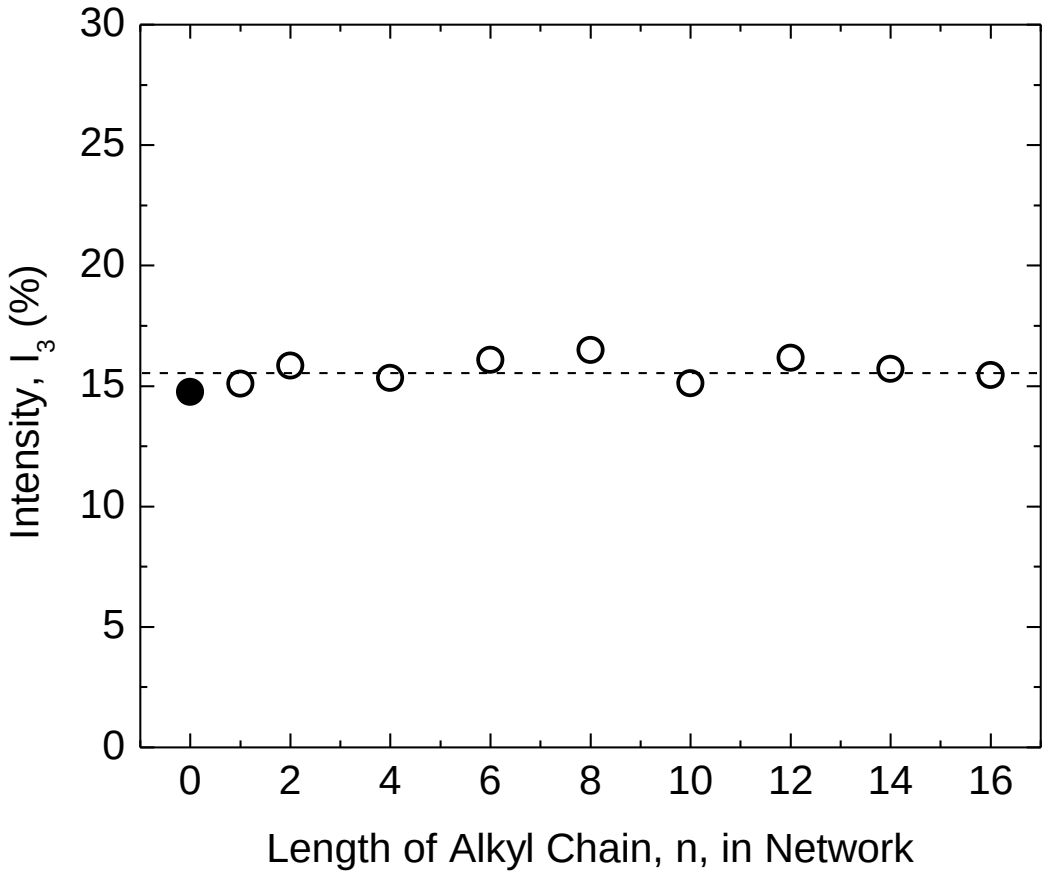

Figure IV-8. Intensity, I_3, of o-Positronium as a function of alkyl chain length demonstrating constant nature of I_3 values. Unmodified thiol-ene network is shown as filled symbol.

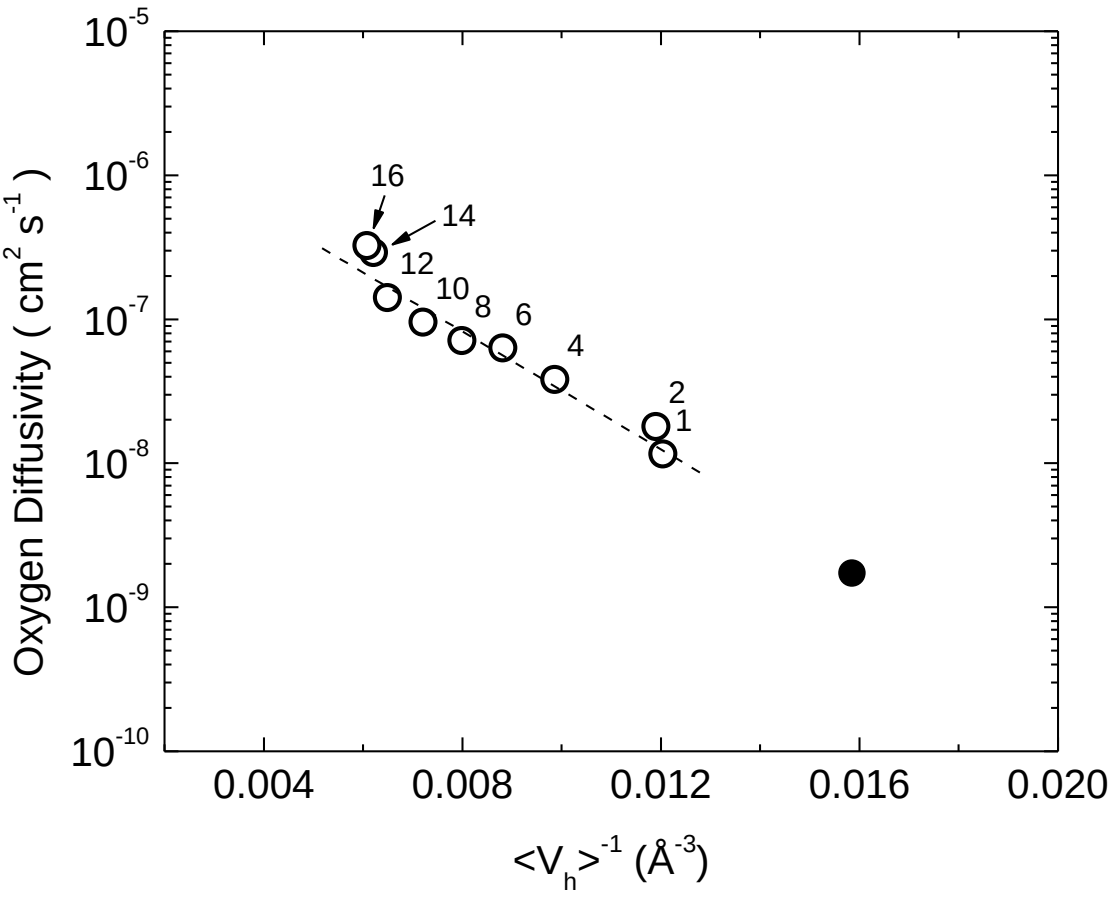

Figure IV-9. Relationship between oxygen diffusivity and the inverse of mean hole free volume via PALS for all networks. n-Alkyl derivatized networks denoted by the length of alkyl chain, n. Unmodified network shown as filled symbol.

Hole free volume can also be related to specific volume (V_{sp}) via Equation 5:[48]

$$V_{Sp} = V_{occ} + N_h \cdot V_h \tag{5}$$

where V_{occ} is the specific occupied volume, which includes van der Waals and interstitial free volumes, and N_h is the number of holes per gram of polymer. Traditionally, specific volume data derived from pressure-volume-temperature (PVT) measurements have been

combined with hole free volume from PALS temperature scan measurements to calculate N_h and V_{occ}.[48-49] In this work, a similar correlation can be made however using density and PALS measurements at room temperature from the systematic variation in the alkyl chain length within the network instead of temperature data. This correlation is shown in Figure IV-10 for the alkyl chain derivatized thiol-ene networks. An excellent linear fit of the experimental data was achieved. This excellent fit of the experimental data at room temperature for the thiol-ene networks indicates that N_h is relatively constant for each network regardless of the alkyl chain length. This result is in agreement with the fact that I_3, which has been related to the concentration of holes, is also constant.[39] Using Equation 5, $V_{occ} = 0.668 \pm 0.005$ cm^3/g and $N_h = 10.21 \pm 0.46 \times 10^{20}$ holes/g. The range of N_h previously reported for different polymeric systems varied from about 2×10^{20} to 9×10^{20} holes/g.[50-51] Therefore N_h found for the alkyl chain modified thiol-ene networks is reasonable though somewhat on the high end. We also speculate that N_h values from PVT and PALS temperature measurements would be in agreement with N_h calculated via the method reported here although this is currently being investigated.

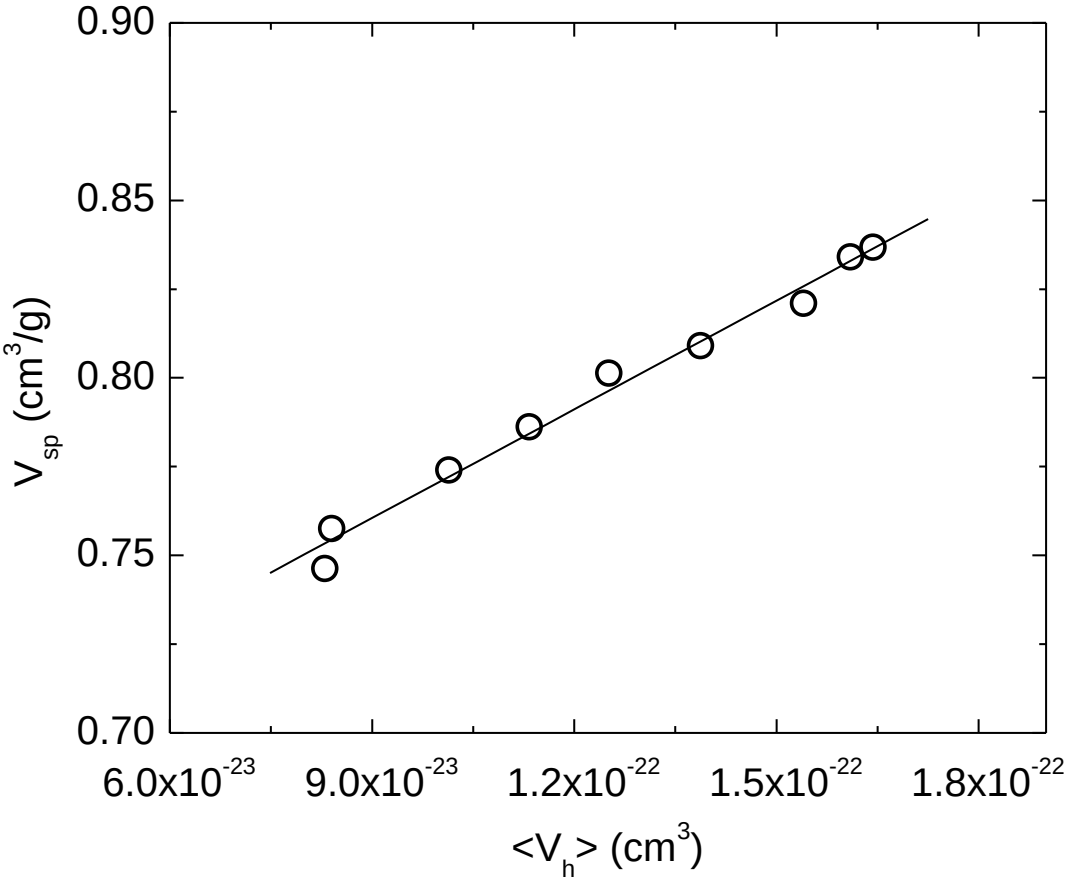

Figure IV-10. Correlation between specific volume (V_{sp}) and average hole free volume (V_h) for measurements conducted at room temperature while varying the length of the alkyl chain, n, in the thiol-ene network.

Glass Transition and Surface Tension

The length of alkyl side chains can have a profound effect on T_g in linear and lightly crosslinked polymers as mentioned in the Introduction. It was beneficial to explore this effect for the family of n-alkyl derivatized thiol-ene networks. Experimental DSC scans are provided in Figure IV-11 and experimental DMTA tan delta and storage

modulus (E') plots are provided in Figure IV-12 for the n-alkyl derivatized thiol-ene networks. T_g values as a function of alkyl chain length are shown in Figure IV-13. The n-alkyl derivatized thiol-ene networks show a slight decrease followed by a slight increase in T_g via DMTA as n increases; this behavior is consistent with certain reports on linear polymers.[11-12] Glass transitions by DSC, which are only available for n = 1 to 12 due to crystalline melting peaks that appear in the transition region at higher n, are in agreement with DMTA results albeit they are all lower than the DMTA values which is expected. However the change in T_g for the n-alkyl derivatized thiol-ene networks is within a 10 °C window for both DSC and DMTA methods, indicating that the alkyl chains in the crosslinked network do not strongly affect the glass transition. Since these are crosslinked networks, mobility and relaxation modes are restricted as compared to linear polymers. The glass transition appears to be controlled mainly by the rigidity of the thiol and ene monomers that make up the network scaffold and is not so much influenced by the increasing n-alkyl length. Although free volume can be related to T_g as we have done in the past for basic thiol-ene networks of varying structure and rigidity,[28] this is not the case for the n-alkyl derivatized networks which consist of an identical network scaffold. Perhaps this methodology may be applied to other networks to maintain a similar T_g but vastly increase the free volume. Shown also in Figure IV-12b are E' plots for the n-alkyl derivatized network. Rubbery modulus values at T_g + 40 °C as a function of alkyl chain length are shown as an inset on this figure. These moduli were within a window of about a factor of 2 and no readily apparent trend was observed. This result suggests that the crosslink density, upon which the rubbery modulus is dependent, is not measurably influenced by the presence or the length of the alkyl chains

for this series of thiol-ene networks. Furthermore note that there is no crystallinity at the testing temperature (23 °C) in any of the networks.

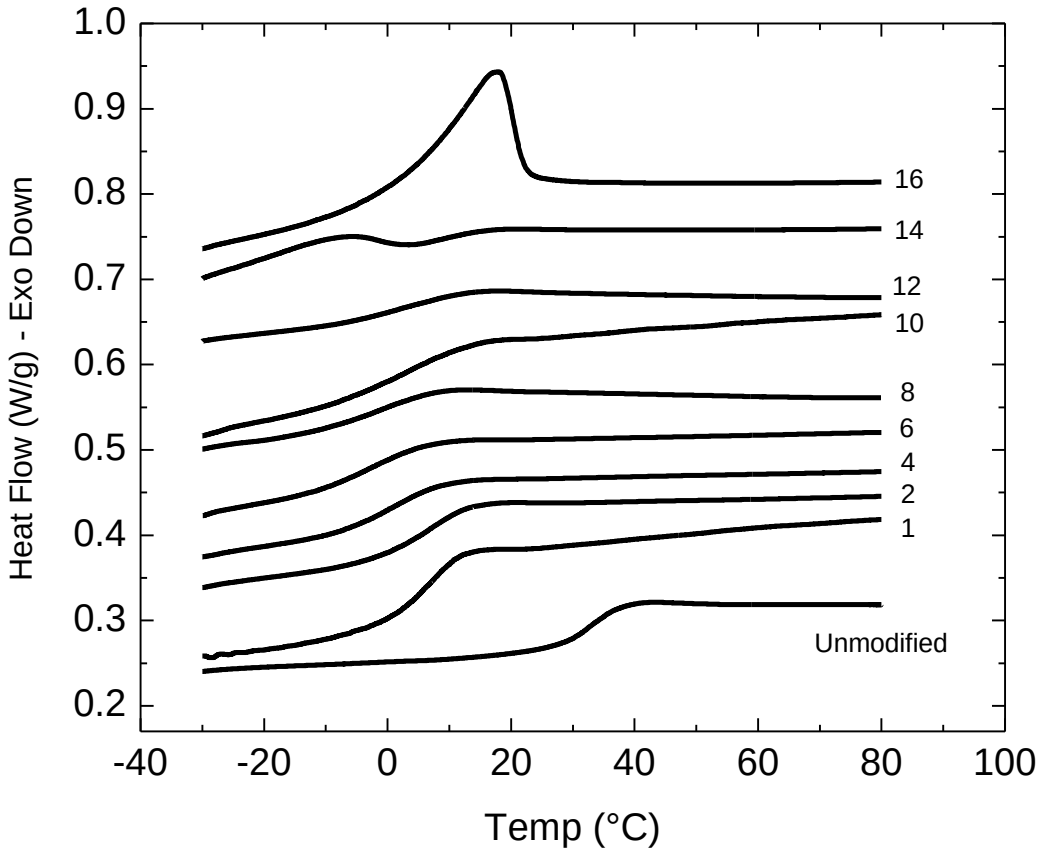

Figure IV-11. DSC 2nd heating scans for n-alkyl derivatized thiol-ene networks. Labels denote length of alkyl chain in network.

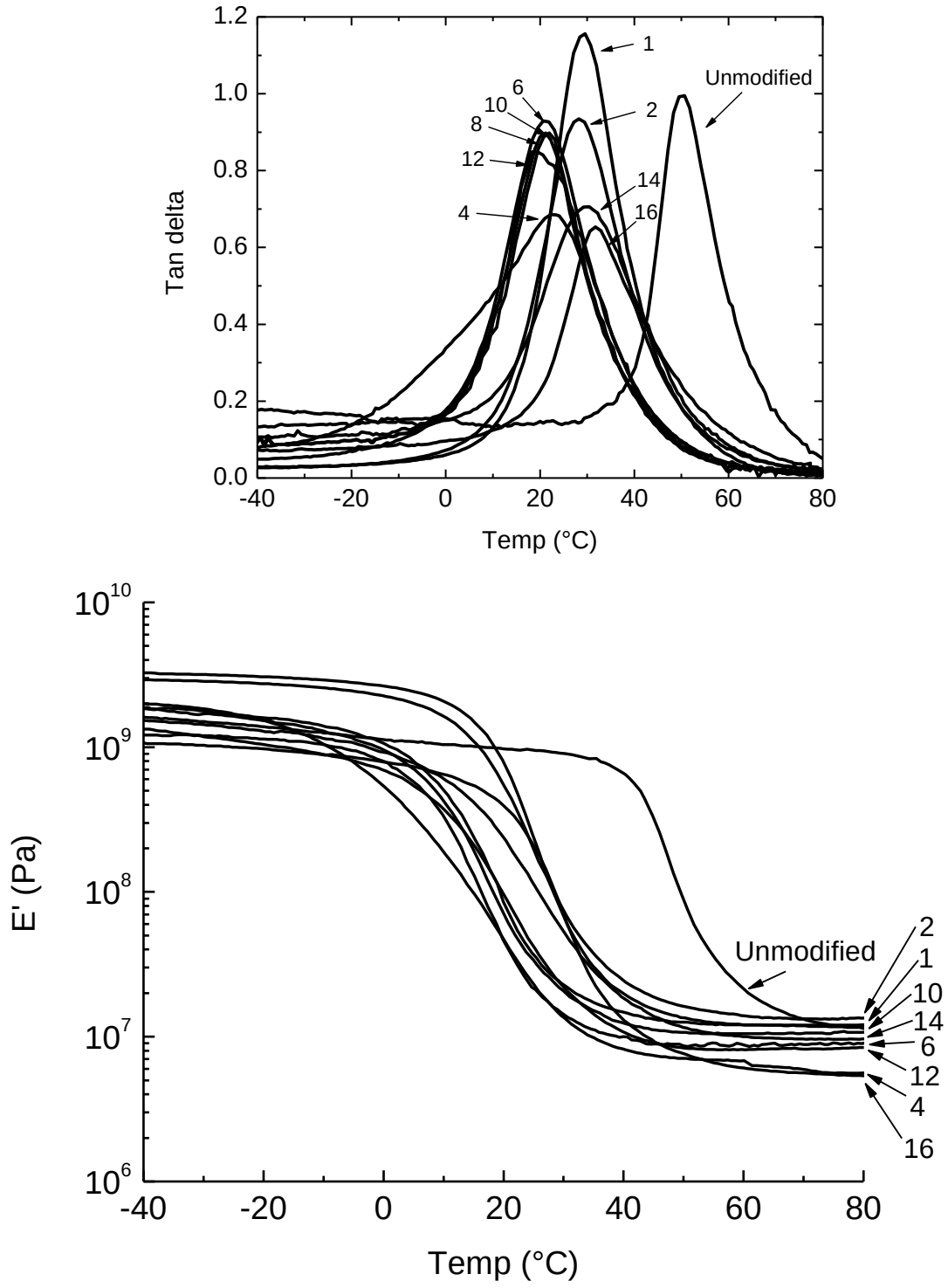

Figure IV-12. (a) DMTA tan delta plots and (b) DMTA E' plots for n-alkyl derivatized thiol-ene networks. Labels denote length of alkyl chain in network.

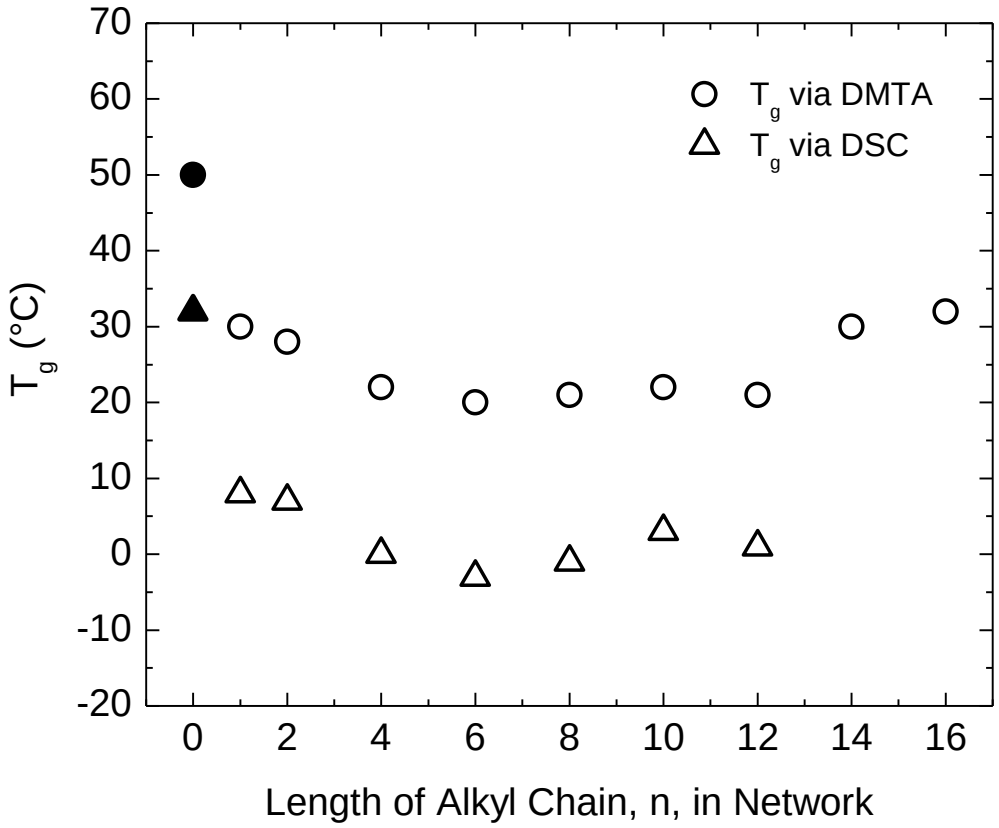

Figure IV-13. Glass transition temperatures via DSC and DMTA. Unmodified thiol-ene network indicated as filled symbols.

Since increasing alkyl chain length brings about compositional changes in the thiol-ene networks, i.e., an increasing concentration of hydrocarbon moities, it is worthwhile to discuss surface tension as a function of increasing alkyl chain length. Water contact angle measurements on the n-alkyl derivatized thiol-ene networks showed increasing contact angle as n increases according to Figure IV-14. As expected, the most

hydrophobic behavior was observed for the n = 16 derivatized network which is indicative of the highest number of methylene groups per structural network unit. Summarizing, it is apparent that the n-alkyl chains modify the surface energy of the thiol-ene networks in agreement with results for linear n-alkyl (meth)acrylates.[14]

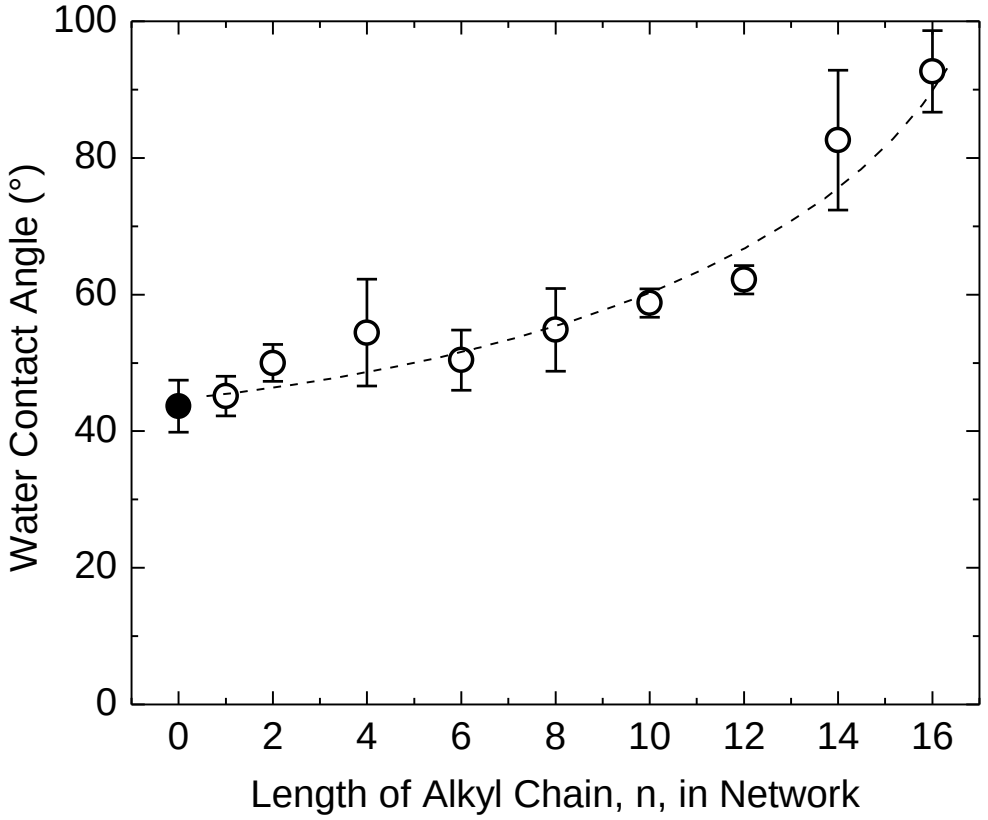

Figure IV-14. Water contact angle as a function of alkyl chain length. Filled symbol is unmodified thiol-ene network.

Conclusions

N-alkyl modified thiol-ene networks, from n = 1 to = 16 in alkyl chain length, were fabricated by photopolymerizing n-alkyl acrylate-derivatized multifunctional thiol monomers with a conventional trifunctional ene monomer. High functional group conversions for both the thio-Michael derivatization reaction and the network photopolymerizations were achieved for all lengths of n. Free volume increased greatly as alkyl chain length increased, doubling in magnitude from n = 1 to n = 16. The free volume increase was verified by bulk density measurements which revealed significant dedensification as a result of increasing alkyl chain length. As a result of the free volume increase, oxygen permeability, diffusivity, and solubility each increased. It was proposed that the covalently bound alkyl chains acted as pillars or spacers expanding the free volume. T_g of the n-alkyl derivatized networks were relatively constant, remaining in a window of 10 °C. Lastly, surface energy was also greatly influenced as evidenced by water contact angle measurements, leading to hydrophobic behavior at longer alkyl chain lengths. Furthermore, this report demonstrates the ease of tuning and forming crosslinked networks at room temperature in the bulk using thiol-ene click chemistry as well as the significant property variations that were observed in these systematically modified materials. Present work is aimed at incorporating fluoroalkyl chains into the network as well as measuring CO_2 and N_2 transport for potential membrane applications. Additionally, PVT and PALS temperature sweep measurements are underway with the goal of comparing N_h values from temperature data with those from varying the length of the alkyl chain as presented in this work.

References

1. Jordan, Jr., E. F.; Smith, Jr., S.; Koos, R. E.; Barker, W. F.; Artymyshyn, B.; Wrigley, A. N. *J. Appl. Polym. Sci.* **1978**, *22*, 1509.

2. Qiao, X.; Wang, X.; Mo, Z. *Synth. Met.* **2001**, *118*, 89.

3. Hsu, W-P.; Levon, K.; Ho, K-S.; Myerson, A. S.; Kwei, T. K. *Macromolecules* **1993**, *26*, 1318.

4. Lee, C.; Kim, K. J.; Rhee, S. B. *Synth. Met.* **1995**, *65*, 295.

5. Mogri, Z.; Paul, D. R. *Polymer* **2001**, *42*, 7765.

6. Kirkland, B. S.; Paul, D. R. *Polymer* **2008**, *49*, 507.

7. Beiner, M. *Macromol Rapid Commun.* **2001**, *22*, 869.

8. Pinnau, I.; Morisato, A.; He, Z. *Macromolecules* **2004**, *37*, 2823.

9. Dorkenoo, D. K.; Pfromm, P. H.; Rezac, M. E. *J. Polym. Sci., Part B: Polym. Phys.* **1998**, *36*, 797.

10. Matsumoto, A.; Oki, Y.; Otsu, T.; *Polym. J.* **1991**, *23*, 201.

11. Wisian-Neilson, P.; Bailey, L.; Bahadur, M. *Macromolecules* **1994**, *27*, 7713.

12. Overberger, C. G.; Frazier, C.; Mandelman, J.; Smith, H. F. *J. Am. Chem. Soc.* **1953**, *75*, 3326.

13. Wisian-Neilson, P.; Xu, G. *Macromolecules* **1996**, *29*, 3457.

14. Clarke, M. L.; Chen, C.; Wang, J.; Chen, Z. *Langmuir* **2006**, *22*, 8800.

15. Mukbaniani, O.; Titvinidze, G.; Tatrishvili, T.; Mukbaniani, N.; Brostow, W.; Pietkiewicz, D. *J. Appl. Polym. Sci.* **2007**, *104*, 1176.

16. Thami, T.; Nasr, G.; Bestal, H.; van der Lee, A.; Bresson, B. *J. Polym. Sci., Part A: Polym. Chem.* **2008**, *46*, 3546.

17. Li, F.; Liu, W. G.; Yao, K. D. *Biomaterials*, **2002**, *23*, 343.

18. Hoyle, C. E.; Lee, T.Y.; Roper, T. *J. Polym. Sci., Part A: Polym. Chem.* **2004**, *42*, 5301.

19. Jacobine, A. F. In *Radiation Curing in Polymer Science and Technology*; Fouassier, J. P., Rabek, J. F., Eds.; Elsevier Applied Science: London, **1993**; Vol. III, pp 219−268.

20. Becer, C. R.; Hoogenboom, R.; Schubert, U. S.; *Angew. Chem. Int. Ed.*, **2009**, *48*, 2.

21. Iha, R. K.; Wooley, K. L.; Nystrom, A. M.; Burke, D. J.; Kade, M. J.; Hawker, C. J. *Chem. Rev.* **2009**, *109*, 5620.

22. Sumerlin, B. S.; Vogt, A. P. *Macromolecules* **2010**, *43*, 1.

23. Khire, V. S.; Benoit, D. S. W.; Anseth, K. S.; Bowman, C. N. *J. Polym. Sci., Part A: Polym. Chem.* **2006**, *44*, 7027.

24. Khire, V. S.; Lee, T. Y.; Bowman, C. N. *Macromolecules*, **2007**, *40*, 5669-5677.

25. Clark, T.; Kwisnek, L.; Hoyle, C. E.; Nazarenko, S. *J. Polym. Sci., Part A: Polym. Chem.* **2009**, *47*, 14.

26. Chan, J. W.; Yu, B.; Hoyle, C. E.; Lowe, A. B. *Polymer* **2009**, *50*, 3158.

27. Chan, J. W.; Hoyle, C. E.; Lowe, A. B.; *J. Am. Chem. Soc.* **2009**, *131*, 5751.

28. Kwisnek, L.; Nazarenko, S.; Hoyle, C. E. *Macromolecules* **2009**, *42*, 7031.

29. Shin, J.; Nazarenko, S.; Hoyle, C. E. *Macromolecules* **2009**, *42*, 6549.

30. Hiltner, A.; Liu, R. Y. F.; Baer, E. *J. Polym. Sci., Part B: Polym. Phys.* **2005**, *43*, 1047.

31. Schrader, D. M.; Jean, Y. C., Eds. *Positron and and Positron Chemistry*, Elsevier, Amsterdam, **1988**.

32. Pethrick, R. A. *Prog. Polym. Sci.* **1997**, *22*, 1.

33. Tao, S. J. *J. Chem. Phys.*, **1972**, *56*, 5499.

34. Kobayashi, Y.; Zheng, W.; Meyer E. F.; McGervey, J. D.; Jamieson, A. M. *Macromolecules* **1989**, *22*, 2302.

35. Kluin, J. E.; Yu, Z.; Vleeshouwers, S.; McGervey, J. D.; Jamieson, A. M.; Simha, R. *Macromolecules* **1993**, *26*, 1853.

36. Chang, G. W.; Yu, Z.; Jamieson, A. M.; McGervey, J. D. *J. Appl. Polym. Sci.*, **1997**, *63*, 483.

37. Kirkegard, P.; Eldrup, M.; Morgesen, O. E.; Pedersen, N. J. *Comput. Phys. Commun.*, **1981**, *23*, 307.

38. Cohen, M. H.; Turnbull, D. *J. Chem. Phys.* **1959**, *31*, 1164.

39. Ito, K.; Saito, Y.; Yamamoto, T. ; Ujihira, Y.; Nomura, K. *Macromolecules* **2001**, *34*, 6153.

40. Park, J. Y.; Paul, D. R. *J. Membr. Sci.* **1997**, *125*, 23.

41. Hill, A. J.; Weinhold, S.; Stack. G. M.; Tant, M. R. *Eur. Polym. J.* **1996**, *32*, 843.

42. Tanaka, K.; Kawai, T.; Kita, H.; Okamoto, K.; Ito, Y. *Macromolecules* **2000**, *33*, 5513.

43. Nagel, C.; Gunther-Schade, K.; Fritsch, D.; Strunskus, T.; Faupel, F. *Macromolecules* **2002**, *35*, 2071.

44. Hu, Y. S.; Liu, R. Y. F.; Zhang, L. Q.; Rogunova, M.; Schiraldi, D. A.; Nazarenko, S.; Hiltner, A.; Baer, E. *Macromolecules* **2002**, *35*, 7326.

45. Ponangi, R.; Pintauro, P. N.; De Kee, D. *J. Membr. Sci.* **2000**, *178*, 151.

46. Villaluenga, J. P. G.; Seoane, B.; Compan, V. *J. Appl. Polym. Sci.* **1998**, *70*, 23.

47. Tanaka, K.; Kita, H.; Okano, M.; Okamoto, K. *Polymer* **1992**, *33*, 585.

48. Dlubek, G.; Stejny, J.; Alam, M. A. *Macromolecules* **1998**, *31*, 4574.

49. Kilburn, D.; Bamford, D.; Dlubek, G.; Pionteck, J.; Alam, M. A. *J. Polym. Sci., Part B: Polym. Phys.* **2003,** *41*, 3089.

50. Goyanes, S.; Rubiolo, G.; Marzocca, A.; Salgueiro, W.; Somoza, A.; Consolati, G.; Mondragon, I. *Polymer* **2003,** *44*, 3193.

51. Dlubek, G.; Pionteck, J.; Sniegocka, M.; Hassan, E. M.; Krause-Rehberg, R. *J. Polym. Sci., Part B: Polym. Phys.* **2007,** *45*, 2519.

CHAPTER V

EFFECT OF FLUOROALKYL CHAIN LENGTH ON GAS PERMEATION BEHAVIOR OF CHEMICALLY MODIFIED THIOL-ENE NETWORKS

*Luke Kwisnek, James Goetz, Brian M. Greenhoe, and Sergei Nazarenko**

Abstract

This report details the physical and transport properties of a new family of photopolymerized, hydrophobic, highly permeable membranes. Crosslinked networks were formed using a simple two-step approach. In the first step, a tetrathiol monomer with fluoroalkyl groups of varying lengths using a nucleophile-catalyzed thiol-acrylate Michael addition reaction. Complete derivatization, verified through ^{1}H NMR by the disappearance of double bond shifts, was achieved regardless of fluoroalkyl length. Derivatized thiols were then combined with an isocyanurate-based triene monomer and UV-cured rapidly to form robust crosslinked polymer networks. Conversions in excess of 90% for both thiol and ene groups were measured by real-time FTIR. These fluoroalkyl-modified networks interestingly exhibited comparable T_g despite the substantial increase in fluoroalkyl length. Oxygen permeability increased dramatically as fluoroalkyl length increased, indicative of looser packing and increased free volume. Water vapor permeability of each material, measured at two different conditions, also increased with increasing fluoroalkyl length at least up to the n = 8 perfluorooctyl-derivatized network. The n = 10 material, or perfluorodecyl-derivatized network, exhibited a water vapor permeability less than expected from the increasing trend. This decline in water vapor permeability may be caused by aggregation or liquid crystalline

order or by decreased water vapor solubility from a high concentration of fluorine. Hydrophobocity, probed by static water contact angle measurements, and bulk density both increased due to increasing concentration of fluorine resulting from increased fluoroalkyl length.

Introduction

Polymer modification via covalently bound functional groups is a historically common and useful approach to increase the performance of preexisting polymers. Fluorinated groups specifically offer unique and attractive property enhancements like chemical and thermal stability and low surface energy.[1-3] Permselective polymer membranes have also been the beneficiaries of the outstanding properties of fluorinated groups. Fluoroalkyl groups, typically attached as pendants, were shown to reduce chain packing and increasing free volume and permeability in a variety of linear polymer gas separation membranes.[4-14] Early work focused on short trifluoromethyl side groups as replacements for basic methyl side groups.[4-5] This sort of simple modification generally yielded vast improvements: gas permeability was increased by a factor of 3-5 without greatly sacrificing gas selectivity in polycarbonate and polyimide membranes.[4-5] Over time, longer fluoroalkyl side groups have been incorporated in a multitude of different membrane materials including polyimide[6-8] and polyetherimide,[9] polyetheramide,[10] polynorbornene,[11] polyphosphazene,[12-13] and even the highly permeable poly(trimethylsilylpropyne),[14] all demonstrating noteworthy increases in gas permeability. This behavior is likely due to the unique combination of bulkiness and thermodynamic frustration imparted by covalently bound fluorinated moieties.

Polymeric materials with extremely high gas permeability, particularly for water vapor, are useful as breathable membranes. One approach to forming several commercial breathable materials is to create microporous or similar morphology. Perhaps the most well known of these materials is expanded microporous PTFE or GORE-TEX.[15-16] Another class of waterproof-breathable membranes are hydrophilic phase-separated block copolymers based on polyethers.[17-19] Each of the materials mentioned is waterproof yet extremely permeable to gaseous water vapor. In addition to athletic wear and other established applications, breathable polymer membranes are being explored for suits protective against chemical agents[20-21] as well as membranes for gas dehydration.[17] Considering that these materials are all linear thermoplastic polymers, their processing is widely used and well understood.[22] However, this processing is nevertheless energy intensive[22] and also perhaps impractical in applying as a coating especially onto delicate substrates. The post-processing steps that GORE-TEX and similar materials must undergo (i.e. drawing/stretching) to form microporous structure[15] introduces yet more complexity.

As an alternative, we are exploring UV-initiated photopolymerization as a processing approach to form breathable coatings and free-standing films. UV curing, as this processing method is known industrially, employs liquid mixtures of various reactive components which are rapidly polymerized into crosslinked network materials via initiation by UV light.[23-27] The fluoroalkyl modification which demonstrated promising results for permselective membranes was implemented in this work. The intention was to increase free volume and breathability while also enhancing hydrophobicity toward UV-curable, water-repellant breathable films. This work is a continuation of our previous

work on alkyl chain incorporation, photopolymerized fluoroalkyl-derivatized thiol-ene networks were formed using a simple, two step approach. The effect of fluoroalkyl chain length on oxygen and water vapor permeability as well as various physical properties in robust, uniform, and rapidly processed thiol-ene polymer networks is presented.

Experimental

Materials

Tetrafunctional thiol monomer pentaerythritol tetrakis(3-mercaptopropionate) (4T) was supplied by Bruno Bock Thiol-Chemical-S. Trifunctional ene monomer triallyl-1,3,5-triazine-2,4,6(1*H*,3*H*,5*H*)-trione (TTT) was supplied by Sartomer. Photoinitiator alpha,alpha-dimethoxy-alpha-phenylacetophenone was purchased from Aldrich. Nucleophilic catalyst dibutylamine was obtained from Aldrich. Fluoroalkyl acrylates, from n = 2 to n = 10 in total alkyl length were obtained from Synquest Labs and Fluoryx, Inc. All materials, shown in Chart V-1, were used as received.

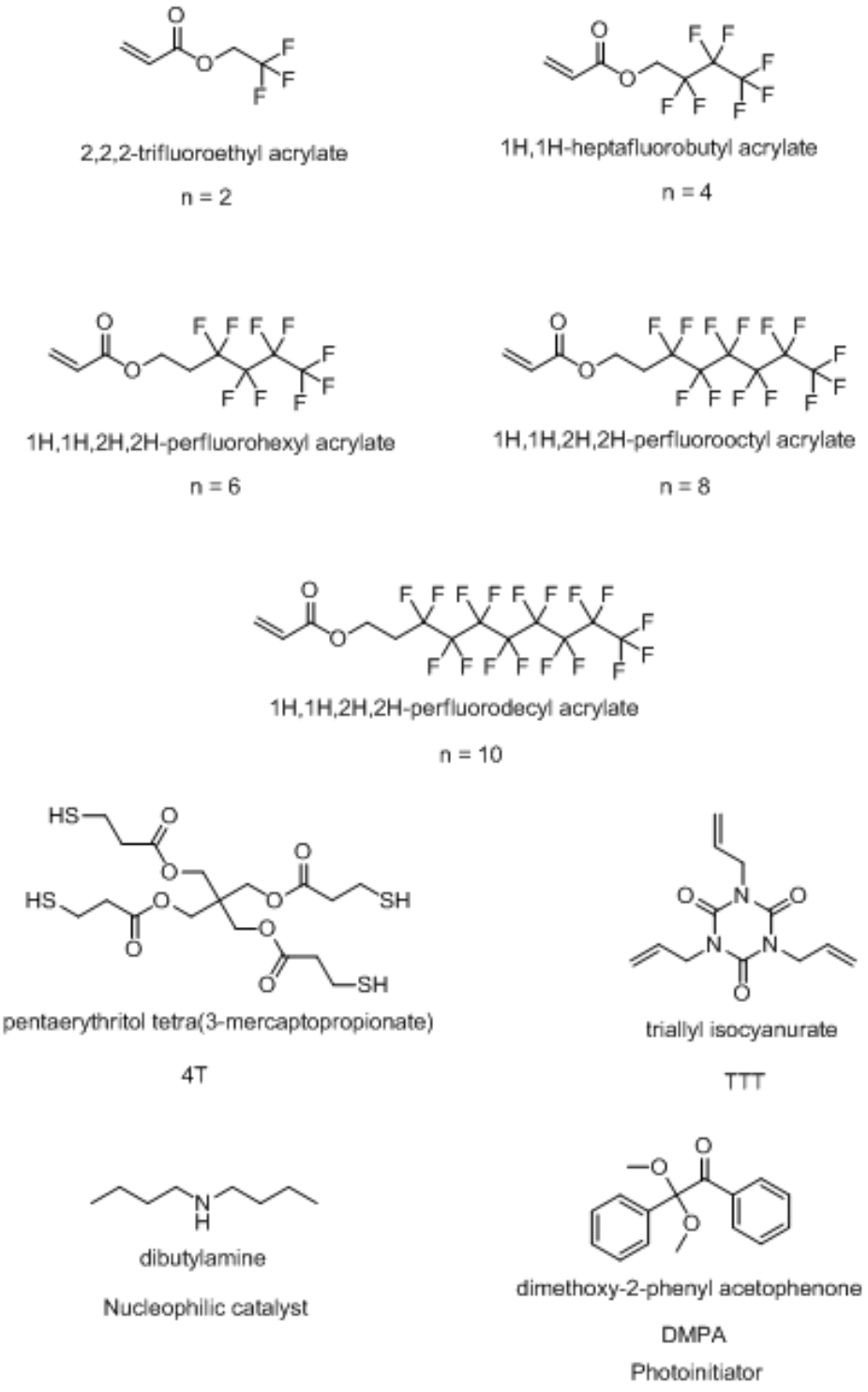

Chart V-1. Chemical structures of fluoroalkyl acrylates, tetrathiol, triene, amine catalyst, and photoinitiator.

Synthesis of Fluoroalkyl Derivatized Thiol Monomers

Fluoroalkyl derivatized trifunctional thiol monomers were synthesized using a nucleophile-catalyzed thio-Michael reaction represented in Scheme V-1. An example synthesis procedure for 4T derivatized with trifluoroethyl acrylate (which is named n = 2 due to the two carbon length chain) is given as follows. An amount of 4T was introduced to a round bottom flask along with 1 mol% dibutylamine. In a separate vial, an equal molar quantity of ethyl acrylate was weighed out and then added dropwise to the 4T/catalyst mixture at approximately 1 mL/min under mild stirring. The flask was then sealed and allowed to stir overnight. The resulting product, a distribution of structures which is on average a trifunctional thiol with an attached fluoroalkyl acrylate group, was not purified and used as-synthesized. This procedure was also used to synthesize the n = 4 fluoroalkyl acrylate-derivatized thiol. However, a modified procedure was used to synthesize longer fluoroalkyl acrylate-derivatized thiols since the high fluorine content caused miscibility problems. To remedy this situation, acetone was added to the thiol/catalyst mixture and then the longer fluoroalkyl acrylate was again added dropwise at 1 mL/min under mild stirring. The following day, acetone was removed using a rotovap distillation and this product was used without further purification.

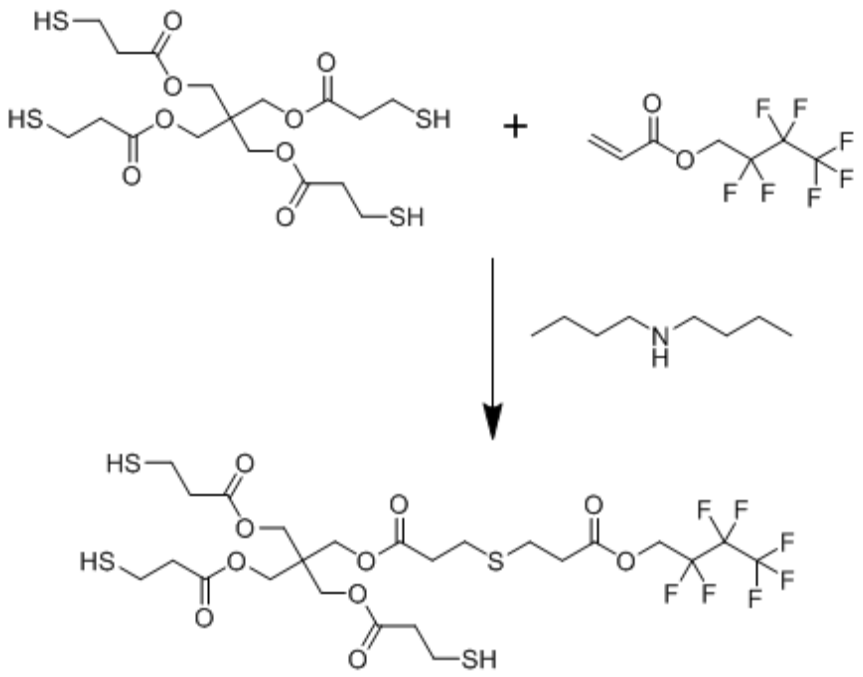

Scheme V-1. Thio-Michael addition reaction scheme for 4T adding to a representative fluoroalkyl acrylate (in this case, "n = 4") with dibutylamine catalyst. Product shown is representative of predominant structure in mixture. The same scheme was followed to form the remaining derivatized thiols: n = 2, n = 6, n = 8, and n = 10 (not shown).

Characterization of Products and Network Conversion

Derivatized thiol monomers were characterized by ^{1}H NMR using a Varian Mercury 200 MHz NMR spectrometer in acetone-D6. Functional group conversions were monitored using a Thermo Fisher Scientific Nicolet 8700 FT-IR spectrometer modified with a fiber-optic cable to irradiate liquid samples. Sample preparation involved placing a droplet of sample liquid (approximately 0.03 mL) on top of a salt plate, followed by complete spreading of this droplet by a top salt plate creating a sample sandwich. Change in peak area of thiol –SH groups at 2570 cm^{-1} (S-H stretch) and ene C=C groups at 3080 cm^{-1} (vinyl C-H stretch) were monitored as a function of irradiation

time. An OmniCure Series 1000 light source with light intensity of 450 mW/cm^2 at 365 nm was used to irradiate the samples and invoke photopolymerization.

Film Formation

All of the fluoroalkyl-derivatized thiol monomers were readily miscible in TTT ene monomer (1:1 molar ratio) at room temperature with only mild sonication, resulting in optically clear, homogeneous liquid mixtures. Free-standing thin films of all thiol-ene formulations were made by dissolving 1 wt% 1,1-dimethoxy-1-phenylacetophenone (Irgacure 651) photoinitiator into the thiol-ene mixture by sonication for approximately 10 minutes. These mixtures were then drawn down onto glass substrates using drawdown bars. The networks formed by copolymerization of the derivatized thiols with TTT are subsequently referred to by the number, n, of the carbons attached to the acrylate group regardless of the number of carbons with fluorination. For example n = 2 describes a network of 4T derivatized with trifluoroethyl acrylate and copolymerized with TTT, n = 4 describes a network of 4T derivatized with 1H,1H-heptafluorobutyl acrylate and copolymerized with TTT, and so on. In these recipes, stoichiometry of thiol, ene, and fluoroalkyl acrylate are equivalent (0.33 M each) in the final films. Films were cured using 10 passes under a Fusion UV curing line system with a D bulb (400 W with belt speed of 3 m/min and 3.1 W/cm^2 irradiance). All films were normalized in air for 3-5 days prior to testing.

Oxygen Permeation Testing

Oxygen permeation tests were conducted at 23 °C and 0% RH on Mocon OX-TRAN® 2/21 instruments using a continuous-flow testing cell method approved by the ASTM (D3985). Further details on this method were reported elsewhere.[28] Special care was taken to evaluate films of approximately uniform thickness; thickness averages were obtained by measuring at multiple locations. No degassing was performed on the samples prior to testing. Preliminary work revealed that steady-state was reached quickly and the overall permeability was quite high so no transient-state, Ficking style curves were obtained for this study.

Water vapor permeation was measured at 23 °C and 100% relative humidity and also at 37 °C and 100% relative humidity conditions using a Mocon PERMATRAN-W 3/31. As with the oxygen permeation tests, no degassing procedure was performed prior to testing. Only the steady-state water vapor flux was recorded allowing the calculation of permeability via multiplying by the sample thickness.

Miscellaneous Physical Properties

A TA Instruments Q1000 DSC with heating rate of 10 ^{o}C/min was used to investigate the glass transition temperature of film samples between 8 and 12 mg. Dynamic mechanical properties were evaluated using a Rheometric Scientific DMTA V with a frequency of 1 Hz, strain rate of 0.05%, and heating rate of 5 °C/min. T_g values were taken as the mid-point of the inflection from DSC scans and as the peak maximum in tan delta plots from DMTA. Density measurements were conducted at room

temperature via the Archimedes method with a modified analytical balance and water as the buoyant fluid. Samples were film squares of approximately 1 g and masses were recorded to the third decimal place. Ambient atmosphere water contact angle measurements were conducted using a Ramé-Hart model 200-00 standard goniometer. Deionized water droplets of approximately 5 mm in diameter were applied to thin films via a 0.6 mm diameter syringe; three droplets for each film, with 5 measurements per drop, were recorded.

Results and Discussion

Derivatization and Network Conversion

Derivatization of thiol monomers was verified via ^{1}H NMR after reaction completion. Figure V-1 shows ^{1}H NMR spectra for each modified monomer mixture. Success of the thio-Michael reaction was verified by the disappearance of the acrylate double bond proton shifts at ~6 ppm. For comparison, the ^{1}H NMR spectrum of an unreacted mixture of 4T and trifluoroethyl acrylate sans amine catalyst is shown (labeled as "Unreacted"). Following NMR verification, the monomer mixtures were not purified and used as-synthesized as mentioned in the Experimental section.

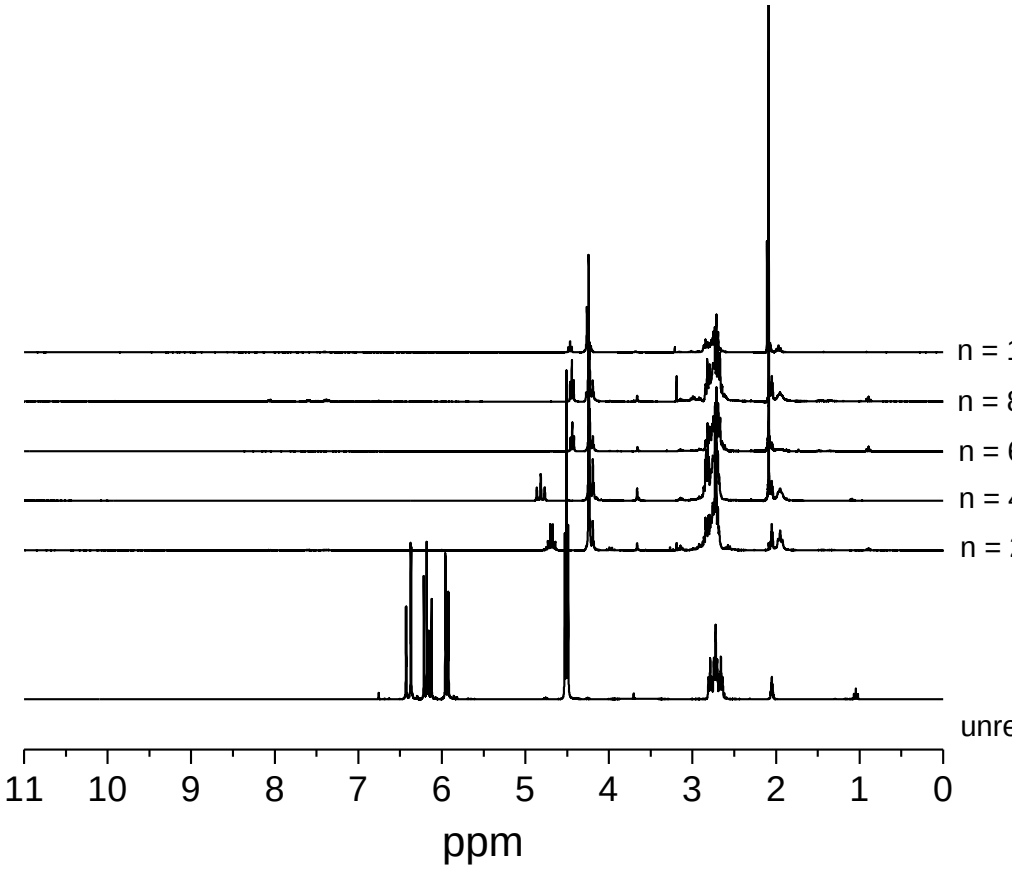

Figure V-1. ^{1}H NMR spectra for fluoroalkyl derivatized thiol monomers synthesized via Scheme 1; monomers denoted by length of fluoroalkyl chain, n, where n = 2 is 4T + trifluoroethyl acrylate, n = 10 is 4T + 1H,1H-perfluorodecyl acrylate, etc. Disappearance of acrylate double bond proton shifts at ~6ppm indicated successful thio-Michael derivatization. Unreacted spectrum is a mixture of 4T and trifluoroethyl acrylate without amine catalyst for comparison.

The issue of the fluoroalkyl chains interfering with functional group conversion during polymerization is a valid one, especially given that increasing n-alkene lengths led to decreased conversions for n-alkene grafting-to reactions in siloxane networks.[29-30] Issues with miscibility and aggregation of the fluoroalkyl groups would likely cause even

greater complications. To address these concerns, real-time FTIR measurements were conducted on liquid monomer mixtures as detailed in the Experimental section. Figure 2 shows conversion versus irradiation time plots for each fluoroalkyl-derivatized thiol-ene network. Conversions in excess of 90% for both thiol and ene groups were achieved. Thiol and ene conversion are also relatively comparable within each formulation indicating a proper stoichiometric balance of thiol and ene groups. Fluoroalkyl chain length had no measurable effect on the ultimate conversion of thiol and ene groups during photoinitiated polymerization. Such high conversions despite structural challenges are not uncommon with thiol-ene chemistry.[27]

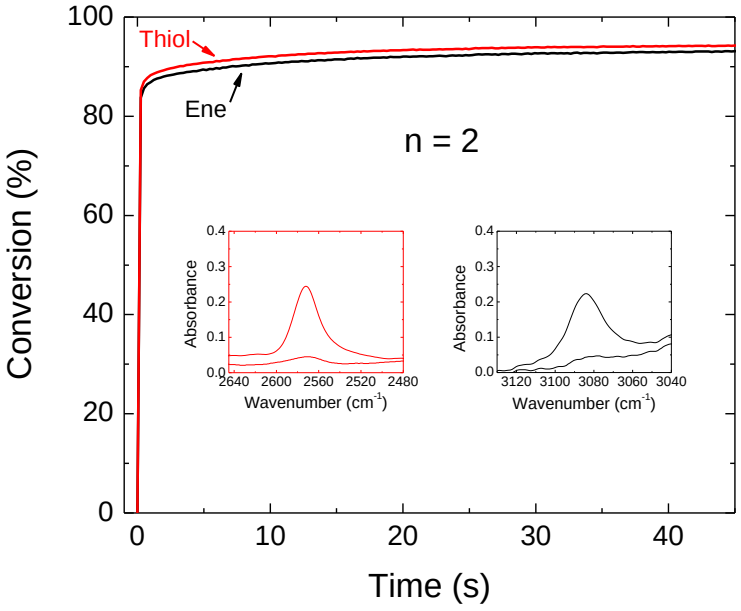

Figure V-2. RT-FTIR conversion-time plots of the thiol (2570 cm^{-1}) peaks and ene (3080 cm^{-1}) peaks for each fluoroalkyl derivatized thiol-ene network. High conversions (90+%) were obtained for each network. Plot labels denote length of fluoroalkyl chain in network.

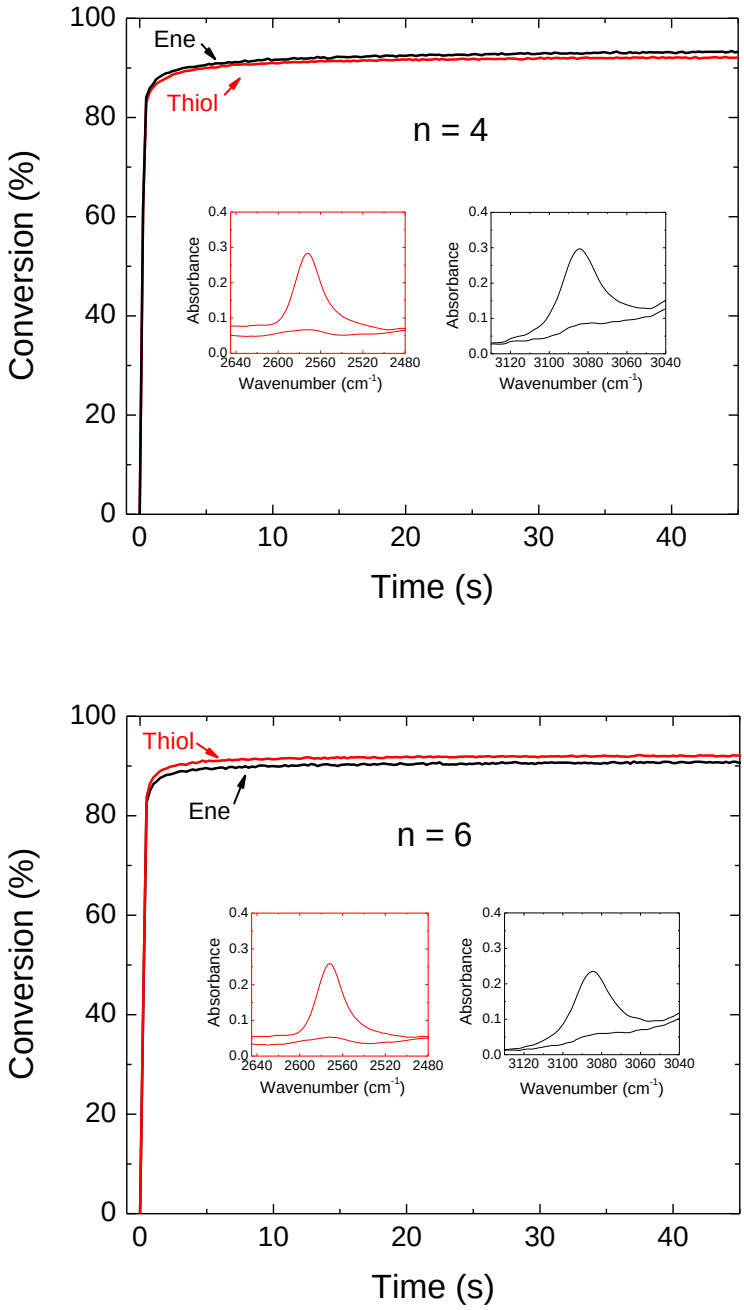

Figure V-2 (continued).

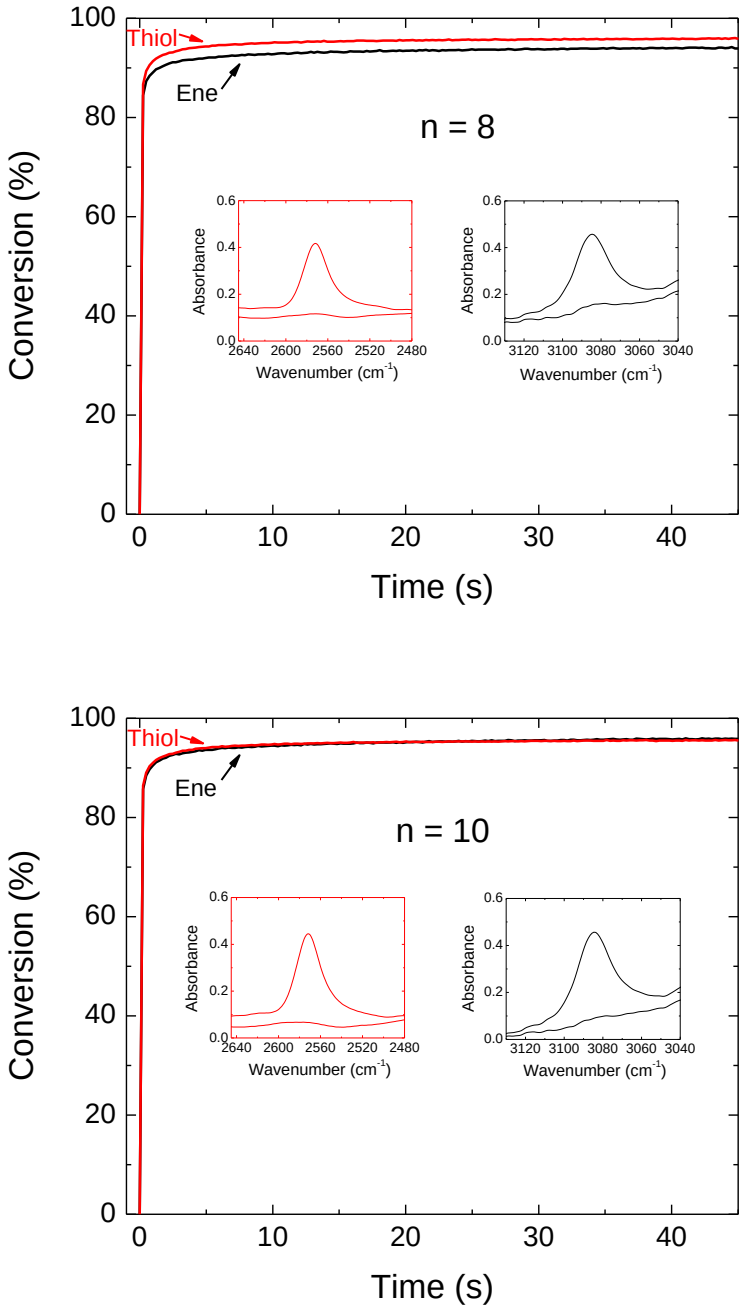

Figure V-2 (continued).

Physical and Transport Properties

After verifying high conversion of each network and essentially no change in conversion as a function of fluoroalkyl length, efforts turned toward an investigation of physical properties. Each material was optically transparent and quite robust regardless of the fluoroalkyl length. Our previous study on n-alkyl derivatized thiol-ene networks showed that despite increasing n-alkyl length from 1 to 16, glass transition temperature remained within a small window.[28] In similar fashion, T_g according to tan delta peak via DMTA for the fluoroalkyl derivatized thiol-ene networks also remained in a small window as shown in Figure V-3. This small effect on T_g as a function of increasing side chain length is peculiar and especially surprising given the mass of the long fluoroalkyl chains. Typically, increasing side chain length causes a significant decrease in T_g related to reduced packing and increased segmental mobility. So far our investigations into alkyl derivatized thiol-ene networks[28] and fluoroalkyl derivatized networks in this work reveal that the glass transition is only somewhat perturbed and so must be controlled by the network scaffold or backbone which was identical for each network. Tan delta peak height, however, tended to decrease as fluoroalkyl length increased; this effect could be due to increasing amount of dangling fluoroalkyl side groups which do not contribute to tan delta, an alpha relaxation related to main chain or network backbone/scaffold motion.

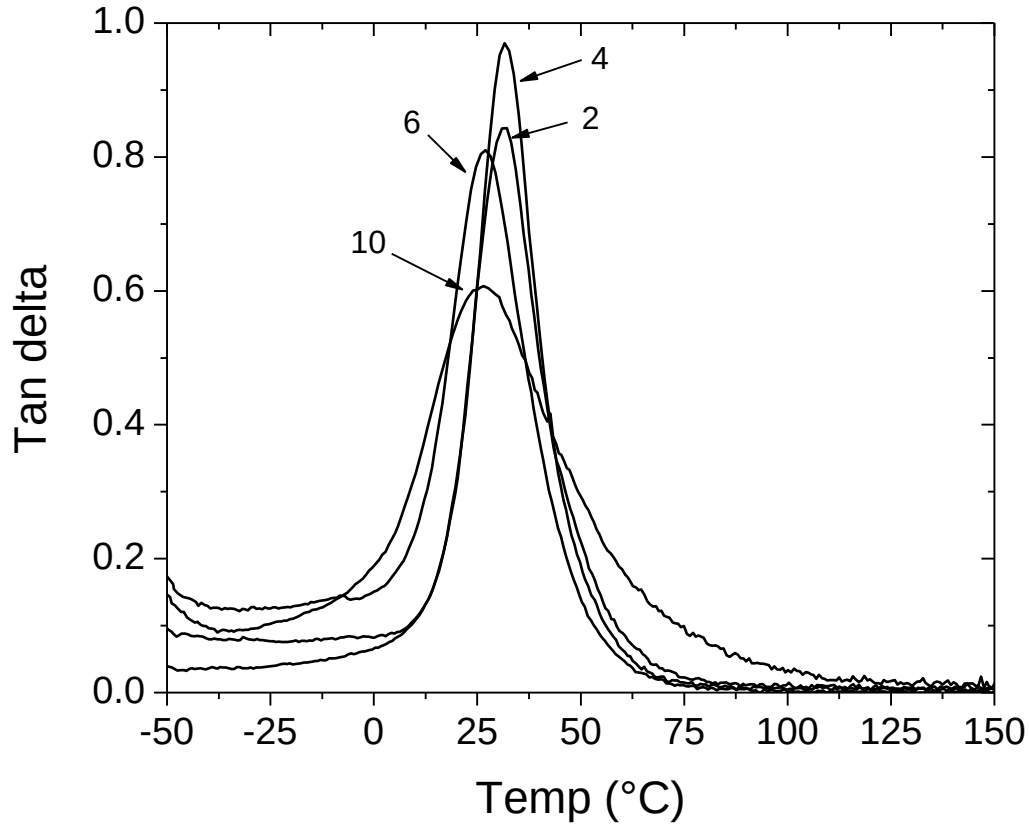

Figure V-3. Tan delta versus temperature plots for each fluoroalkyl derivatized thiol-ene network. Labels indicate length of fluoroalkyl chain in network.

While the glass transition in alkyl derivatized thiol-ene networks was not greatly affected, oxygen permeability increased greatly due to an increase in free volume. Free volume increases were attributed to looser packing of the network provided by the alkyl chains acting as pillars or spacers. Increasing fluoroalkyl length brought about a similar though much sharper increase in oxygen permeability. Figure V-4 is a semi-log plot of oxygen permeability measured at 23 °C and 0% RH, as described in the Experimental section, versus the length of the (fluoro)alkyl chain embedded in the network. Oxygen permeability for the n= 2 fluoroalkyl derivatized network was roughly comparable to that

of the same length alkyl chain modified network. However the fluoroalkyl modified networks deviate from the alkyl chains as the length increases. The n = 10 fluoroaklyl derivatized network demonstrated oxygen permeability around 80 cc(STP) cm m^{-2} day^{-1} atm^{-1} which is extremely high: this value is four times greater than that of LDPE[31] and approaches the level of highly breathable commercial materials. This strong increase in permeability can again be attributed to an increase in free volume. The fluoroalkyl chains, like the related alkyl chains, acted as pillars which limited packing and expanded the free volume of the network. This structural effect may also be coupled with a thermodynamic effect related to the frustration between fluoroalkyl groups and the network scaffold.

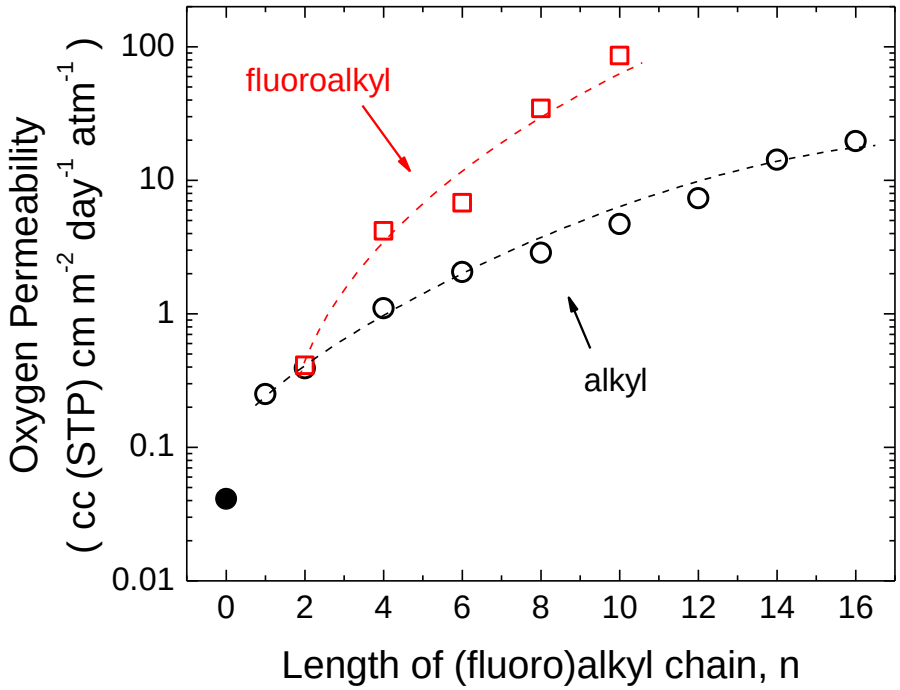

Figure V-4. Semi-log plot of oxygen permeability versus the length of alkyl and fluoroalkyl chain in the thiol-ene network. Shaded symbol represents unmodified thiol-ene network.

Owing to the vast increase in oxygen permeability which was comparable or even greater than standard highly permeable polymers, it was interesting to consider if the fluoroalkyl chains would have the same effect on water vapor permeability. Water vapor permeability did indeed increase as fluoroalkyl length increased at least up to the n = 8 material as seen in Figure V-5. This material, a thiol-ene network derivatized with perfluorooctyl groups, exhibited a water vapor permeability of approximately 4 g cm m^{-2} day^{-1} at 37 °C. This specific testing environment is the standard ASTM condition for simulating human body conditions. A value of 4 is quite promising although not quite in the range of commercial breathable membranes with water vapor permeability around 10 to 20 g cm m^{-2} day^{-1} or higher.[17-19] The generally high water vapor permeability for these materials is not entirely in accord with non-porous fluorinated polymers. Fluoropolymers such as PVF and PVDF exhibit low water vapor permeability and are often used as water vapor barriers. These materials are high molecular weight linear polymers with fluorine pendant to the backbone. However, fluorine in the fluoroalkyl modified thiol-ene networks are present as side groups which limited packing and increased free volume – a different implementation. Therefore the structural effect of the fluoroalkyl groups acting as pillars and increasing free volume is a plausible explanation for the water vapor permeability behavior. However, after n = 8 water vapor permeability declined. The n = 10, perfluorodecyl-derivatized thiol-ene network, demonstrated lower permeability than was expected from the rising trend. The decline could be due to aggregation or phase separation of the fluoroalkyl groups into ordered domains. In support of this explanation is the fact that perfluorodecyl side-chain polymers are known to form liquid crystalline phases whereas perfluorooctyl side-chain polymers are amorphous and do not form

ordered phases. The lower water vapor permeability may also be due to the increase in fluorine which could cause lower water vapor solubility. Regardless, the water vapor permeability behavior of this series of materials is in disagreement with the oxygen permeability behavior. Further investigations underway include wide-angle x-ray diffraction to probe for order and water vapor permeation measurements at different conditions to test the repeatability of the results.

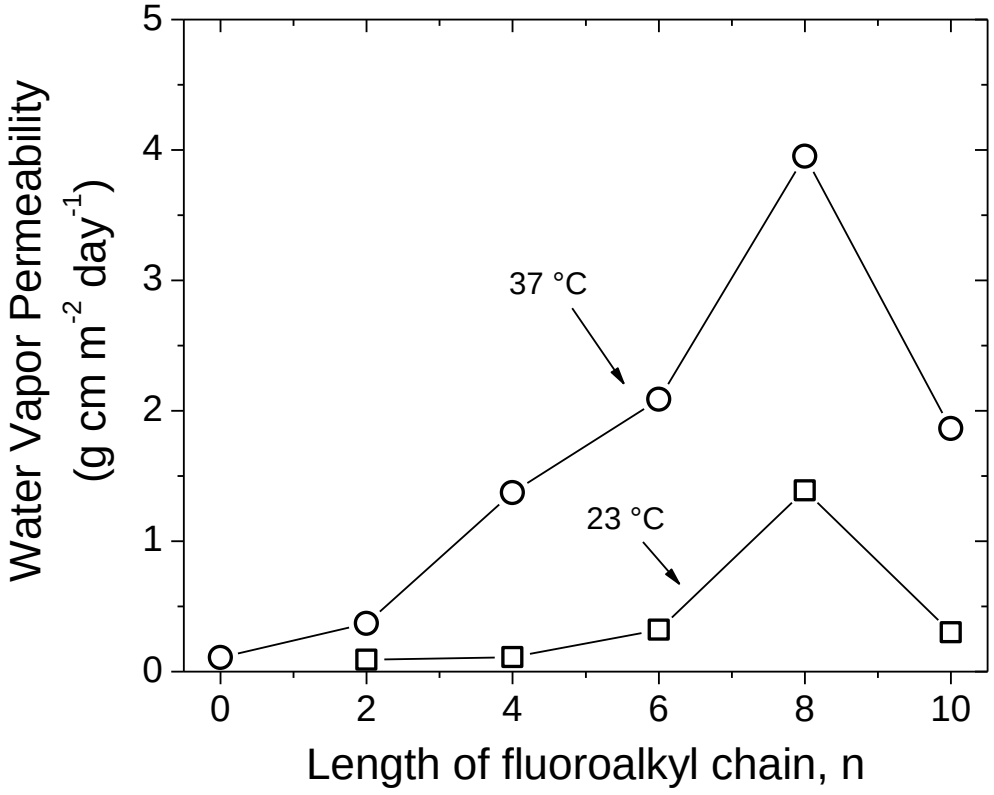

Figure V-5. Water vapor permeability at 23 °C and 37 °C, both at 100% RH, plotted versus the length of fluoroalkyl chain in the network. Material shown at n = 0 represents unmodified thiol-ene network.

As fluoroalkyl length increased so did the concentration of fluorine in the network. Because of fluorine's relatively large mass as compared to hydrogen, bulk density increased for the fluoroalkyl derivatized networks as shown in Figure V-6. Despite a likely increase in free volume indirectly probed by oxygen and water vapor permeability, the fluoroalkyl chains caused densification due to an increasing concentration of fluorine which overpowered the free volume increase.

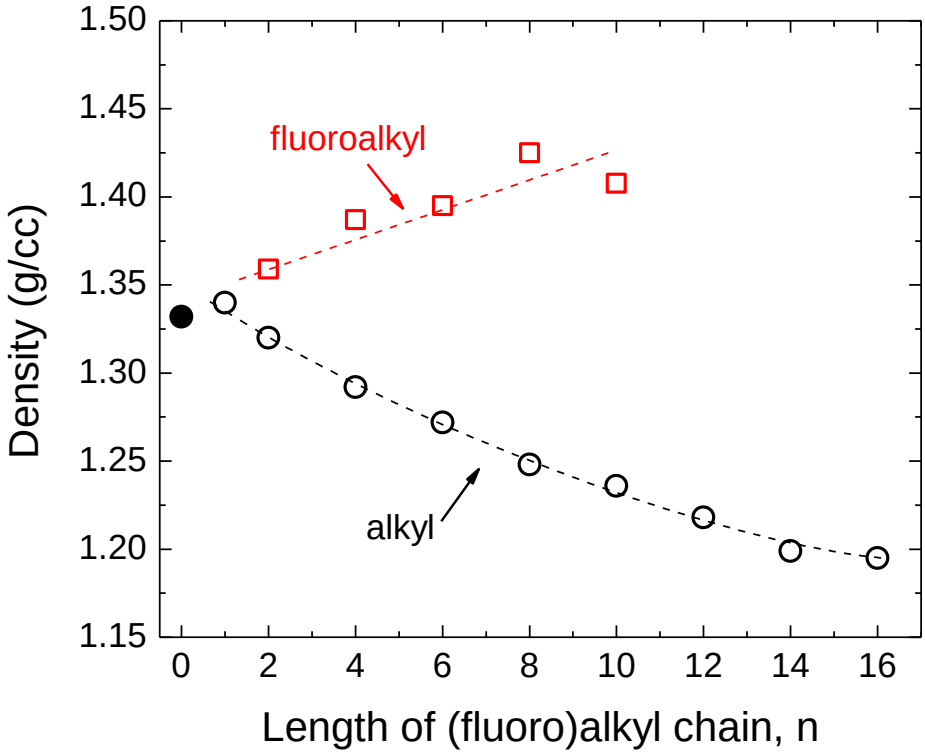

Figure V-6. Bulk density as a function of the length of fluoroalkyl and alkyl chain in the network. Shaded symbol represents unmodified thiol-ene network.

Perhaps the most well known and valuable property of fluorinated polymers is their surface energy. The unique properties of the carbon-fluorine bond allow for only weak intermolecular interactions and thus extremely low surface energy and anti-fouling properties, making fluoropolymers irreplaceable for a variety of applications. Increasing fluoroalkyl length in the photopolymerized thiol-ene networks caused an increase in static water contact angle according to Figure V-7. The strong hydrophobic behavior observed for these materials was due simply to the increased concentration of fluorine in the bulk. Additionally, the fluoroalkyl-derivatized networks displayed greater water contact angle over the corresponding length alkyl-derivatized networks. The water contact angle for the fluoroalkyl series approached 110 °C, a value comparable to that of Teflon.[2]

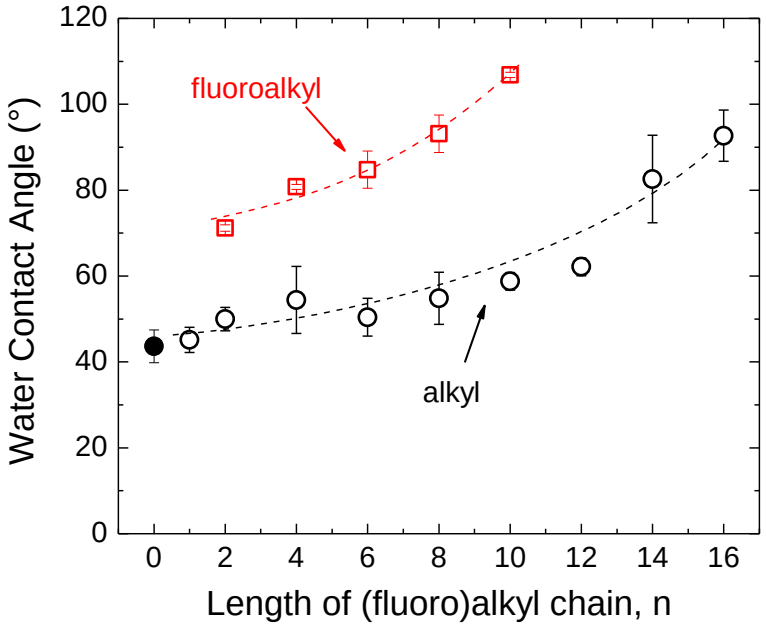

Figure V-7. Static water contact angle versus the length of alkyl and fluoroalkyl chain in the network. Shaded symbol represents unmodified thiol-ene network.

Conclusions

A two-step approach, used successfully to form n-alkyl derivatized thiol-ene networks in previous work, was employed in this work to form fluoroalkyl derivatized thiol-ene networks. The first step was thio-Michael addition of a tetrathiol to various fluoroalkyl acrylates, from two to ten carbons in length. Complete disappearance of double bond shifts in ^{1}H NMR confirmed successful attachment acrylate "tails" to the thiol monomer. These new derivatized thiols were combined with an isocyanurate-based trifunctional ene and a common photoinitiator. Surprisingly the fluoroalkyl derivatized thiols readily combined with the triene without the use of solvents, enabling UV-curing in the bulk forming optically clear and robust crosslinked networks.

High conversions, in excess of 90% for both thiol and ene groups, were obtained for the photopolymerization of each formulation as measured by real-time FTIR. Fluoroalkyl-derivatized thiol-ene networks exhibited similar T_g despite substantial structural changes. The glass transition of these networks was likely controlled by the network backbone or scaffold which consisted of the thiol and ene monomers. Oxygen permeability for fluoroalkyl-derivatized networks was higher than for alkyl-derivatized networks of corresponding carbon chain length.

Oxygen permeability for the n = 10, perfluorodecyl-derivatized, thiol-ene network was approximately 80 cc(STP)cm $m^{-2}day^{-1}atm^{-1}$ which is in the range of materials considered highly permeable. Water vapor permeability also generally increased as a function of fluoroalkyl length. Because of increasing concentration of fluorine, density and water contact angle increased with increasing fluoroalkyl length. Static water contact angle for the most hydrophobic material, n = 10, was comparable to that of Teflon. This

approach thus demonstrates the potential for UV-curing of highly breathable, water-repellant materials using thiol-ene chemistry.

References

1. Drobny, J. G., ed. *Technology of Fluoropolymers, 2nd edition*, CRC Press, Boca Raton, **2009**.
2. Wall, L. A., ed. *Fluoropolymers*, Wiley, New York, **1972**.
3. Kobayashi, H.; Owen, M. J.; *Surface Properties of Fluorosilicones*, Trends in Polymer Science, **1995**, 3, 330-335.
4. Hellums, M. W.; Koros, W. J.; Husk, G. R.; Paul, D. R.; *Journal of Membrane Science*, **1989**, 46, 93-112.
5. Tanaka, K.; Kita, H.; Okano, M.; Okamoto, K-i.; *Polymer*, **1992**, 33, 585-592.
6. Kim, J-H.; Chang, B-J,; Lee, S-B.; Kim, S. Y.; *Journal of Membrane Science*, **2000**, 169, 185-196.
7. Kim, J-H.; Lee, S-B.; Kim, S. Y.; *Journal of Applied Polymer Science*, **2000**, 77, 2756-2767.
8. Chang, B-J.; Chang, Y-H.; Kim, D-K.; Kim, J-H; Lee, S-B.; *Journal of Membrane Science*, **2005**, 248, 99-107.
9. Sen, S. K.; Dasgupta, B.; Banerjee, S.; *Journal of Membrane Science*, **2009**, 343, 97-103.
10. Maji, S.; Banerjee, S.; *Journal of Membrane Science*, **2010**, 349, 145-155.
11. Vargas, J.; Santiago, A. A.; Tlenkopatchev, M. A.; Lopez-Gonzalez, M.; Riande, E.; *Journal of Membrane Science*, **2010**, 361, 78-88.
12. Allcock, H. R.; Nelson, C. J.; Coggio, W. D.; Manners, I.; Koros, W. J.; Walker, D. R. B.; Pessan, L. A.; *Macromolecules*, **1993**, 26, 1493-1502.
13. Wisian-Nelson, P.; Xu, G-F.; *Macromolecules*, **1996**, 29, 3457-3461.

14. Nagase, Y.; Sugimoto, K.; Takamura, Y.; Matsui, K.; *Journal of Applied Polymer Science*, **1991**, 43, 1227-1232.

15. W.L. Gore and Associates, Inc., U.S. patent 3953566, April **1976**.

16. W.L. Gore and Associates, Inc., U.S. patent 4194041, March **1980**.

17. Metz, S. J.; van de Ven, W. J. C.; Potreck, J.; Mulder, M. H. V.; Wessling, M.; *Journal of Membrane Science*, **2005**, 251, 29-41.

18. Gebben, B.; *Journal of Membrane Science*, **1996**, 113, 323-329.

19. Meng, Q. B.; Lee, S-I.; Nah, C.; Lee, Y-S.; *Progress in Organic Coatings*, **2009**, 66, 382-386.

20. Lu, X.; Nguyen, V.; Zeng, X.; Elliot, B. J.; Gin, D. L.; *Journal of Membrane Science*, **2008**, 318, 397-404.

21. Gin, D. L.; Bara, J. E.; Noble, R. D.; Elliott, B. J.; *Macromol. Rapid Commun.*, 29, **2008**, 367-389.

22. Rosato, D. V., Rosato, D. V., Rosato, M. G. *Injection Molding Handbook, 3rd edition*; Kluwer Academic Publishers: Massachusets, **2000**; pp. 1335.

23. Yagci, Y.; Jockusch, S.; Turro, N. J.; *Macromolecules*, 43, **2010**, 6245-6260.

24. Fouassier, J. P.; *An Introduction to the Basic Principles in UV Curing*, in: Fouassier, J. P. and Rabed, J. F. (Eds.), Radiation Curing in Polymer Science and Technology – Volume I, Elsevier Applied Science, New York, **1993**, pp. 49-117.

25. Hoyle, C.E.; *Photocurable Coatings*, in: C.E. Hoyle, J.F. Kinstle (Eds.), Radiation Curing of Polymeric Materials, ACS, Washington D.C., **1990**, pp. 1-16.

26. Lee, T. Y.; Roper, T.; Hoyle, C. E.; *Journal of Polymer Science: Part A: Polymer Chemistry*, 42, **2004**, 5301-5338.

27. Hoyle, C. E.; Bowman, C. N.; *Angewandte Chemie International Edition*, 49, **2010**, 1540-1573.

28. Kwisnek, L.; Kaushik, M.; Hoyle, C. E.; Nazarenko, S.; *Macromolecules*, 43, **2010**, 3859-3867.

29. Mukbaniani, O.; Titvinidze, G.; Tatrishvili, T.; Mukbaniani, N.; Brostow, W.; Pietkiewicz, D. *J. Appl. Polym. Sci.* **2007**, *104*, 1176.

30. Thami, T.; Nasr, G.; Bestal, H.; van der Lee, A.; Bresson, B. *J. Polym. Sci., Part A: Polym. Chem.* **2008**, *46*, 3546.

31. Pauly, S. "Permeability and Diffusion Data," in *Polymer Handbook*, Eds. J. Brandrup et al., John Wiley & Sons, **1999**.

CHAPTER VI

MULTIFUNCTIONAL THIOLS AS ADDITIVES IN UV-CURED PEG-DIACRYLATE MEMBRANES FOR CO_2 SEPARATION

*Luke Kwisnek, Stephen Heinz, Jeffrey S. Wiggins, Sergei Nazarenko**

Abstract

The utility of incorporating only 20 mol% of multifunctional thiols into UV-cured poly(ethyleneglycol)diacrylate (PEGDA) membranes for CO_2 separation is presented. Five different multifunctional thiols were investigated, spanning a range of functionalities from 2 to 4 and also different rigidities. All thiol-modified networks exhibited lower modulus values according to both small-strain and large-strain mechanical testing. This decrease in modulus was primarily attributed to a decrease in crosslink density via the step-growth thiol-acrylate reaction. Decreased crosslink density was more pronounced for dithiol additives which formed a "train-like" topology of connected PEGDA segments. Because of this more linear topology, dithiol-modified networks exhibited increases in gas permeability and strain at break. CO_2 selectivity of each thiol-modified network was nearly comparable to the unmodified PEGDA network. Each network rapidly reached 100% conversion under a nitrogen atmosphere. However in air, the pure acrylate network reached negligible conversion while the networks modified with tri and tetrathiols reached noticeably higher conversions. Outdoor sunlight curing revealed that all thiol-modified networks were tack-free after only several minutes depending on thiol functionality. In contrast, the pure acrylate membrane remained tacky and uncured on

the surface indefinitely. This study emphasizes the importance of thiol monomer selection in diminishing oxygen inhibition in UV-initiated acrylate polymerization as well as marked improvement in permeability for this specific PEGDA network via the incorporation of dithiols.

Introduction

Gas separation is an important industrial process with applications such as hydrogen recovery, air separation, and natural gas purification.[1] Often, costly and/or polluting methods like distillation and amine treatment are used. Membrane separation is an environmentally friendly alternative to these methods and polymeric membranes in particular could be manufactured in large quantities and at low cost making them extremely attractive.[1-4]

Since the early 1980s, it has been well documented that membranes based on poly(ethylene glycol) (PEG) have a high selectivity for carbon dioxide (CO_2),[5-9] a common contaminant in many industrial gas purification processes as well as a key component in atmospheric packaging for certain foods.[10] It was suggested that the reason for this selectivity is a Lewis acid-base interaction between the polar, electron-rich ether units on the polymer backbone (the Lewis base) and CO_2 (the Lewis acid).[5] This electronic interaction promotes a high CO_2 solubility in PEG. Solubility selectivity is an attractive quality since low T_g, rubbery materials may be used. Such materials do not undergo physical aging and can also have extremely high permeability. While it has a low T_g, solid polymeric PEG unfortunately crystallizes to approximately 70 vol% which severely reduces the permeability of the membrane.[8-9] Because gas separation

membranes must be highly permeable as well as highly selective,[11-12] semi-crystalline PEG would not meet performance requirements for industrial separations.

One solution to the problem of PEG crystallinity is to crosslink PEG, limiting the molecular weight of linear segments between junction points therefore preventing crystallinity.[7-9] The Freeman research group has reported on a multitude of crosslinked amorphous PEG-based membranes made with UV-initiated radical photopolymerization of acrylates based on PEG.[13-16] These membranes show high performance compared to other polymeric CO_2 separation membranes while at the same time employing the inherent advantages of UV-curing such as rapid preparation of large areas of material, no solvents (100% reactive liquid components), energy efficient processing compared to thermal methods, and enormous latitude in formulations due to the variety of commercially-available UV-curable monomers and oligomers.[17-18] UV-curable materials might also be used to repair defects in gas separation membranes or as coatings to upgrade existing units.

An important drawback to acrylate photopolymerization is oxygen inhibition.[17-18] When cured in an oxygen-containing atmosphere, acrylate radicals react with oxygen forming peroxy radicals. These peroxy radicals are relatively unreactive toward acrylate double bonds thus limiting the overall conversion of these materials when cured in air. As a result, acrylate-based materials are often prepared under a controlled nitrogen atmosphere in order to reach optimal conversions and to prevent an uncured, tacky surface. Thiol-ene photopolymerization, which proceeds via a step-growth free-radical polymerization process compared to the chain-growth acrylate polymerization process, is

known for its insensitivity towards oxygen.[19-21] Peroxy radicals formed during polymerization in air readily abstract hydrogen from thiols, generating thiyl radicals which react with double bonds continuing the polymerization process. This thiol-ene photopolymerization process consumes oxygen that diffuses into the liquid mixture and reaches high conversion as in a controlled inert atmosphere. An extensive review of the problems and solutions associated with oxygen inhibition in UV-cured materials is available in reference 22. In this work, one solution to oxygen inhibition in acrylate photopolymerizations was investigated.[22] By incorporating multifunctional thiols into the acrylate formulation, the effect of oxygen inhibition was diminished. It was hypothesized that polymer system viscosity was a controlling factor for the extent of oxygen inhibition: higher viscosity reduced oxygen diffusion into the system thus decreasing oxygen inhibition.[22]

We previously studied oxygen transport and free volume in a variety of basic and modified thiol-ene networks all UV-cured in air.[23-24] It is our intent to expand the range of applicability of UV-cured thiol-enes into membrane applications while employing the advantages of the well-defined and robust thiol-ene reaction. In this paper, we demonstrate the benefits of incorporating only a small amount of various multifunctional thiols into a PEG-based acrylate membrane, poly(ethyleneglycol)diacrylate. Multifunctional thiol monomers will be ranked based on how they affect gas separation performance as well as their efficacy towards correcting the oxygen inhibition problem during UV-initiated processing.

Experimental

Materials

The thiol monomers glycol di(3-mercaptopropionate) (2T), trimethylolpropane tri(3-mercaptopropionate) (3T), and pentaerythritol tetra(3-mercaptopropionate) (4T) were supplied by Bruno Bock Thio-Chemical-S. Thiol monomer ethylenedioxy diethanethiol (2TE) was obtained from Aldrich. Thiol monomer tris[2-(3-mercaptopropionyloxy)ethyl] isocyanurate (3TI) was obtained from Wako Pure Chemical Industries. Acrylate oligomer poly(ethylene glycol) diacrylate (PEGDA) with average M_n = 700 g/mol was obtained from Aldrich. All mixtures were initiated using the photoinitiator 2,2-dimethoxy-2-phenylacetophenone (DMPA) which was also obtained from Aldrich. All materials, shown in Figure VI-1, were used as received.

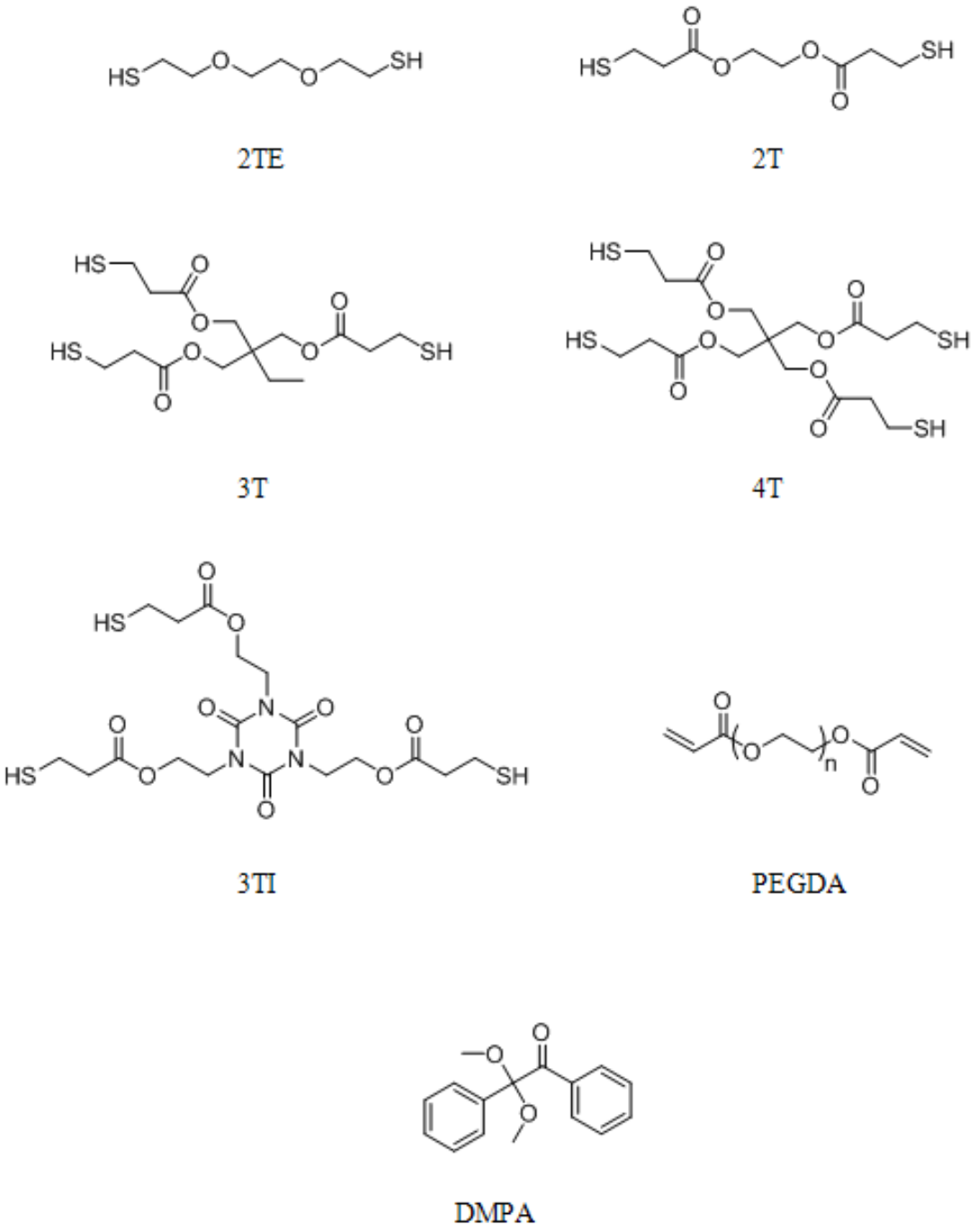

Figure VI-1. Structures of thiol monomers, acrylate oligomer, and photoinitiator.

Sample Preparation

Membrane samples for gas permeation measurement were prepared as follows. For the control material, pure PEGDA, 1 wt% DMPA was added to PEGDA and then sonicated for 10 minutes. This mixture was then poured onto a glass plate and sandwiched by another glass plates with a 1mm shim to control the thickness. This glass plate/oligomer sandwich was then cured using 10 passes (5 one side, 5 opposite side) at 10 ft/min feed speed under a Fusion UV curing line system with a D bulb (400 W with belt speed of 10 feet/min and 3.1 W/cm^2 irradiance). For thiol-modified PEGDA membranes, 80/20 mol% mixtures of acrylate groups (C=C)/thiol groups (–SH) were prepared. This ratio was chosen as large enough to gain the advantages of the uninhibited thiol-acrylate reaction without having excess, unreacted thiols. DMPA was then incorporated at 1 wt%, sonicated, and cured as already described. Presented in Table VI-1 are the compositional data for each liquid mixture. Additionally, DMTA samples were carefully cut from the material prepared as described for the membrane samples. Tensile "dogbone" samples were also prepared via a glass sandwich except a 3.5 mm rubber mold with "dogbone" cutouts was used as the spacer – this procedure was used so that samples for tensile testing were as pristine as could be managed.

Table VI-1. Compositional Information for Each Liquid Mixture.

Material	mol% thiol groups in liquid mixture	wt% thiol monomer in liquid mixture	wt% ethylene glycol in liquid mixture
PEGDA	0	0	83
PEGDA+2TE	20	6.1	79
PEGDA+2T	20	7.8	77
PEGDA+3T	20	8.7	76
PEGDA+4T	20	7.8	77
PEGDA+3TI	20	11.1	74

Characterization

Functional group conversions for all networks were monitored using a Thermo Fisher Scientific Nicolet 8700 FT-IR spectrometer modified with a fiber-optic cable to irradiate liquid samples. Sample preparation involved placing a droplet of sample liquid (approximately 0.03 mL) on top of a salt plate, followed by complete compression and spreading of this droplet by a top salt plate which was subsequently removed leaving a thin layer of material to be monitored for conversion. The conversion of acrylate double bonds at 812 cm^{-1} were monitored as a function of irradiation time. An OmniCure Series 1000 light source with light intensity of 20 mW/cm^2 at 365 nm was used to irradiate the samples and invoke photopolymerization. Special care was taken to ensure that absorbances at 812 cm^{-1} were comparable (i.e. comparable thickness at the location of the IR beam) for all samples before polymerization. Both nitrogen purge and air purge atmospheres were explored.

Tack-free time studies for films cured in sunlight were conducted on the roof of the USM School of Polymers and High Performance Materials building. Liquid formulations were drawn down at 100 micron thickness onto steel substrates. Total solar radiation was 50 mW/cm^2 and the UV index was 4 as recorded by a Davis Advantage Pro 2 weather station. Tack-free time was noted as when liquid material would cease to transfer to a gloved finger lightly pressed onto the membrane. Dynamic mechanical properties were evaluated using a Rheometric Scientific DMTAV with a frequency of 1 Hz, strain rate of 0.05%, and heating rate of 5 °C/min. T_g values were taken as the peak maximum of tan delta plots. Tensile tests were performed on miniature "dogbone" samples (5 mm wide, ~3.5 mm thick, 12 mm gage length) with an MTS Insight 10 electromechanical test frame equipped with a 2.5 kN load cell. Tests were conducted in duplicate at a strain rate of 1.3 mm/min strain rate to ensure failure between one and three minutes. A Brookfield CAP 2000+ parallel plate viscometer was used to measure the viscosity of liquid oligomer mixtures. Viscosity measurements were conducted at 500 RPM, 6,667 s^{-1} shear rate, and a controlled 23 °C temperature.

Permeation of nitrogen, oxygen, and carbon dioxide were measured using a custom-built gas permeation device based on a constant-volume, variable pressure (manometric) technique similar to those described in the literature.[8,25-27] Upstream feed gas pressure was monitored with an Omega Engineering PX181-300G5V pressure transducer. For this study all experiments were conducted at 3.5 atm applied upstream pressure. Downstream permeated gas pressure was monitored with an MKS 226A differential pressure transducer. Both transducers were connected to a computer for real-time data collection. The permeation cell was maintained at a constant temperature, i.e.

23 °C, via a recirculating chiller. All film samples were degassed under high vacuum for 24 hours prior to testing. Experimental curves provided in Figure VI-2 exhibit typical Fickian behavior, with well-defined steady-state slopes, and are representative of those not shown. The black dashed lines are experimental data reported by the differential pressure transducer. The red lines are the steady-state, constant slope, portions of the permeations curves extrapolated down to zero value of downstream pressure. Technically the slopes were determined via conducting a linear fit to the steady-state experimental data using Origin graphing software. Using this slope value along with Equation 1, permeability values were calculated where P is the permeability, V_d is the downstream volume, l is the membrane thickness, p is the applied upstream pressure, A is the testing area, R is the universal gas constant, T is the temperature, and dp/dt is the steady-state slope.[27] Diffusion coefficients were calculated from time lag values, t_L, i.e. the intersections of the steady state line extrapolations with the x-axis according to Equation 2. S was then calculated from known permeability and diffusivity coefficients as follows: $P=DS$.

$$P = \frac{V_d\, l}{p\, A\, R\, T}\left(\frac{dp}{dt}\right) \tag{1}$$

$$D = \frac{l^2}{6t_L} \tag{2}$$

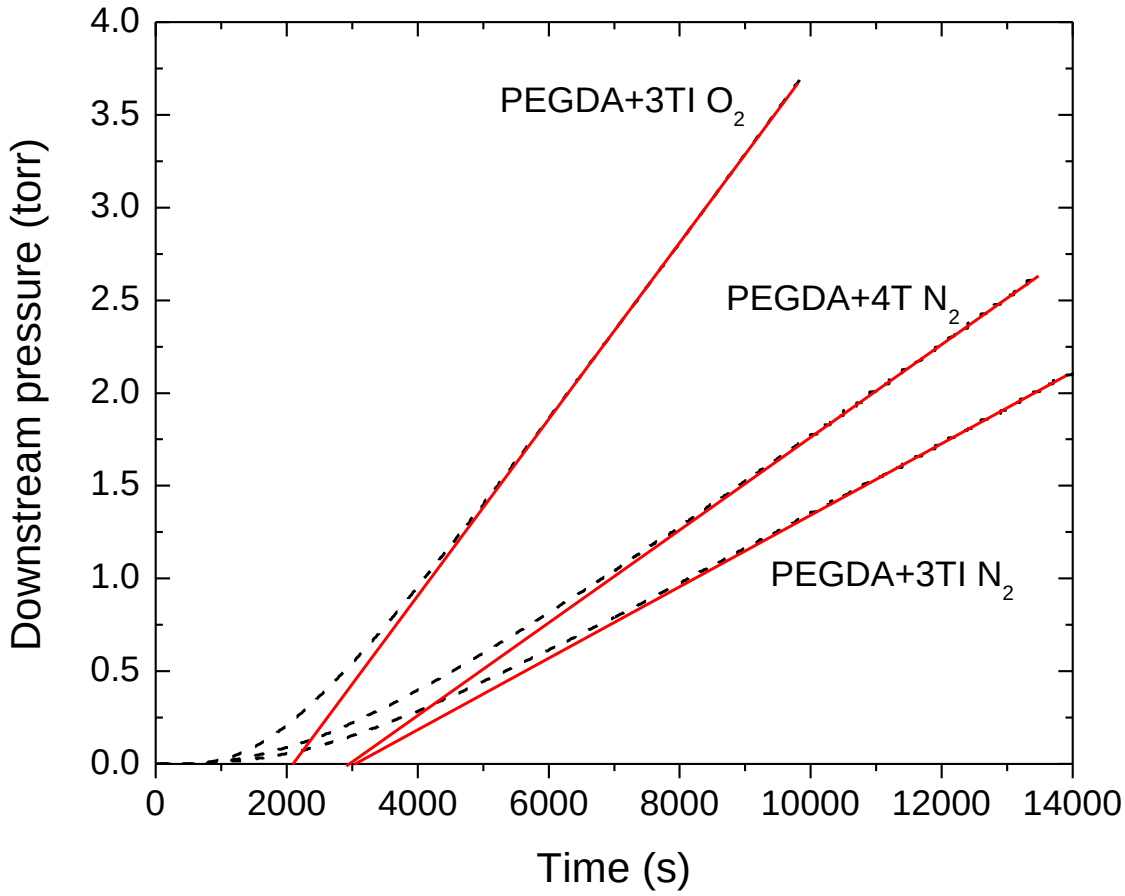

Figure VI-2. Representative permeation curves for various gases and different materials. Dashed lines are experimental downstream pressure data while solid lines are extrapolations of the steady state portion indicating the x-intercepts (which were used to calculate the time lag, t_L).

Results and Discussion

Gas Permeation

From the constant volume, variable pressure gas permeation technique described in the Experimental section, *P*, *D*, and *S* values for O_2, CO_2, and N_2 for each membrane were generated and are listed in Table VI-2A. Table VI-2B includes pure gas selectivity values for each gas pair considered in the study.

Table VI-2A. Permeability, Diffusivity, and Solubility for O_2, CO_2, and N_2 Measured at 23 °C and 3.5 atm Upstream Pressure for Each Network. Also Included for Comparison are Permeability Values for PEGDA from Literature, "XLPEGDA," Calculated for 23 °C.[25]

	Permeability, Barrer			**Diffusivity, 10^{-7} cm^2s^{-1}**			**Solubility, cc (STP) cm^{-3} atm^{-1}**		
Material	**CO_2**	**O_2**	**N_2**	**CO_2**	**O_2**	**N_2**	**CO_2**	**O_2**	**N_2**
PEGDA	53	2.2	0.88	3.8	5.8	4.7	1.06	0.029	0.014
"XLPEGDA"[25]	60	2.9	1.05	-	-	-	-	-	-
PEGDA+2TE	77	3.3	1.35	6.1	11	6.8	0.97	0.022	0.015
PEGDA+2T	66	2.7	1.11	4.7	7.3	4.4	1.06	0.028	0.019
PEGDA+3T	49	2.1	0.81	3.4	6.1	3.5	1.1	0.027	0.018
PEGDA+4T	49	2.3	0.88	3.8	5.5	3.5	1	0.032	0.019
PEGDA+3TI	52	2.4	0.94	3.1	5.1	3.2	1.28	0.036	0.022

Table VI-2B. Pure Gas Selectivities, Including Permeability (overall), Diffusivity, and Solubility Selectivity, for Each Network and Each Gas Pair at 23 °C and 3.5 atm Upstream Pressure. Also included for comparison are overall selectivity values for PEGDA from literature, "XLPEGDA," calculated for 23 °C[25]

	CO_2/N_2 Selectivity			CO_2/O_2 Selectivity		
Material	P_{CO2}/P_{N2}	D_{CO2}/D_{N2}	S_{CO2}/S_{N2}	P_{CO2}/P_{O2}	D_{CO2}/D_{O2}	S_{CO2}/S_{O2}
PEGDA	61	0.81	76	24	0.66	37
"XLPEGDA"[25]	57	-	-	21	-	-
PEGDA+2TE	57	0.9	65	23	0.55	44
PEGDA+2T	59	1.07	56	24	0.64	38
PEGDA+3T	61	0.97	61	23	0.56	41
PEGDA+4T	56	1.09	53	21	0.69	31
PEGDA+3TI	55	0.97	58	22	0.61	36

Gas permeability values for PEGDA in this study were slightly lower than those reported for "XLPEGDA" (calculated for 23 °C via van't Hoff-Arrhenius parameters) although not unreasonably so as seen in Table VI-2A.[25] Differences in sample preparation, especially photoinitiator type and concentration as well as UV light intensity, may have caused differences in network buildup during photopolymerization. Additionally, differences in statistical purity or batch-to-batch variation of the PEGDA chemical may be another source of variation. Selectivity for each gas pair was slightly higher for the PEGDA in this study although again still in reasonable agreement with the selectivity reported for "XLPEGDA." For each network, CO_2 permeability was greater than both O_2 and N_2 permeability due to the high CO_2 solubility of PEG. Table VI-1B indicates that the overall selectivies for both CO_2/N_2 and CO_2/O_2 were derived from the solubility selectivity. CO_2/O_2 selectivities were all quite similar. Interestingly, CO_2/N_2

selectivities were lower for the thiol-modified PEGDA networks but not by much. CO_2/N_2 diffusivity selectivity was slightly improved while CO_2/N_2 solubility selectivity was slightly decreased. The reason for these differences is not exactly clear. Regardless, the thiol-modified membranes remain highly selective of CO_2 despite slightly decreased ethylene glycol content. This result is consistent with literature reports where only a certain weight percentage of ether units is necessary to obtain high CO_2 selectivity as has been well documented.[9] As one specific example of this phenomenon, pure crystalline PEG, which has 100 wt% ethylene glycol, has comparable selectivity to a copolymer membrane containing only 41 wt% ethylene glycol.[28]

While selectivity was roughly equivalent, permeability increased for the membranes containing the dithiols, 2T and 2TE. The increase in gas permeability for these two thiol-modified networks was derived from an increase in diffusivity as shown in Table VI-2A. Dithiols reduced the crosslink density of the PEGDA network by linking PEGDA segments together in a linear "train" fashion. Figure VI-3 illustrates the effect of a dithiol connection in comparison with a crosslinking trithiol additive as well as a pure PEGDA network where crosslinking is strictly chain-growth. It is evident from this graphic that the well-defined step-growth thiol-ene reaction allows tuning of the PEGDA network topology by simply varying the functionality of the thiol additive. The PEGDA+2TE membrane showed a 45% higher CO_2 permeability than the PEGDA control while remaining highly selective. The PEGDA+2T network also improved permeability but to a lesser extent which was probably due to the increased rigidity of 2T as compared with 2TE. In summary there is clear improvement in the permeability of PEGDA networks modified with only 20 mol% dithiols while maintaining comparable

selectivity. The remaining thiol additives do not greatly affect the gas separation performance. Regarding the idealized schematic in Figure VI-3 note that the carbon-centered radicals, which are formed upon addition of a thiyl radical to an acrylate double bond, may undergo either chain-growth crosslinking or chain transfer to another thiol and so Figure VI-3 represents the ideal cases where only chain transfer occurs. However given the changes in permeability and other physical properties which will be discussed, it is likely a satisfactory depiction of the average network connectivity upon incorporation of multifunctional thiols in this system.

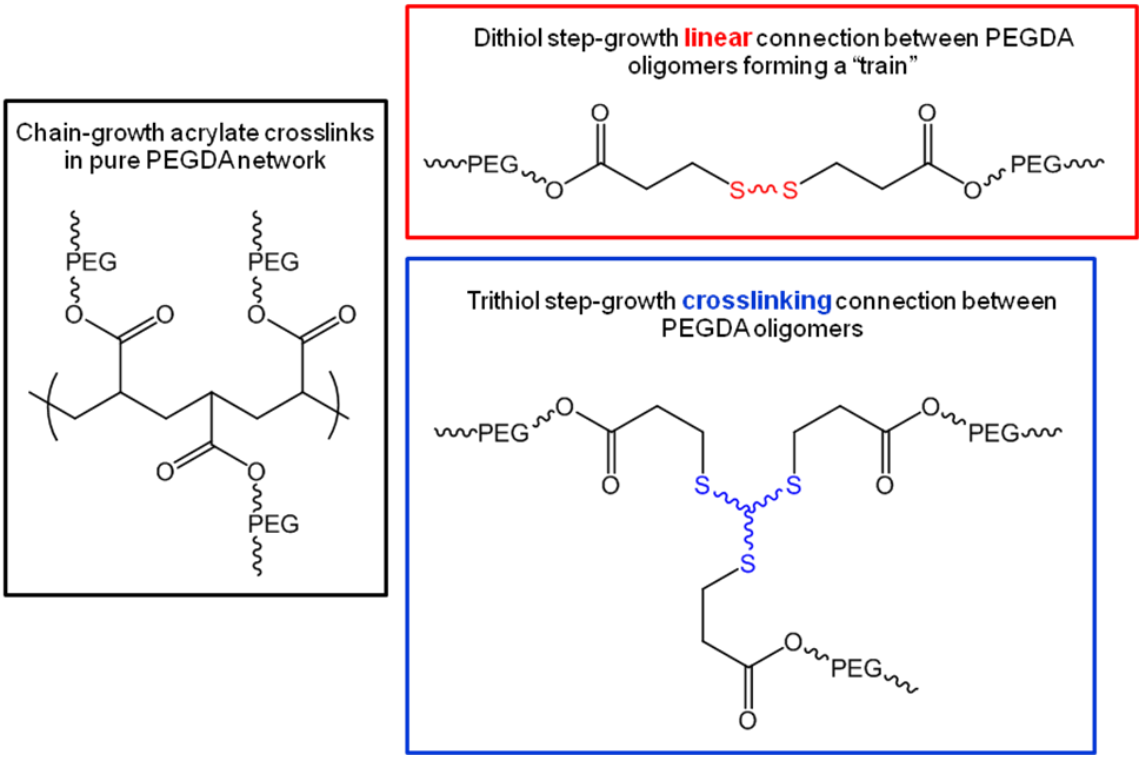

Figure VI-3. Idealized schematics comparing dense chain-growth acrylate connections to two representative thiol-acrylate step-growth connections: trithiol, a crosslinker, and dithiol, which forms linear polymer or a "train" of PEGDA oligomers.

Physical Properties

Mechanical analysis was performed on each network to verify T_g, rubbery modulus, tensile elongation, and tensile modulus as described in the Experimental section. Our interest in these properties lies in the fact that T_g, related to fractional free volume, is often used to interpret gas permeability data. Likewise, modulus (stiffness) is related to the molecular weight between crosslinks according to theories of rubber elasticity. Degree of crosslinking is also influential on gas permeability especially in rubbery polymers due to restrictions in polymer mobility.

With regards to small-strain measurements by DMTA, the experimental tan delta and storage modulus plots for each network are provided in Figures VI-4 and VI-5, respectively. Glass transition temperature values, taken as the tan delta peak, along with rubbery modulus values are reported in Table VI-3. Compared with the glass transition temperature via DMA for "XLPEGDA" from the literature,[29] the PEGDA control exhibited a slightly higher T_g which was not unexpected considering the permeability values for PEGDA fabricated in our labs for this study were also lower than those reported for "XPLEGDA."[25] This slight discrepancy was attributed to differences in sample preparation as mentioned already. Only slight decreases in T_g were observed for the thiol-modified networks with the exception of the PEGDA+3TI network which contains the rigid, isocyanurate-based 3TI thiol. However the T_g values for all networks are near -30 °C and the range is nearly within experimental scatter. The rubbery plateau moduli, shown in Figure VI-5 and tabulated in Table VI-3, indicate a measurable

decrease in modulus for each of the thiol-modified networks with respect to the unmodified PEGDA network. This decrease in modulus can be attributed primarily to a decrease in crosslink density due to the step-growth thiol-acrylate reaction. The pure PEGDA network forms only chain-growth acrylate crosslinks characterized by high crosslink density and carbon-carbon linkages. The thiol-modified PEGDA networks form, in addition to chain-growth acrylate crosslinks, step-growth thiol-acrylate crosslinks. The PEGDA+2TE network in particular has the lowest plateau modulus value which is in agreement with the permeability results. The 2TE thiol is a flexible, difunctional connection between PEGDA segments, decreasing crosslink density and perhaps imparting flexibility. The reduction in rubbery plateau modulus upon incorporation of multifunctional thiols into an acrylate network is consistent with other reports.[30-31]

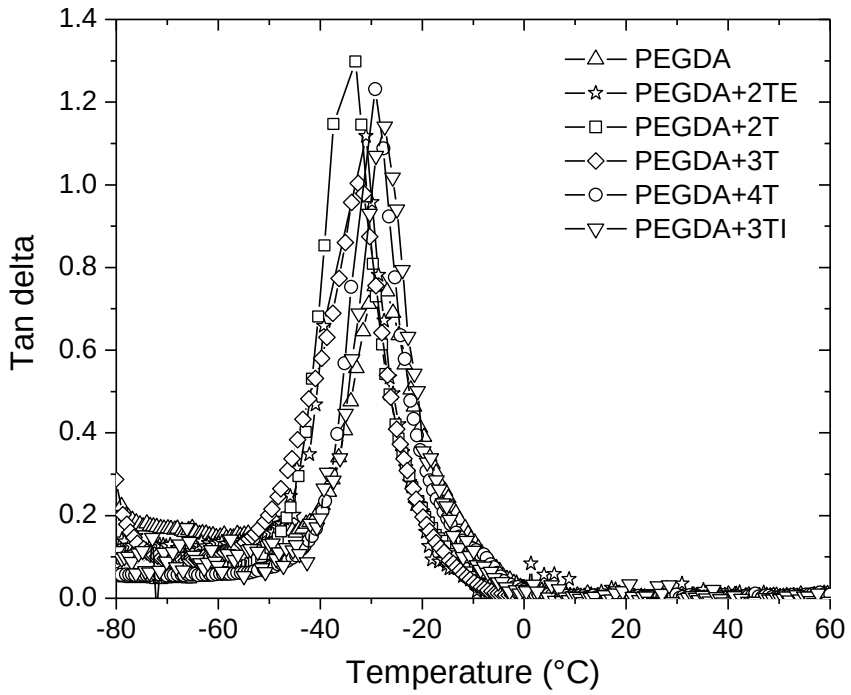

Figure VI-4. Experimental tan delta temperature sweep plots for each network.

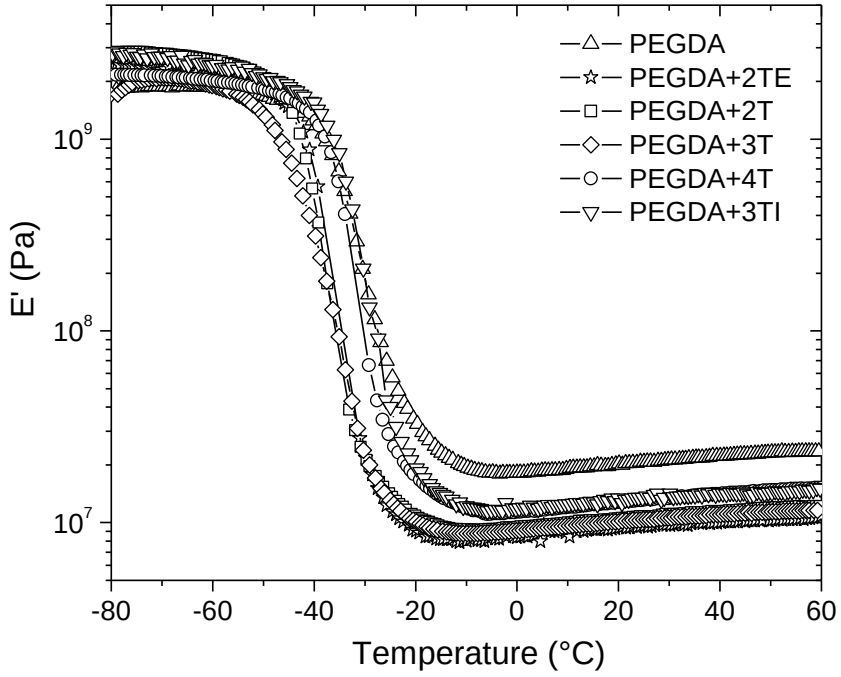

Figure VI-5. Experimental E' (rubbery modulus) temperature sweep plots for each network.

Table VI-3. Glass Transition Temperatures via Tan Delta Peak and E' (rubbery modulii) at (T_g + 50) °C for Each Material Including "XPLEGDA" for Comparison.[29]

Material	T_g (°C)	E' @ T_g + 50 (MPa)
PEGDA	-28	20.4
"XLPEGDA"[29]	-35	-
PEGDA+2TE	-31	9.3
PEGDA+2T	-33	10.4
PEGDA+3T	-33	10
PEGDA+4T	-29	12.9
PEGDA+3TI	-27	13.5

In addition to small-strain measurements, large-strain behavior of these materials was investigated via tensile testing. In a practical membrane setting, mechanical properties may play an important role in the implementation of new materials: deformation behavior and flexibility are especially significant given that gas separation membranes are often assembled in a unique manner (spiral-wound, hollow fiber, etc.) as well as being exposed to large applied pressures. As such an analysis of mechanical properties, not only to understand the effect of thiol modification, but also for the pure PEGDA network, was in order.

Representative experimental stress-strain plots are shown in Figure VI-6. All networks showed relatively low elongation at break indicative of highly crosslinked networks. Clearly the tensile modulii, or slopes, were much lower for the thiol-modified networks as compared with the pure PEGDA control. The 1% secant modulus values, along with standard deviations which were quite low, are listed in Table VI-4. Indeed the thiol-modified networks had noticeably lower modulus values in agreement with the small-strain rubbery plateau modulii obtained via DMTA. Again this decrease in modulus was due both to the decrease in crosslink density from the thiol-acrylate step-growth reaction as well as the formation of thioether (sulfide) crosslinks. Furthermore, PEGDA+2T and PEGDA+2TE, the dithiol-modified networks, showed the lowest secant modulus values while the PEGDA+4T network had the highest of the modified group, indicative of a more highly crosslinked system as compared with the other thiol additives. Strain at break values, also listed in Table VI-4, showed considerable scatter and also quite low values since these materials were highly crosslinked networks. The dithiol-modified PEGDA materials had markedly improved elongations and thus increased

toughness as implied by the area under the stress-strain curve. As these dithiols connect PEGDA segments together like a "train," we feel this topology explains the tensile behavior – less crosslinking and more linear sections allowed larger elongation of the samples. In support of this conclusion are the lower strain at break values for the tri and tetrathiol-modified PEGDA networks which are more highly crosslinked than the networks modified with dithiols.

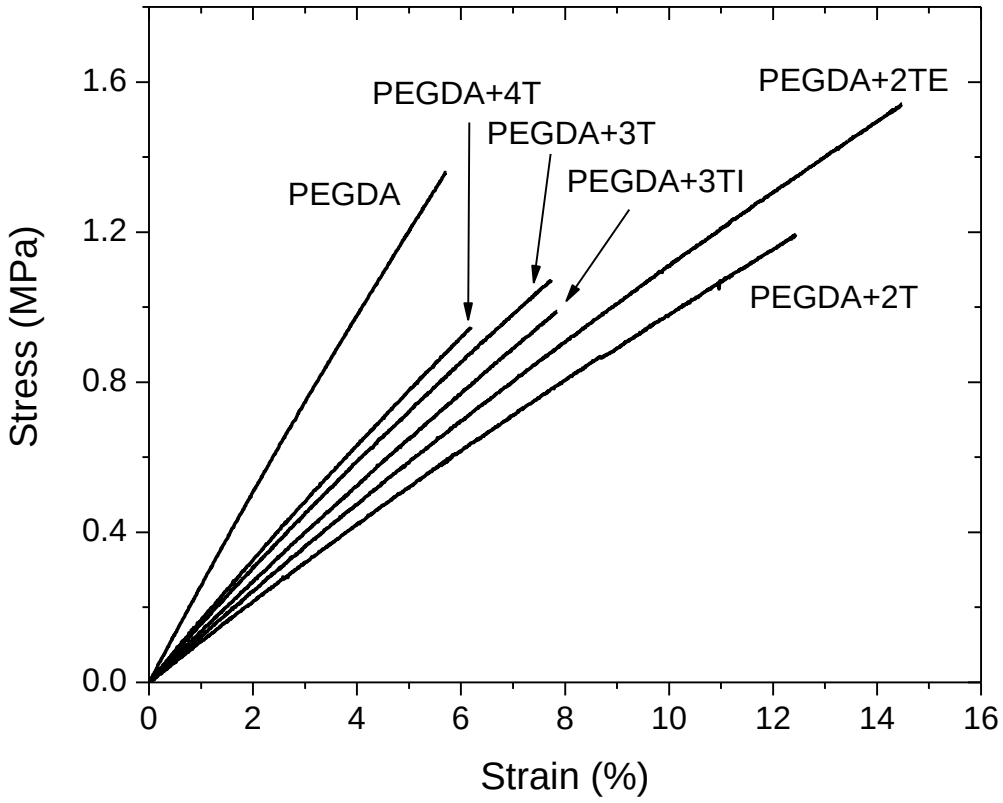

Figure VI-6. Representative experimental stress-strain plots for each material.

Table VI-4. Average Strains at Break and Secant Modulii at 1% Strain for Each Material. Corresponding standard deviations provided in parentheses

Material	Strain at Break, % (st. dev.)	1% Secant Modulus, MPa (st. dev.)
PEGDA	5.1 (0.8)	25.4 (0.6)
PEGDA+2TE	10.9 (5.1)	12.1 (0.5)
PEGDA+2T	9.0 (3.6)	11.5 (0.6)
PEGDA+3T	6.8 (1.3)	15.5 (0.2)
PEGDA+4T	5.2 (1.4)	15.8 (1.3)
PEGDA+3TI	6.3 (2.2)	13.2 (0.5)

Effect of Curing Atmosphere

Owing to the advantages of the robust and well-defined thiol-ene reaction, not only can the physical and transport properties of this system be improved, but the processing as well. The decreased oxygen inhibition of the thiol-ene reaction allowed curing of the membranes in the air and in sunlight. Acrylate group conversions were studied as a function of UV irradiation time as described in the experimental section. Under a nitrogen atmosphere all networks rapidly reached 100% conversion of acrylate groups as shown in Figure VI-5. In the case of the thiol-modified acrylate systems, the acrylate double bonds homopolymerize while the thiols add to the acrylate double bonds simultaneously. No significant differences in rate or total conversion were observed given that all systems rapidly reached 100% conversion. However in air, the conversion of each system is quite different as seen in Figure VI-8.

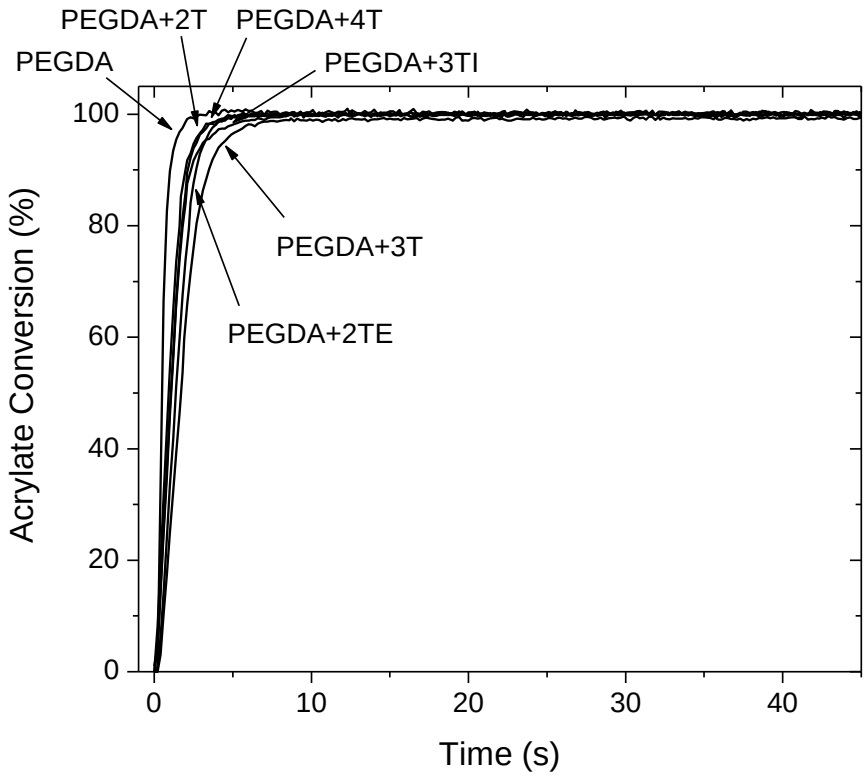

Figure VI-7. Acrylate conversion for each network under nitrogen atmosphere.

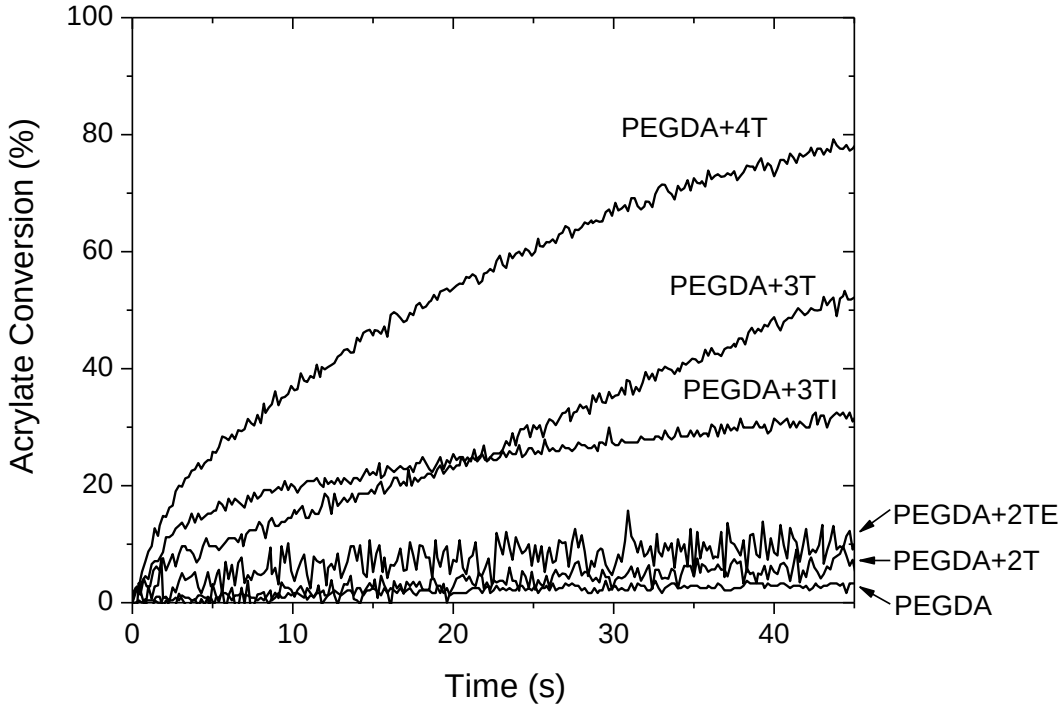

Figure VI-8. Acrylate conversion for each network under air atmosphere.

The PEGDA control network reached only 5% conversion over 45 seconds, indicative of the oxygen inhibition effect for this sample. In contrast, the PEGDA+4T thiol-modified network attained nearly 80% conversion after 45 seconds. 3T and 3TI modified networks also demonstrated strong deviations from the control network, reaching 50% and 30% acrylate conversions, respectively. The dithiols did not noticeably improve the conversion in air for this specific thickness and light intensity combination; the behavior of these dithiols compared with the higher functional thiols will be addressed later in the paper according to a viscosity effect. Overall these results highlight the value of incorporating a multifunctional thiol into a PEG-based diacrylate oligomer when curing in an air (oxygen) atmosphere. The free-radical, step-growth thiol-ene reaction is known for minimal oxygen inhibition while the free-radical, chain-growth acrylate homopolymerization reaction is hindered by oxygen due to the formation of unreactive peroxy radicals.[17]

To further demonstrate the reduced oxygen inhibition by incorporating multifunctional thiols into the acrylate mixture, tack free time studies were performed on 100 micron thick films of each network using sunlight in outdoor ambient air. As seen in Table VI-5, sunlight was able to cure (at least to the point of a non-tacky surface) all of the thiol-modified networks in a matter of minutes. The PEGDA control was still tacky on the surface after nearly 4 hours. The PEGDA membrane should indeed remain tacky on the surface indefinitely due to the constant diffusion of oxygen into the surface of the liquid film.

In terms of the outdoor sunlight curing analysis, the best performing mixture was PEGDA+4T which was tack-free in 7 minutes under these specific conditions. Following closely in tack-free time was the PEGDA+3TI system at 8 minutes and 45 seconds. The longest tack free time for the thiol-modified acrylate systems was observed for the PEGDA+2T network, tack free after 33 minutes. The differences in tack free times, as well as the real-time FTIR results, indicate that the tri and tetrathiols had a greater impact on reducing the effects of oxygen inhibition. This effect can be explained from the system viscosities.

While the viscosities of the uncured liquid mixtures are comparable according to Table VI-4, we believe that the viscosities deviate dramatically during polymerization depending on the functionality of the thiol additive. As the uninhibited thiol-acrylate reaction occured, consuming dissolved oxygen, molecular weight increased along with a concomitant increase in system viscosity/decrease of free volume. In turn reduced free volume led to decreased oxygen permeation back into the liquid mixture. Indeed, it is broadly accepted that viscosity is predominantly determined by free volume. The ranking of the thiol monomers in tack-free time during curing (an intermediate state) closely paralleled the rankings of the final cured membranes in terms of gas permeability. The tri and tetrathiol modified PEGDA membranes showed the lowest gas permeabilities as well as the shortest tack free times, reinforcing the free volume explanation.

As the uninhibited thiol-acrylate reaction occured, viscosity increased due to molecular weight buildup, decreasing concentration of chain ends, and thus decreasing free volume. This effect was more pronounced for the tri and tetrathiol additives since

they are crosslinkers; in contrast the dithiols would form only linear polymer as the thiol-acrylate reaction occurred. Additionally, each of the thiol monomers considered, with the exception of 2TE, have the same reactive groups based on mercaptopropionate. The 2TE thiol monomer may have a greater reactivity than 2T which would explain the shorter tack free time for this mixture.

Table VI-5. Tack Free Times for Each Membrane When Cured with Sunlight Under Ambient Outdoor Conditions Along With Viscosities of the Uncured Liquid Mixtures

Material	Tack-free Time (s)	Viscosity of Liquid Mixture (Poise)
PEGDA	--	1.12 ± 0.01
PEGDA+2TE	1260	0.91 ± 0.01
PEGDA+2T	1980	1.15 ± 0.02
PEGDA+3T	780	1.14 ± 0.01
PEGDA+4T	420	1.19 ± 0.00
PEGDA+3TI	525	1.37 ± 0.03

The tack-free time study, along with the curing atmosphere investigations using RT-FTIR, demonstrated that thiol-acrylate UV-curable PEG membranes may be fabricated in air and perhaps at increased line speeds and lower light intensity than a pure acrylate PEGDA membrane. If optimum curing efficiency of this PEGDA system was the goal, the 4T multifunctional thiol is recommended due to the highest conversion in IR measurements and the shortest tack-free time during sunlight curing under the conditions considered. If gas separation performance was the concern, 2TE would be the ideal

additive since it increased permeability without sacrificing selectivity. We also suppose that the ranking in curing efficiency as a result of this work would be similar for other acrylate systems but this speculation remains to be experimentally verified. Additionally, shelf life is another factor that is worth taking into account when considering thiol-acrylate mixtures.

Conclusions

An assortment of multifunctional thiols, varying in functionality and rigidity, were added to PEG-diacrylate. These mixtures were subsequently UV-cured forming new membranes for CO_2 separation. Each thiol monomer was incorporated at 20 mol% of functional groups with respect to the total amount of functional groups in the mixture. Thermomechanical analysis revealed comparable T_g and decreased rubbery modulus for each of the thiol-modified networks. The decrease in modulus was due to the step-growth thiol-acrylate reaction which reduced crosslink density. Gas permeation measurements revealed that CO_2/N_2 and CO_2/O_2 selectivities were roughly equivalent for each network regardless of the thiol monomer additive. Permeability was increased for membranes modified with dithiols while membranes modified with tri and tetrathiols showed no measurable change in permeability, both with respect to the pure PEGDA control. With regards to network topology, dithiols connected the PEGDA segments in a linear, "train-like" fashion as opposed to tri and tetrathiols which were crosslinkers. The reduction in crosslink density imparted by the dithiol additives also led to increased tensile strains at break and improved toughness. Real-time FTIR was used to monitor acrylate conversion in each system during UV-initiated polymerization in both nitrogen

and air environments. All mixtures rapidly reached 100% conversion of acrylate groups under a nitrogen atmosphere. Under air, however, the PEGDA control and the dithiol-modified PEGDA mixtures exhibited significant oxygen inhibition and reached only minuscule percent conversions. The tri and tetrathiol-modified PEGDA mixtures reached much higher conversions in only 45 seconds. This difference in conversion was likely due to an increase in system viscosity as the thiol-acrylate reaction proceeded. In the case of dithiols, the increase in viscosity is less than tri and tetrathiols which are crosslinkers and increased the system viscosity more rapidly, reducing oxygen diffusion back into the sample and allowing higher conversion of acrylate groups. As a practical demonstration of the utility of the thiol-ene reaction, 100 micron samples of the thiol-modified PEGDA mixtures were cured outdoors using sunlight. Tack-free times for these materials ranged from 7 minutes to just over 30 minutes and followed a functionality trend in accordance with the IR results (i.e., tri and tetrathiol-modified PEGDA systems were tack-free in a shorter time than PEGDA modified with dithiols). The pure PEGDA control remained uncured and tacky on the surface indefinitely. In summary, only a small amount of multifunctional thiol additives were used to increase permeability as well as to enable environmentally friendly and robust processing for this specific PEGDA membrane system without compromising mechanical properties or gas selectivity.

References

1. Bernardo, P.; Drioli, E.; Golemme, G. *Ind. Eng. Chem. Res.* **2009**, *48*, 4638-4663.
2. Koros, W. J.; Coleman, M. R.; Walker, D. R. B. *Annu. Rev. Mater. Sci.* **1992**, *22*, 47-89.
3. Stern, S. A.; Frisch, H. L. *Ann. Rev. Mater. Res.* **1981**, *11*, 523-550.
4. Koros, W. J.; Fleming, G. K. *J. Membr. Sci.* **1993**, *83*, 1-80.
5. Kawakami, M.; Yamashita, Y.; Yamasaki, M.; Iwamoto, M.; Kagawa, S. *J. Polym. Sci. Polym. Lett. Ed.* **1982**, *20*, 251-257.
6. Okamoto, K.; Fujii, M.; Okamyo, S.; Suzuki, H.; Tanaka, K.; Kita, H. *Macromolecules* **1995**, *28*, 6950-6956.
7. Hirayama, Y.; Kase, Y.; Tanihara, N.; Sumiyama, Y.; Kusuki, Y.; Haraya, K. *J. Membr. Sci.* **1999**, *160*, 87-99.
8. Lin, H.; Freeman, B. D. *J. Membr. Sci.* **2004**, *239*, 105-117.
9. Lin, H.; Freeman, B. D. *J. Mol. Struct.* **2005**, *739*, 57-74.
10. Murphy, T. M.; Offord, G. T.; Paul, D. R. *Fundamentals of Membrane Gas Separation*, in: Drioli, E., Giorno, L., (Eds.), *Membrane Operations: Innovative Separations and Transformations*, Wiley, Weinheim Germany, **2009**, pp. 63-82.
11. Robeson, L. M. *J. Membr. Sci.* **1991**, *62*, 165-185.
12. Robeson, L. M. *J. Membr. Sci.* **2008**, *320*, 390-400.
13. Lin, H.; Van Wagner, E.; Swinnea, J. S.; Freeman, B. D.; Pas, S. J.; Hill, A. J.; Kallakkunnath, S.; Kalika, D. S. *J. Membr. Sci.* **2006**, *276*, 145-161.
14. Lin, H.; Freeman, B. D.; Kalakkunnath, S.; Kalika, D. S. *J. Membr. Sci.* **2007**, *291*, 131-139.

15. Kusuma, V. A.; Freeman, B. D.; Borns, M. A.; Kalika, D. S. *J. Membr. Sci.* **2009**, *327*, 195-207.

16. Kusuma, V. A.; Matteuci, S.; Freeman, B. D.; Danquah, M. K.; Kalika, D. S. *J. Membr. Sci.* **2009**, *341*, 84-95.

17. Kloosterboer, J. G. *Adv. Polym. Sci.* **1988**, *84*, 8-68.

18. Hoyle, C. E.; *Photocurable Coatings*, in: C.E. Hoyle, J.F. Kinstle (Eds.), *Radiation Curing of Polymeric Materials*, ACS, Washington D.C., **1990**, pp. 1-16.

19. Hoyle, C. E.; Lee, T. Y.; Roper, T. *J. Polym. Sci., Part A: Polym. Chem.* **2004**, *42*, 5301-5338.

20. Iha, R. K.; Wooley, K. L.; Nystrom, A. M.; Burke, D. J.; Kade, M. J.; Hawker, C. J. *Chem. Rev.* **2009**, *109*, 5620-5686.

21. Hoyle, C. E.; Bowman, C. N. *Angew. Chem. Int. Ed.* **2010**, *49*, 1540-1573.

22. O'Brien, A. K.; Cramer, N. B.; Bowman, C. N. *J. Polym. Sci., Part A: Polym. Chem.* **2006**, *44*, 2007-2014.

23. Kwisnek, L.; Hoyle, C. E.; Nazarenko, *Macromolecules* **2009**, *42*, 7031-7041.

24. Kwisnek, L.; Kaushik, M.; Hoyle, C. E.; Nazarenko, S. *Macromolecules* **2010**, *43*, 3859–3867.

25. Lin, H.; Freeman, B. D. *Macromolecules* **2006**, *39*, 3568-3580.

26. Barrer, R. M.; Rideal, E. K. *Trans. Faraday Soc.* **1939**, *35*, 628-643.

27. Bondar, V. I.; Freeman, B. D.; Pinnau, I. *J. Polym. Sci., Part B: Polym. Phys.* **2000**, *38*, 2051-2062.

28. Yoshino, M.; Ito, K.; Kita, H.; Okamoto, K.-i. *J. Polym. Sci., Part B: Polym. Phys.* **2000**, *38*, 1707-1715.

29. Kalakkunnath, S.; Kalika, D. S.; Lin, H.; Freeman, B. D. *J. Polym. Sci., Part B: Polym. Phys.* **2006**, *44*, 2058-2070.

30. Cramer, N. B.; Bowman, C. N. *J. Polym. Sci., Part A: Polym. Chem.* **2001**, *39*, 3311-3319.

31. Chan, J. W.; Wei, H.; Zhou, H.; Hoyle, C. E. *Eur. Polym. J.* **2009**, *45*, 2717-2725.

CHAPTER VII

ROBUST, PHOTOCURABLE PEG-BASED THIOL-ENE NETWORKS FOR MEMBRANE CO_2 SEPARATION

*Luke Kwisnek, Stephen R. Heinz, Jeffrey S. Wiggins, Sergei Nazarenko**

Abstract

The mechanical properties and CO_2 separation performance of a robust new family of photopolymerized ethyleneglycol-containing crosslinked networks formed using thiol-ene chemistry are reported. Starting with a highly-crosslinked ethyleneglycol-containing thiol-ene network, the crosslink density was gradually decreased along with a concomitant increase in ethyelenglycol content by diluting the formulation with an ethyleneglycol-containing dithiol. Both thiol and ene groups for each formulation rapidly reached 100% conversion. Glass transition temperature and rubbery plateau modulus both decreased with increasing dithiol content. Glass transition temperature leveled off, however, for the materials containing the highest concentrations of dithiol. This leveling off was corroborated by gas permeation analysis which revealed nearly a four-fold increase in gas permeability and a subsequent leveling off for the same materials. It was proposed that chain entanglements, acting as physical crosslinks, restricted the further increase in free volume which likely controlled both T_g and permeability for this series of networks. CO_2 selectivity over both O_2 and N_2 was high for each material; the selectivity was derived from high CO_2 solubility which is typical for PEG-based membranes. Interestingly, despite increasing the PEG content from 38

wt% to 67 wt% across the series, solubility of each gas remained relatively constant. Increases in permeability were thus due solely to increased diffusivity. Improvements to gas separation performance were coupled with increases in the mechanical integrity of the films: the addition of dithiol evolved the films from a brittle material (no dithiol) to a truly robust, elastomeric material at the highest concentrations of dithiol. The equation of state for ideal rubbers was applied to stress-strain data which allowed calculation of M_c, the number-average molecular weight between crosslinks. M_c derived from this experimental approach was on average two times greater than the ideal M_c predicted via stoichiometry. This systematic variation was reconciled using a front factor correction of ~0.5 for the equation of state model.

Introduction

Polymeric membrane gas separation is a large and rapidly growing industry. While the gas combinations involved in separations are quite varied, CO_2 is a key component in numerous processes including natural gas purification, power plant flue gas capture, modified atmosphere packaging for fresh produce, and hydrogen purification.[1-3] Poly(ethyleneglycol) (PEG) is known for its high CO_2 solubility selectivity and has been researched extensively as a selectivity-providing component in all sorts of polymer membranes.[1-10] The affinity-based selectivity that PEG provides is an attractive quality since low T_g, rubbery materials may be used. Such materials do not undergo physical aging and can also have extremely high permeability. Unfortunately pure PEG crystallizes to ~70 vol% resulting in low gas permeability.[4,8] In order to achieve high permeability membranes, PEG has been employed in phase-separated blends of block

copolymers made via solution casting[10-13] and in UV-cured (meth)acrylate-functional amorphous crosslinked networks.[4,7,9,15]

Photopolymerizing a basic PEG-diacrylate yielded membranes with high PEG content, selectivity comparable to pure semi-crystalline PEG, while increasing CO_2 permeability by an order of magnitude.[4] This basic material is highly crosslinked though and it is known that crosslinking generally limits gas permeability due to mobility and free volume restrictions. This limitation is undesirable for commercial membranes which must be highly permeable as well as highly selective.[15] Decreasing the crosslink density of PEG-diacrylate networks by incorporating PEG-monoacrylates (such as PEG-methyletheracrylate, PEGMEA), was shown to dramatically improve permeability while maintaining CO_2/non-polar gas selectivity.[16-17] This performance improvement was attributed to a decrease in crosslink density and an increase in the number of methylether end groups, both of which dramatically increased free volume and thus permeability.[16-17]

The PEG-based acrylate family of crosslinked network membranes, in addition to demonstrating promising separation performance, employ the inherent advantages of UV cured or photopolymerized materials.[18-20] Among these advantages are the use of eco-friendly, solvent-free, 100% reactive component liquids, rapid processing of large areas of material, and high energy efficiency as compared with traditional thermal processing methods.[18-20] For these reasons, photopolymerized acrylates in particular are in widespread use as adhesives, coatings, and inks in a multitude of applications.[18-20] It is likely that the fabrication of permselective membranes would also benefit from these advantages.

With these advantages come two specific drawbacks to UV-cured acrylates: oxygen inhibition and high shrinkage.[18-20] UV-cured thiol-enes, in contrast, are insensitive to oxygen and have inherently low shrinkage because of the step-growth nature of the thiol-ene reaction.[21-23] The processing of thiol-enes is more energy efficient and forgiving as a result of these differences. We have been involved in exploring UV-cured thiol-ene materials for barrier and membrane applications.[24-26] Recently, our group showed that a small amount of multifunctional thiol additives could be used to improve the processing, gas separation performance, and mechanical properties of PEG-diacrylate membranes.[26] The work reported herein presents a new, mechanically robust family of photocurable PEG-containing membranes using only thiol-ene chemistry. Similar to the work by Freeman[16-17] and Hirayama,[7] we start with a highly crosslinked PEG-containing polymer network. By diluting the original formulation with increasing amounts of a PEG-containing dithiol while maintaining a 1:1 thiol:ene ratio, crosslink density will be decreased while simultaneously increasing PEG content. These modifications are expected to yield overall performance enhancements over the initial highly crosslinked and brittle material. Relationships between PEG content, crosslink density, gas permeation and selectivity, and mechanical properties will be elucidated for this robust, photocurable, PEG-based membrane platform.

Experimental

Materials

Ethyleneglycol-containing components, specifically the diene, triethyleneglycol divinylether (TEGDVE), and the dithiol, ethylenedioxy diethanethiol (EDDT), were

obtained from Aldrich. Multifunctional thiol crossslinker, trimethylolpropane tri(3-mercaptopropionate) (3T), was provided by Bruno Bock. The photoinitiator, 2,2-dimethoxy-2-phenylacetophenone (DMPA), was also obtained from Aldrich. All materials, shown in Figure VII-1, were used as received.

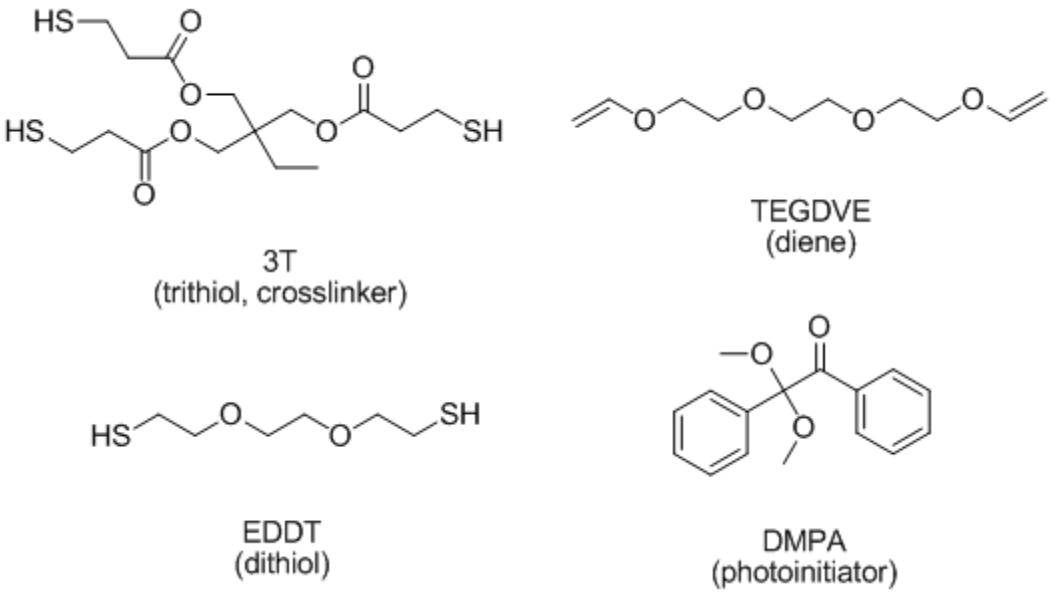

Figure VII-1. Chemical structures used in this work.

Sample Preparation

Each membrane prepared for this work was fabricated by incorporating the thiol and ene monomers (according to the recipes shown in Table 1) into a vial, adding 1 wt% DMPA photoinitiator, followed by sonication for ~10 mins to dissolve the initiatior and remove any bubbles. These mixtures were then poured onto glass plates and sandwiched by a top glass plate with shims to control the thickness to ~0.5 mm and cured by 10 passes (5 top side, 5 reverse side) at 3 m/min belt speed under a high-intensity Fusion UV

EPIQ 6000. Prior to performing any characterization or testing, films were normalized at room temperature in air for several days. The compositional information for each formulation is provided in Table VII-1. The percent of thiol groups from EDDT was increased while simultaneously decreasing the amount of 3T in order to maintain 1:1 thiol:ene stoichiometry. In this manner, each membrane material will be referred to by the percent contribution of thiol groups from the dithiol; as the percentage number increases, crosslink density decreases. For example, 0% represents a network composed solely of 3T and TEGDVE while 95% denotes a membrane where 95% of the thiol groups are provided by EDDT and only 5% via 3T. The 95% formulation approached the limit of forming a solid film – higher percentages of EDDT resulted in tacky samples unsuitable for testing. A hypothetical formulation of 100% would yield linear polymer although such a formulation, when UV cured, only increases in viscosity and does not solidify. Note that for each formulation, the molar concentration of TEGDVE is identical since this is the only ene component. This naming scheme was borrowed from similar work on elastomeric, lightly crosslinked thiol-ene networks with tuned moduli.[27]

The general fabrication procedure already described was employed for forming the membrane samples for gas permeation analysis. Additionally, DMTA samples were carefully cut from the material prepared in the same way. Tensile "dogbone" samples were prepared using custom-made silicone rubber molds with dimensions according to ASTM D638 Type V specimens with 1.5 mm mold depth. Mold features were filled with formulation mixtures and then covered with glass plates and cured under a medium pressure mercury lamp with light intensity of xx mW/cm^2 at 254 cm^{-1} for 30 seconds of

exposure time. Cured tensile samples were then easily peeled from the mold and excess flash was carefully trimmed with a razor blade.

Table VII-1. Compositional Information for Each Formulation. "Parts" columns denote relative molar amount of each component.

Formulation Name	Parts EDDT	Parts 3T	Parts TEGDVE	wt% ethyleneglycol
0%	0	67	100	38
20%	20	53	100	43
40%	40	40	100	49
60%	60	26.7	100	55
80%	80	13.3	100	62
90%	90	6.7	100	65
95%	95	3.3	100	67

Characterization

Functional group conversions were monitored using a Thermo Fisher Scientific Nicolet 8700 FT-IR spectrometer modified with a fiber-optic cable to irradiate liquid samples. Sample preparation involved sandwiching a droplet of sample liquid (approximately 0.03 mL) between two salt plates. Change in peak area of thiol –SH groups at 2570 cm^{-1} (S-H stretch) and ene C=C groups at 3080 cm^{-1} (vinyl C-H stretch) were monitored as a function of irradiation time. An OmniCure Series 1000 light source with light intensity of 20 mW/cm^2 at 365 nm was used to irradiate the samples and invoke photopolymerization under a nitrogen purge.

Dynamic mechanical properties were evaluated using a Rheometric Scientific DMTAV with a frequency of 1 Hz, strain rate of 0.05%, and heating rate of 5 °C/min. T_g

values were taken as the peak maximum of tan delta plots. Tensile tests were performed on ASTM D638 Type V specimens at ambient conditions using an MTS Insight 10 electromechanical test frame equipped with a 2.5 kN load cell. Tests were conducted in duplicate at a strain rate of 1.3 mm/min strain rate and 30 mm gage length. Bulk density was recorded at ambient conditions via the Archimedes method using an analytical balance; mass was recorded to the fourth decimal place and each sample was measured in duplicate.

Permeation of nitrogen, oxygen, and carbon dioxide were measured using a custom-built gas permeation device based on a constant-volume, variable pressure (manometric) technique as previously described by our group.[26] This apparatus is also similar to those described in the literature.[8-10] All permeation measurements were conducted at 3.5 atm applied upstream pressure. The permeation cell was maintained at a constant temperature, i.e. 23 °C, via a recirculating chiller. All film samples were degassed under high vacuum for 24 hours prior to testing. Experimental curves provided in Figure VII-2 exhibit typical Fickian behavior with well-defined steady-state slopes, and are representative of those not shown. The black dashed lines are experimental data reported by the differential pressure transducer. The red lines are the steady-state, constant slope, portions of the permeations curves extrapolated down to a zero value of downstream pressure, the x-intercept. Technically the slopes were determined via conducting a linear fit to the steady-state experimental data using Origin graphing software. Using this slope value along with Equation 1, permeability values were calculated where P is the permeability, V_d is the downstream volume, l is the membrane thickness, p is the applied upstream pressure, A is the testing area, R is the universal gas

constant, T is the temperature, and dp/dt is the steady-state slope.[8] Diffusion coefficients were calculated from time lag values, t_L, i.e. the intersections of the steady state line extrapolations with the x-axis according to Equation 2. S was then calculated from known permeability and diffusivity coefficients as follows: $P=DS$.

$$P = \frac{V_d l}{pART}\left(\frac{dp}{dt}\right) \quad (1)$$

$$D = \frac{l^2}{6t_L} \quad (2)$$

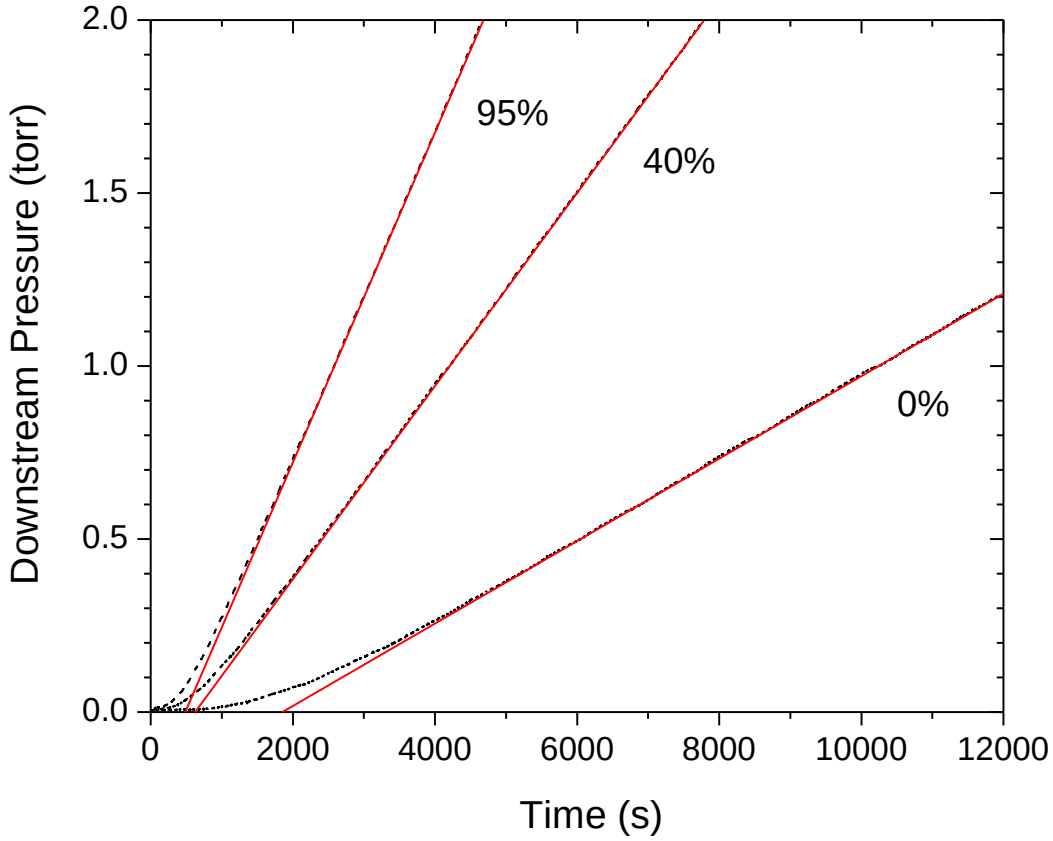

Figure VII-2. Representative nitrogen permeation curves at 23 °C and 3.5 atm upstream pressure for three materials denoted by the percent EDDT in the formulation. Black dashed lines are experimental downstream pressure data while red lines are extrapolations of the steady state portion indicating the x-intercepts (which were used to calculate the time lag, t_L).

Results and Discussion

Analysis of Functional Group Conversion

A relevant first step in the verification of new polymer materials is the analysis of functional group conversion. Conversion is especially important in photopolymerized crosslinked networks since linear sections and crosslinks are built up simultaneously sometimes leading to complications. In order to verify high functional group conversion

of each material for this new family of crosslinked networks, real-time FTIR was employed as described in the Experimental section. Thiol and ene conversions as a function of UV irradiation time are shown in Figures VII-3A and VII-3B, respectively. Each formulation rapidly reached 100% conversion of both thiol and ene groups. A slight dependency of polymerization rate on EDDT content was observed: formulations containing more EDDT, the dithiol, and less 3T, the crosslinker, reached maximum conversion at earlier times. This was due to increased mobility and decreased crosslinking in materials with increasingly greater amounts of EDDT. However, these differences were minuscule especially considering the relatively low light intensity used for this specific experiment. While it is unclear how the different reactivity between EDDT and 3T would affect network buildup, the light intensity used for curing films for physical testing was much higher and so we assume a negligible effect from reactivity differences.

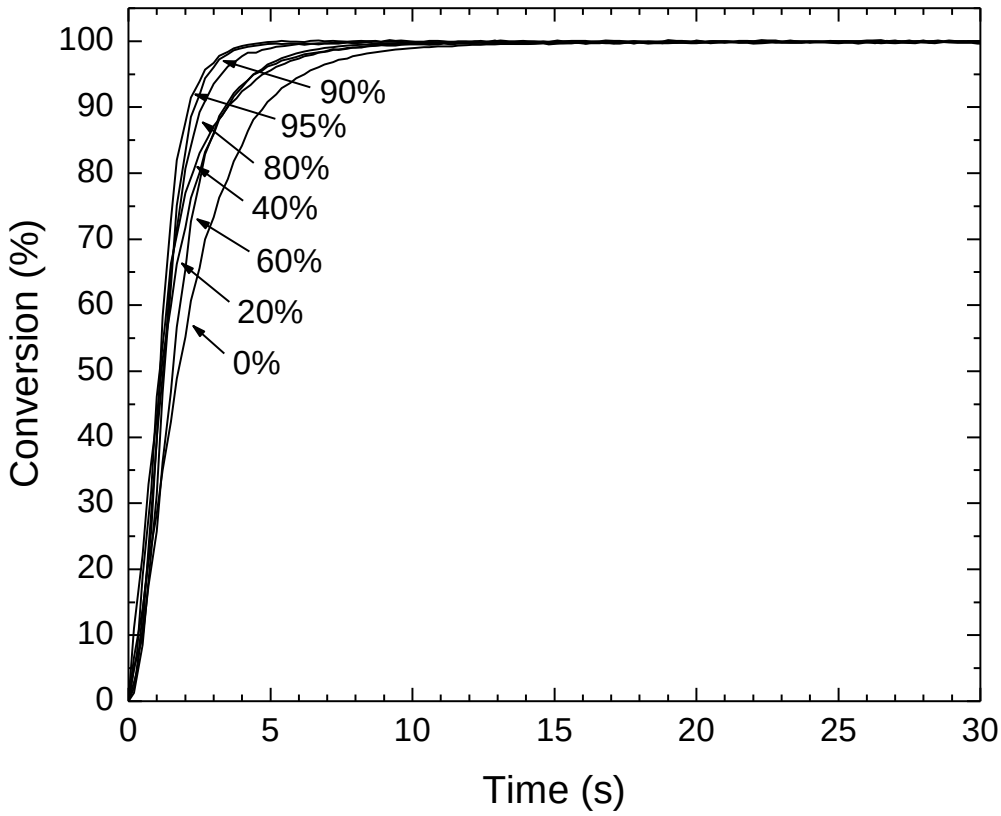

Figure VII-3A. Thiol (S-H stretch at 2570 cm^{-1}) conversion versus time. Labels indicate percent of thiol groups from EDDT.

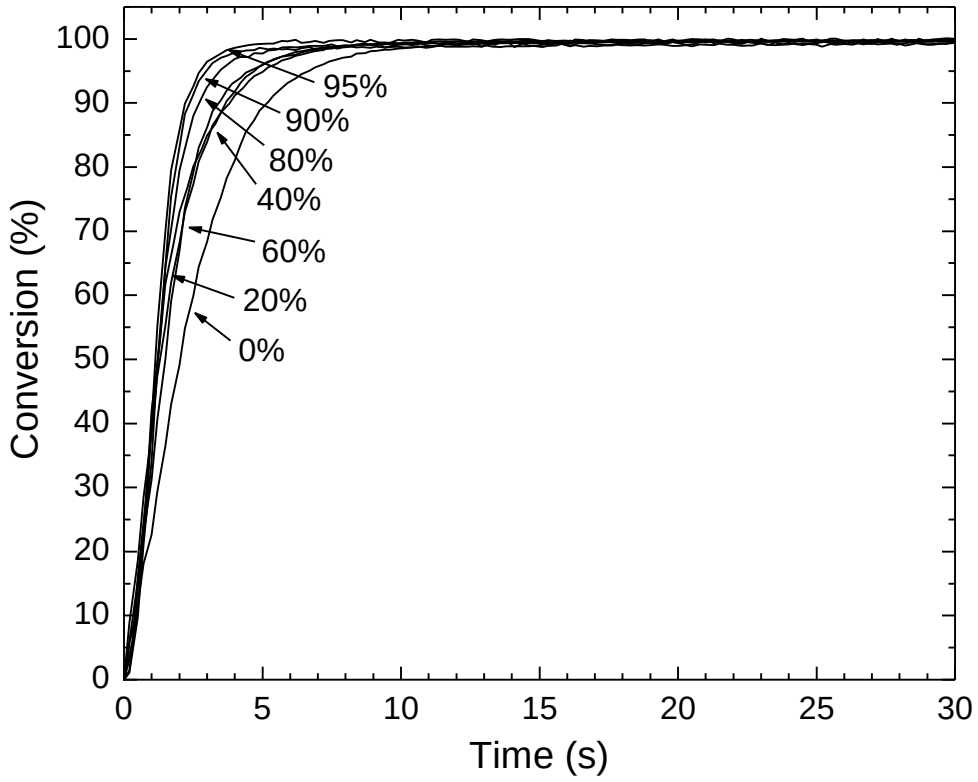

Figure VII-3B. Ene (vinyl C-H stretch at 3080 cm^{-1}) conversion versus irradiation time. Labels indicate percent of thiol groups from EDDT.

Investigation of Mechanical Properties

Because T_g is known to influence gas permeability and also owing to the strong relationship between modulus and crosslink density in polymer networks, a mechanical property investigation including both small strain and large strain measurements was in order. Small strain DMTA temperature sweep measurements were conducted in duplicate on each material according to specifications given in the Experimental section. Experimental curves, although not shown, all exhibited narrow glass transitions which are characteristic of the uniformity of thiol-ene networks in general. Rubbery plateau

moduli, taken at 23 °C, and T_g values, taken as tan delta peak, for duplicate measurements were averaged and are presented as a function of EDDT content in Figure VII-4A and VII-4B, respectively. Error bars represent +/- one standard deviation. Rubbery modulus displayed a general decreasing trend as a function of EDDT content shown in Figure VII-4A. This trend, which spanned nearly an order of magnitude, was expected due to the significant decrease in 3T crosslinker across the series of networks. T_g also decreased linearly but only up to the 80% formulation. The 90% and 95% formulations deviated from this trend by exhibiting T_g values higher than expected. T_g for these sparsely crosslinked networks appeared to level off or even increase slightly as a function of EDDT content. It is suspected that this deviation is due to entangelements. As the crosslink density decreases, leading to higher molecular weight between crosslinks, the linear sections are able to entangle subsequently limiting long-range segmental motion. These mobility-restricting entanglements likely prevented further free volume increases, causing T_g to level off. We suspect that the physical crosslinks are not strong enough to influence the rubbery plateau modulus which does not show the deviation observed for T_g. The glass transition, in contrast, is based on chain dynamics and is likely more sensitive to weak entanglement forces. Average values for T_g and rubbery plateau modulus are also shown in Table VII-2 for convenience.

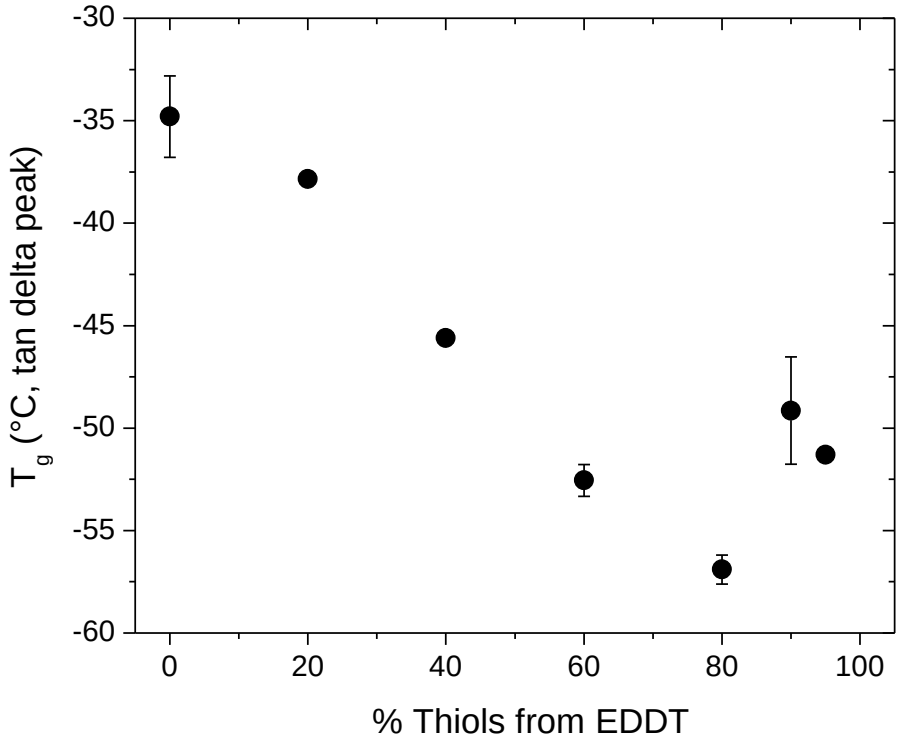

Figure VII-4A. T_g via tan delta peak as a function of EDDT content. Error bars represent +/- one standard deviation.

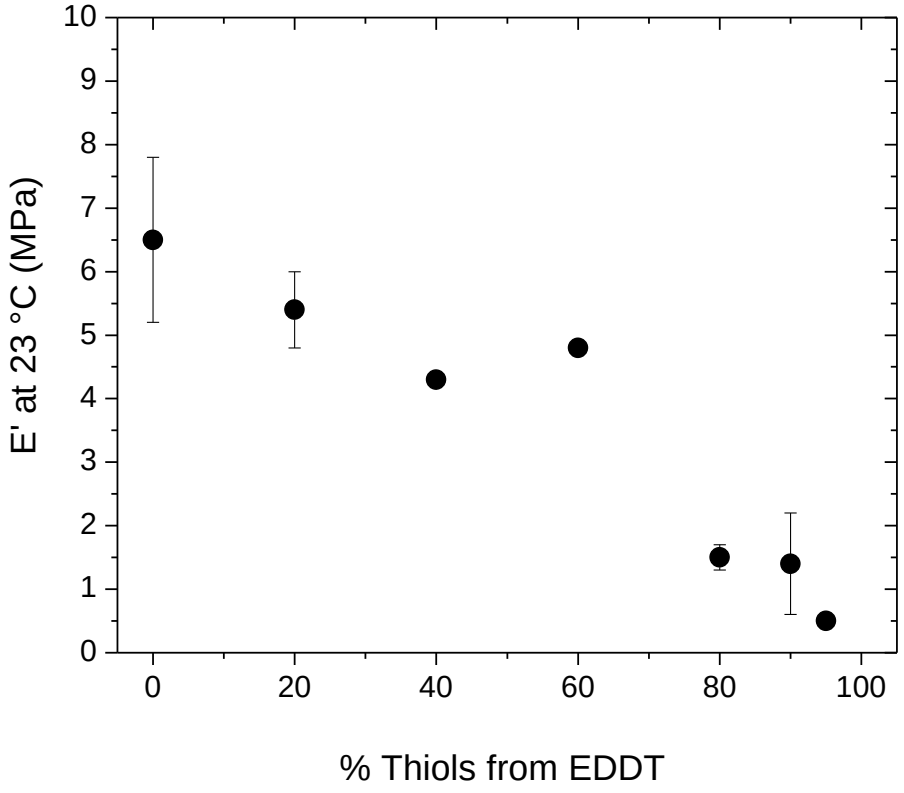

Figure VII-4B. Rubbery plateau modulus at 23 °C as a function of EDDT content. Error bars represent +/- one standard deviation.

The crosslinking reduction strategy used in this approach brought about significant changes to the overall mechanical properties as well. As EDDT content increased the materials became more flexible and also more elastomeric/stretchy. Tensile testing was used to characterize these observations more clearly. As detailed in the Experimental section, tensile tests were performed in duplicate. Figure VII-5 reports one representative experimental stress-strain curve for each material. As EDDT content increased, as denoted by the labels, tensile modulus (slope) significantly decreased. The

decrease in average modulus, reported in Table VII-2 as 1% secant modulus, is in excellent agreement with the decrease in rubbery plateau modulus via DMTA measurements and was due to the decreased crosslink density as EDDT content increased. Elongation at break, however, was not so straightforward.

A break in the strain axis was required to properly display each curve. The axis break also indicates that there were two distinct groups within this material family: those with elongation at break less than 20%, and those with elongation at break greater than 50%. Average values for elongation at break are included in Table VII-2 for completeness. Disparity between the two material sub-groups occurred between 80% and 90% thiols from EDDT in the formulation. The low elongation of the first group, indicative of brittle failure, is typical for highly crosslinked networks. The high elongation of the second group is typical of elastomeric behavior due high molecular weight between crosslinks. These linear sections follow random coil behavior in the relaxed state. When elongated or stretched, the random coils straighten and orient along the axis of draw. The 90% and 95% materials, which exhibited random coil elastomeric tensile behavior, were also the materials which deviated from the T_g trend via DMTA. It is likely that the two phenomena are related. In the relaxed, random coil state, the long polymer chains between junction points are somewhat entangled which may limit long-range segmental motion and free volume which control the glass transition.

The elastomeric quality of the high elongation materials, known as 90% and 95%, may be important for modified atmosphere food packaging films or other emerging applications where membrane flexibility and durability are important. Also note that the mechanical behavior reported for this family of UV-cured, PEG-containing thiol-ene

membrane materials are superior to the mechanical behavior of PEG-containing acrylate networks such as PEGDA which exhibit low elongation, poor flexibility, and brittle failure.[26]

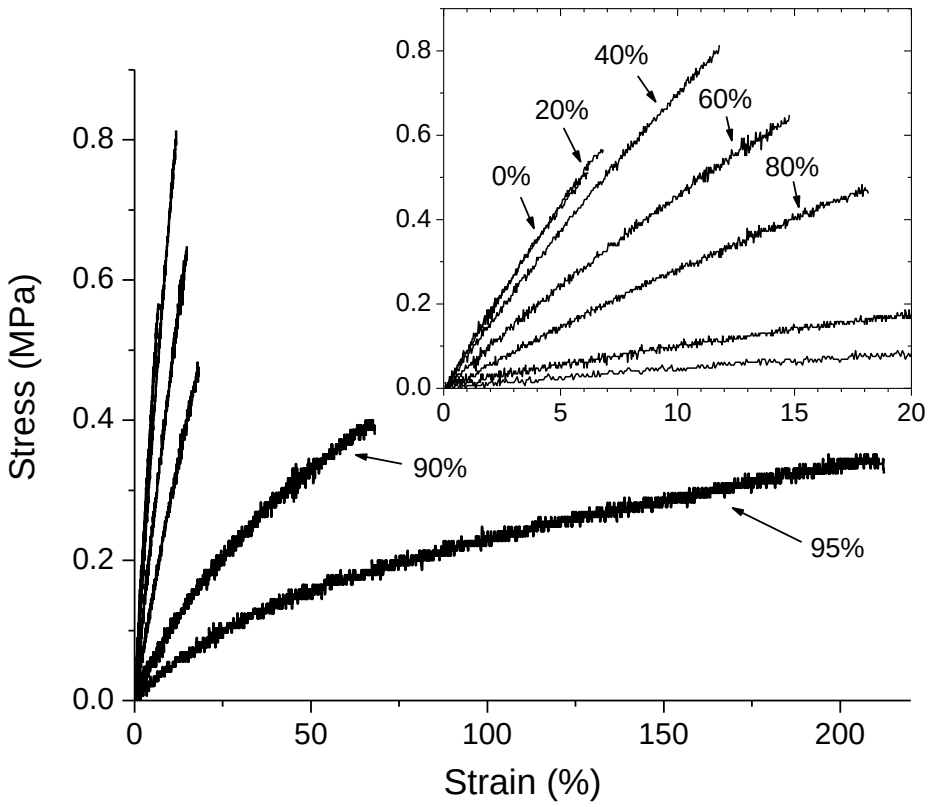

Figure VII-5. Representative experimental stress-strain curves for each material. Inset provides rescaled plot for detail of materials with relatively low elongation at break. Labels indicate percent of thiol groups from EDDT.

Table VII-2. Average T_g via DMTA Tan Delta Peak, Average E' Rubbery Plateau Modulus via DMTA at 23 °C, and Average 1% Secant Modulus and Average Elongation at Break via Tensile Testing. Material designation indicates percent thiol groups from EDDT

Material	T_g (°C)	E' @ 23 °C (MPa)	1% Secant Modulus (Mpa)	Elongation at Break (%)
0%	-35	6.5	10.44	5.9
20%	-38	5.35	10.04	6.8
40%	-46	4.25	8.14	11
60%	-53	4.8	5.21	14
80%	-57	1.45	3.69	18
90%	-49	1.43	1.23	70
95%	-51	0.53	0.74	224

Owing to the quality of the stress-strain data, the vast window of crosslink density explored, as well as the absence of dangling chain ends at least hypothetically, we felt that this series of thiol-ene networks presented an opportunity to employ a stress-strain model in order to extract useful parameters such as M_c, the number-average molecular weight between crosslinks. The model chosen for this work was the basic equation of state for an ideal rubber given in Equation 3.[28-30]

$$\sigma = \frac{A\rho RT}{M_C}\left(\alpha - \frac{1}{\alpha^2}\right) \tag{3}$$

This model considers the rubber as a perfect continuum with affine deformation characteristics.[28-30] Model parameters include ρ the bulk density in g/cc, α the elongation ratio or L/L_0, a unitless parameter, R the gas constant taken as 8.314 J/K mol, T the temperature in Kelvin, and stress in MPa. Unit conversions were made when necessary

for calculation. There is sometimes a front factor or similar variable applied to the right hand side, denoted as A, in order to account for crosslink functionality or other effects.[28] For fitting of experimental data the front factor was assumed to be unity. Fitting required a plot of stress versus the quantity in parentheses yielding the slope as the combined outer factor which is sometimes referred to as the Young's modulus, E. Figure VII-6 demonstrates the excellent fit of this model where filled circles are actual experimental data and the red lines are the fit to Equation 3. The excellent fit of the entire curves, at least for samples containing up to 80% thiol groups from EDDT, are direct evidence of the uniformity or ideal nature of thiol-ene networks. Our evidence supports the numerous reports in the literature with regard to uniformity of thiol-ene networks as indicated by their narrow glass transition regions, their tendency to gel at high conversion, and their low shrinkage. Past 0.5 on the x-axis scale the model deviates from a linear fit. Deviation was only observed for the two elastomeric materials, i.e. the 90% and 95% formulations. Although not shown, the stress values for these materials decreased with increasing x-axis values, a classic example of temporary physical crosslinks from entanglements.[31] The entanglements are temporary, or deformation dependent, since as the samples are elongated and the random coils straighten, the entanglements unravel causing a reduction in stress and thus modulus as a function of increasing elongation.[31]

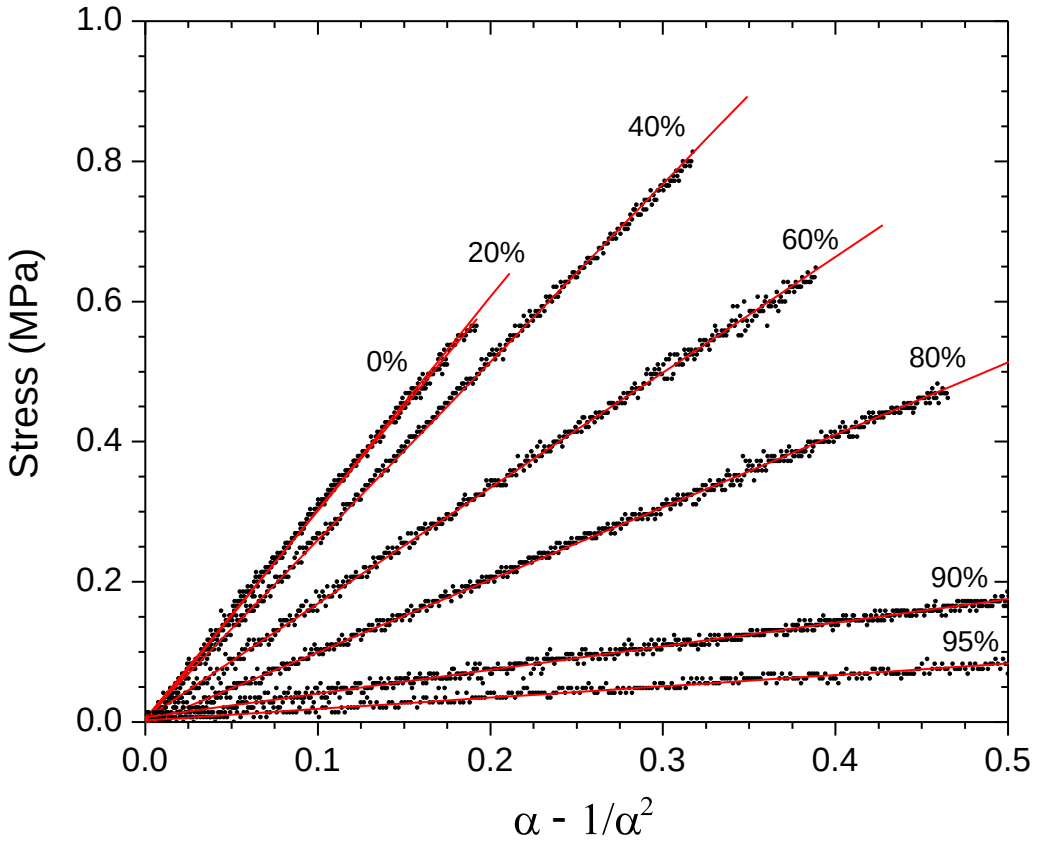

Figure VII-6. Representative model fits of experimental stress-strain data to Equation 3. The fit was satisfactory in each case including those not shown with R^2 values generally greater than 0.99. Labels indicate percent of thiol groups from EDDT.

The average slope of each material was obtained via Equation 3 and reported in Table VII-2. Combining these values with bulk density at ambient conditions as discussed in the Experimental section, the number-average molecular weight between crosslinks, M_c, was determined. A predicted M_c was also calculated using stoichiometry where each 3T represents a junction point for 1.5 active chains.[31] This simple calculation considers the crosslinked polymer as a completely connected network with no dangling

ends which is appropriate for this series of thiol-ene networks.[31] Both experimental and hypothetical M_c values are included in Table VII-2 and are also plotted in Figure VII-7. A systematic variation was observed. The slope of this plot is 0.54 with $R^2 = 0.989$ indicating with some confidence that the real M_c determined experimentally was roughly one-half the M_c predicted by stoichiometry. Surprisingly the relationship held quite well across a vast window of crosslink density. Different explanations for this variation were explored. Intramolecular crosslinks like cyclic/loops, structures which do not contribute to the modulus, could offer an explanation. However, it has been shown that thiol-ene networks undergo only negligible cyclization or intramolecular crosslinking events due to the free-radical step-growth thiol-ene mechanism.[32-33] Furthermore, the observed difference between experiment and prediction was systematic. A more appropriate explanation lies in a front factor correction for the model which would affect all of the data equally.

Front factors generally begin at 1, the ideal case, and decrease. Often the front factor accounts for non-Gaussian chain statistics as represented by the relation $\overline{r_i^2} / \overline{r_0^2}$.[28-30] Chemical crosslinks restrict chain segments from the complete freedom of mobility that is afforded in linear polymers. Hence $\overline{r_i^2}$ is less than $\overline{r_0^2}$ due to network restrictions resulting in a front factor $\overline{r_i^2} / \overline{r_0^2}$ less than one.[28-30] Other front factor corrections have been explored, including one based on crosslink functionality given by the relation $(f^* - 2)/f^*$ where f* is the functionality of the crosslinker.[28]. For this work, the functionality correction would yield a value of 0.33 due to trifunctional crosslinks. So it appears that a front factor of ~0.5, which would reconcile the differences in M_c values for

this family of thiol-ene networks, is in the normal range of front factor corrections. In support of this finding, there have been several reports on the success of fitting experimental data to the ideal rubber equation of state by employing a front factor of 0.5. A deeper, molecular interpretation of a front factor of 0.5 for this series of thiol-ene networks would be difficult to undertake.

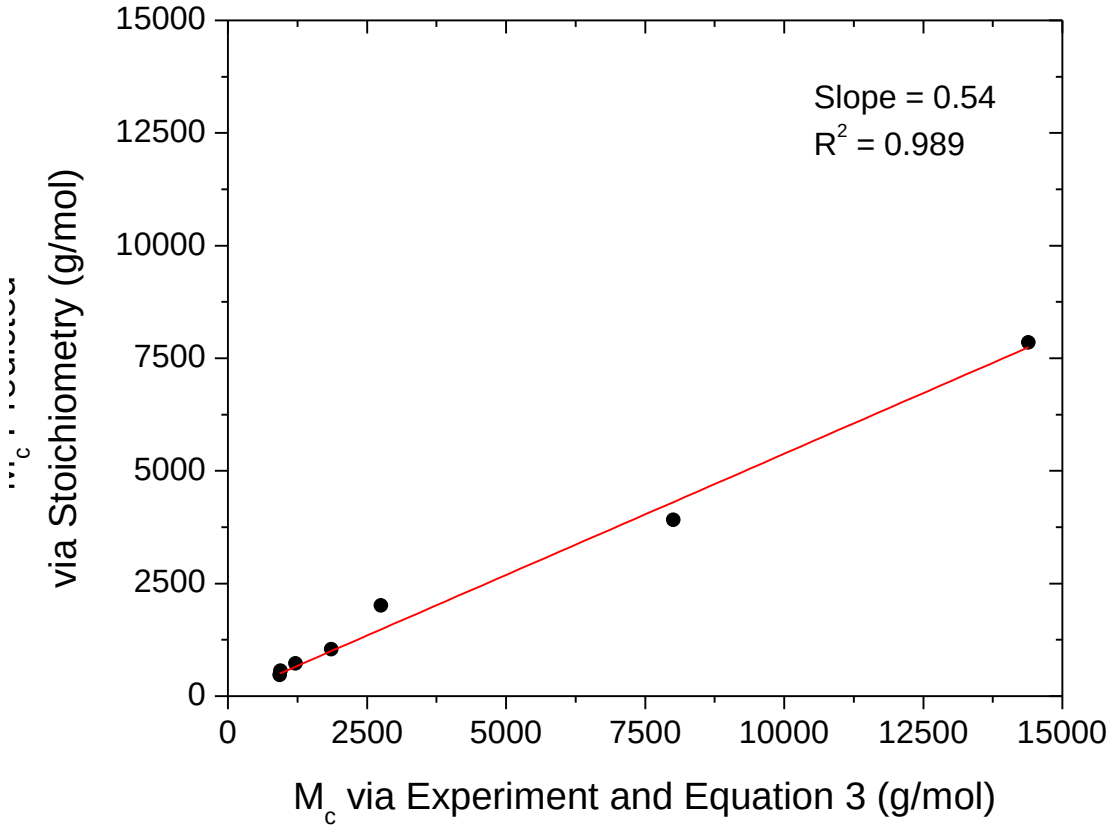

Figure VII-7. Relationship between M_c predicted via stoichiometry and M_c calculated experimentally via stress-strain data and Equation 3.

Table VII-3. Average Values for the Slope of Equation 3 Fit to Experimental Stress-Strain Data (see Figure 5), Average Bulk Density Recorded at Ambient Temperature, Experimental M_c Calculated via Equation 3, and Ideal M_c Predicted via Stoichiometry. Material designation indicates percent thiol groups from EDDT in the network

Material	Slope (Equation 3) (MPa)	Density (g/cc)	M_c via Experiment and Equation 3 (g/mol)	M_c via Stoichiometry (g/mol)
0%	3.17	1.205	936	467
20%	3.13	1.205	949	566
40%	2.41	1.19	1220	724
60%	1.57	1.185	1860	1040
80%	1.05	1.173	2750	2010
90%	0.357	1.16	8010	3910
95%	0.199	1.163	14400	7850

Gas Permeation and Selectivity Analysis

So far in this work we have demonstrated improvements in mechanical properties leading to elastomeric and robust membrane materials. However, as mentioned in the Introduction it was our goal to make overall improvements including gas separation performance. The addition of EDDT resulted in decreased crosslink density and increased ethyleneglycol content, both of which were expected to be favorable for CO_2 separation. From the constant volume, variable pressure gas permeation technique described in the Experimental section, the permeability coefficient of the three test gases (CO_2, O_2, N_2) for each membrane formulation were determined. Figure VII-8 indicates that CO_2 permeability initially increased and then leveled off around 90 Barrer as the EDDT content was increased. The permeability increase translates into nearly a

quadrupling of permeability via this approach but also indicates the limitation encountered at the higher % EDDT formulations. Permeability of N_2 and O_2 both increased and leveled off in similar fashion. The probable cause of this limitation, i.e. the presence of entanglements which act as physical crosslinks, will be addressed in detail later.

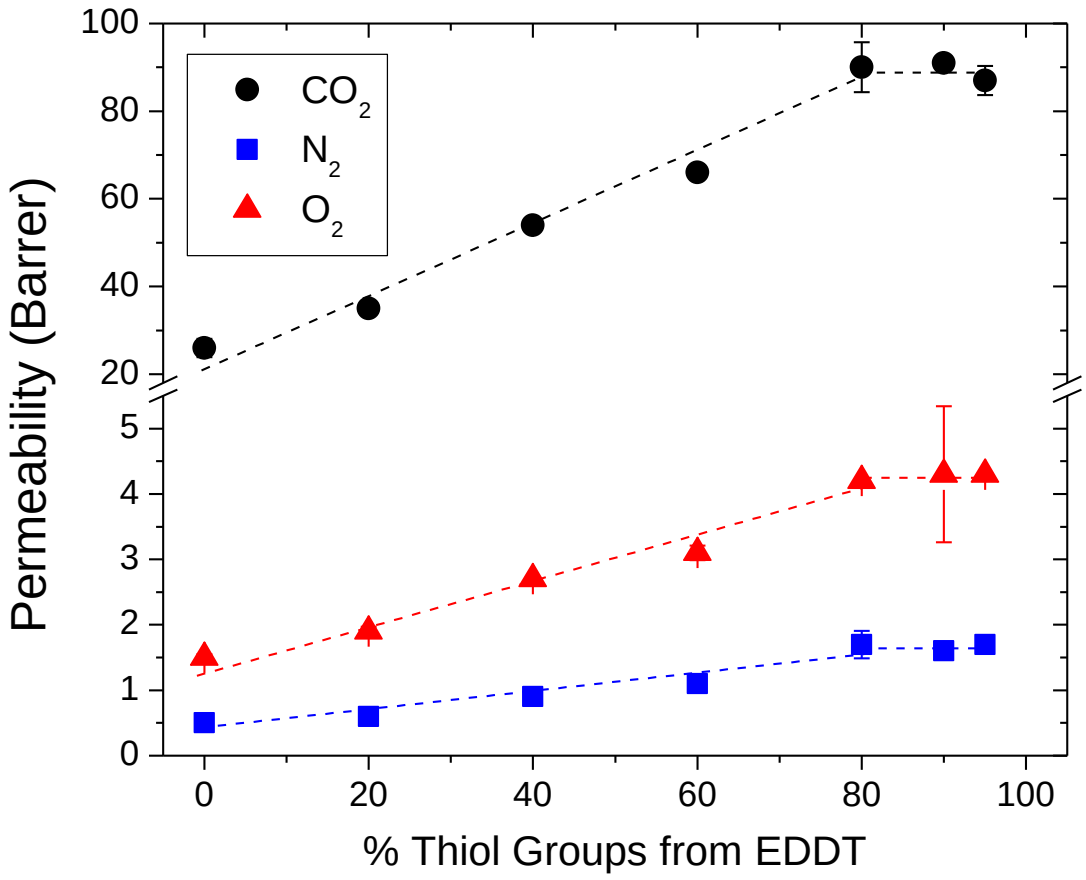

Figure VII-8. Permeability of CO_2, O_2, and N_2 at 23 °C and 3.5 atm upstream pressure plotted as a function of EDDT content. Lines provided to guide the eye.

Pure gas selectivity for the two gas pairs, CO_2/O_2 and CO_2/N_2, are shown in Figure VII-9. Selectivity values were determined via the average pure gas permeation values. It is evident that each formulation, regardless of the EDDT content, exhibited high CO_2 selectivity provided by the EG units. Interestingly, the selectivity for each gas pair remains in a small window despite the vast increase in EG content from 38% to 67%. Also worth mentioning is the fact that the 0% formulation contains only 38% EG and exhibits this high selectivity. Since the selectivity of PEG-based membranes is derived from solubility, it is worthwhile to discuss the solubility and also the diffusion components of the overall permeability. Solubility coefficients were extracted from these experiments via the time lag method as described in the Experimental section and reported in Figure VII-10. Remarkably the solubility of each gas remained essentially unchanged as a function of EDDT content despite enormous structural and compositional differences. The increases in permeability were thus due to increased diffusivity as shown in Figure VII-11. The initial increase followed by a leveling off, the trend observed for permeability, was also observed for diffusivity. Clearly the flexibility and free volume imparted to the network by EDDT had a significant effect on membrane performance. The fact that EDDT provides more PEG content, however, is inconsequential at least regarding solubility selectivity. Also worth mentioning is that there may be a CO_2 solubility enhancement via the sulfide or thioether bonds present in all thiol-ene networks. This effect cannot be ruled out and is likely deserving of another study.

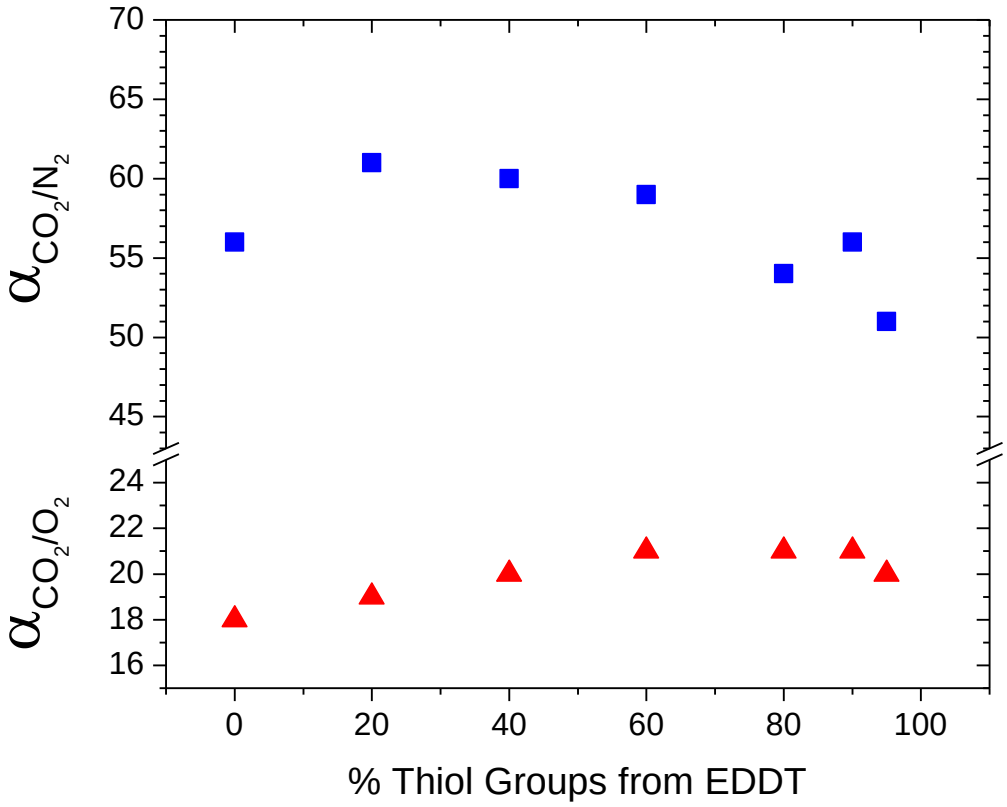

Figure VII-9. Average pure gas selectivity at 23 °C for two gas pairs, CO_2/N_2 and CO_2/O_2, as a function of EDDT content.

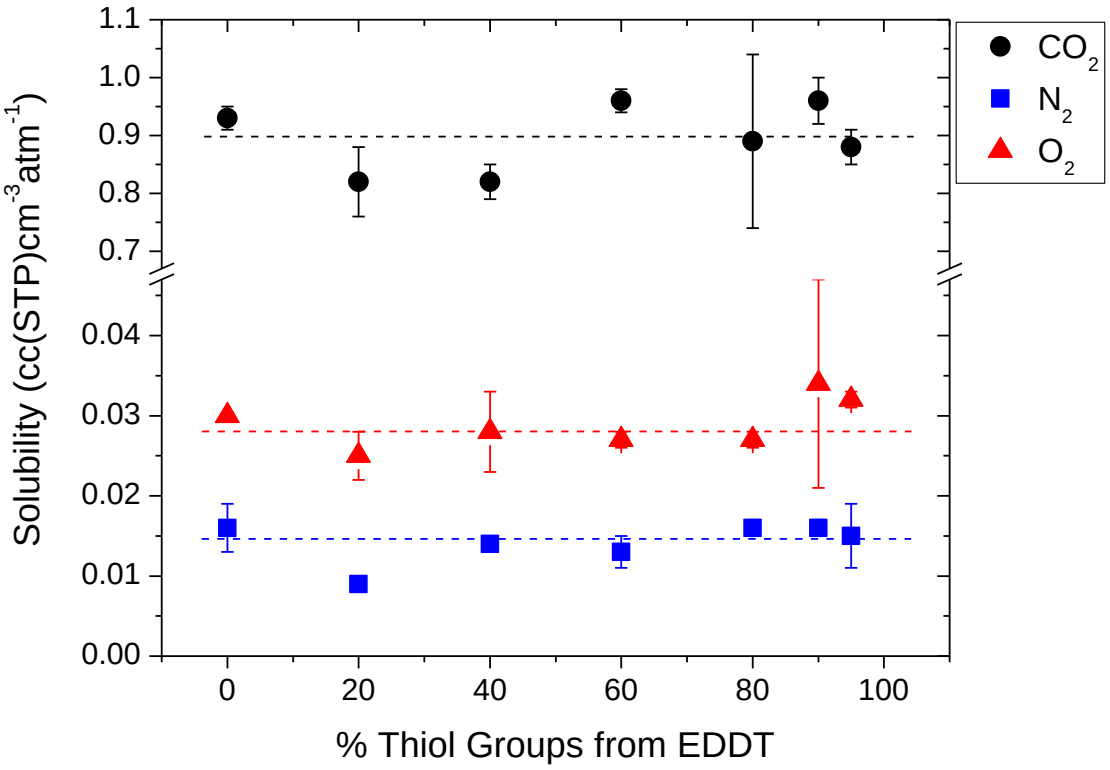

Figure VII-10. Gas solubility at 23 °C as a function of EDDT content. Lines provided to guide the eye.

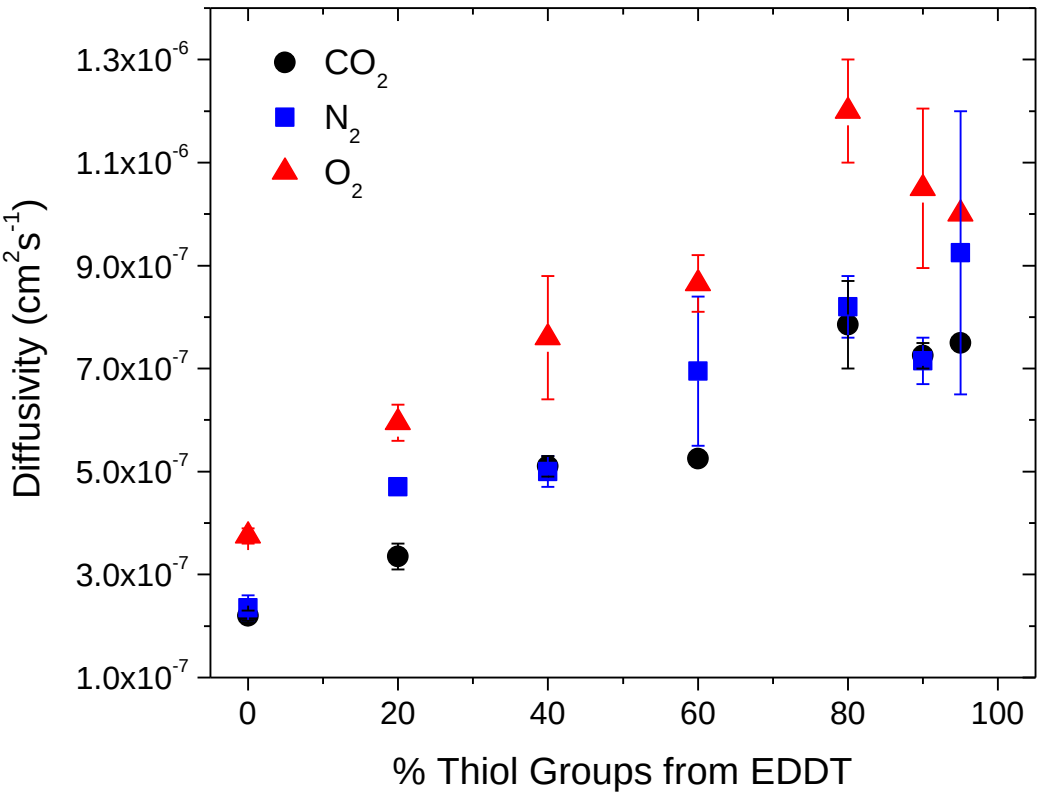

Figure VII-11. Gas diffusivity at 23 °C as a function of EDDT content.

Gas separation membranes are often rated by the combination of their fast gas permeability, in this case CO_2, and the permselectivity over another gas. It is known that a tradeoff between the two parameters exists and the upper bound plot is a good measure of this behavior. Figure VII-12 shows the permeability/selectivity performance of each network compared to the upper bound for the CO_2/N_2 gas pair, a widely studied separation process. The points on this tradeoff plot approach the upper bound as the percent of thiol groups from EDDT was increased. Also included for comparison is

semi-crystalline PEG which was calculated for 23 °C using van't Hoff-Arrhenius parameters from the literature.[8]

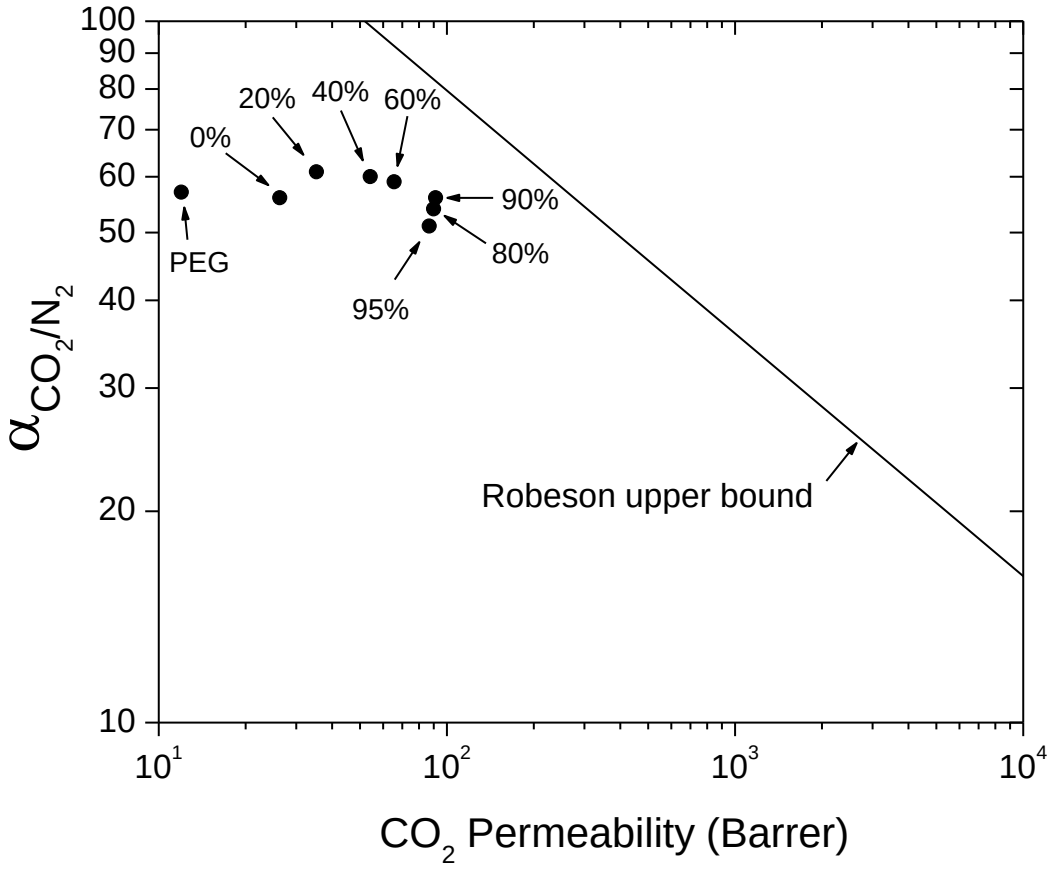

Figure VII-12. Robeson upper bound[15] trade-off plot for CO_2/N_2 demonstrating performance improvement via addition of EDDT for permeation measurements at 23 °C. Semi-crystalline PEG at 23 °C included for comparison.[8] Labels indicate percent of thiol groups from EDDT.

To put these results in perspective, we compared the approach reported in this work to that of Hirayama[7] and Freeman.[16-17] In their strategy, the conventional UV-cured PEG-di(meth)acrylate membranes were diluted with a monofunctional PEG-acrylate.

While crosslink density and chain end concentration were greatly increased as the monofunctional PEG-acrylate content increased, the PEG content remained nearly constant at ~80 wt%. It was shown in these reports that vast increases in gas permeation and thus membrane performance were derived almost entirely from diffusivity. This result was straightforward considering that the PEG content, which provides high CO_2 solubility, was essentially constant. However in our series of thiol-ene membranes the PEG content spanned 38 wt% to 67 wt%. Yet despite this increase in PEG, essentially no change in gas solubility was observed. This leads us to emphasize that apparently only a certain PEG concentration is required to reach the maximum solubility selectivity in low T_g, rubbery PEG-based membranes. The minimum amount of PEG likely varies according to the remaining structures in the material as well as other factors like T_g, crystallinity, additives, etc.

Conclusions

A crosslink reduction strategy was employed to simultaneously increase free volume and ethyleneglycol content in a new family of photopolymerized PEG-based membranes using thiol-ene chemistry. The starting material, a combination of a trithiol crosslinker and an ethyleneglycol-containing diene, was gradually diluted with an ethyleneglycol-containing dithiol while maintaining 1:1 thiol-ene stoichiometry. Each formulation rapidly reached 100% conversion of both thiol and ene groups. A slight increase in polymerization rate was observed for materials with higher dithiol content likely due to increased free volume and decreased viscosity during polymerization. Rubbery plateau modulus decreased by one order of magnitude across the series, albeit gradually, which was a direct consequence of the vast decrease in crosslink density.

Favorable improvements to membrane performance were observed. Glass transition temperature gradually decreased but then leveled off as dithiol content increased. CO_2 permeability leveled off in similar fashion at around 90 Barrer at 23 °C, although it did increase roughly four-fold over the starting material. It was hypothesized that chain entanglements, acting as physical crosslinks, restricted the further increase of free volume which caused both T_g and permeability to level off. CO_2 selectivity over both O_2 and N_2 was high in each case due to the ethyleneglycol which has a strong affinity for CO_2. Interestingly, despite massive compositional changes, i.e. an increase in ethyleneglycol content from 38 wt% to 67 wt%, solubility for all three gases was essentially constant. Increases in permeability were due solely to diffusivity.

Tensile tests revealed that tensile modulus decreased and tensile elongation increased with increasing dithiol content as expected. Materials with the highest concentration of dithiol were indeed elastomeric and mechanically robust in nature due to the random coil behavior of the long polymer chains between crosslinks. The equation of state for ideal rubbers was applied to stress-strain data allowing the calculation of the number-average molecular weight between crosslinks, M_c. M_c calculated from this experimental approach was systematically greater than hypothetical M_c predicted by stoichiometry. This difference was likely due to a front factor value of ~0.5, in agreement with unrelated reports on rubber elasticity in crosslinked polymers.

References

1. Bernardo, P.; Drioli, E.; Golemme, G. *Ind. Eng. Chem. Res.* **2009**, *48*, 4638.
2. T.M. Murphy, G.T. Offord, D.R. Paul, *Fundamentals of Membrane Gas Separation*, in: E. Drioli ,L. Giorno (Eds.), *Membrane Operations: Innovative Separations and Transformations*, Wiley, Weinheim Germany, **2009**, pp. 63-82.
3. Shao, L.; Low, B. T.; Chung, T-S.; Greenberg, A. R. *J. Membr. Sci.* 327, **2009**, 18-31.
4. Lin, H.; Freeman, B. D. *J. Mol. Struct.* **2005**, *739*, 57.
5. Kawakami, M.; Yamashita, Y.; Yamasaki, M.; Iwamoto, M.; Kagawa, S. *J. Polym. Sci. Polym. Lett. Ed.* 20, **1982**, 251-257.
6. Okamoto, K.; Fuji, M.; Okamyo, S.; Suzki, H.; Tanaka, K.; Kita, H. *Macromolecules* 28, **1995**, 6950-6956.
7. Hirayama, Y.; Kase, Y.; Tanihara, N.; Sumiyama, Y.; Kusuki, Y.; Haraya, K. *J. Membr. Sci.* 160, **1999**, 87-99.
8. Lin, H.; Freeman, B. D. *J. Membr. Sci.*, 239, **2004**, 105-117.
9. Lin, H.; Freeman, B. D.; *Macromolecules*, 39, **2006**, 3568-3580.
10. Bondar, V. I.; Freeman, B. D.; Pinnau, I. *J. Polym. Sci., Part B: Polym. Phys.*, 38, **2000**, 2051-2062.
11. Reijerkerk, S. R.; Knoef, M. H.; Nijmeijer, K.; Wessling, M. *J. Membr. Sci.*, 352, **2010**, 126-135.
12. Husken, D.; Visser, T.; Wessling, M.; Gaymans, R. J. *J. Membr. Sci.*, 346, **2010**, 194-201.

13. Yave, W.; Car, A.; Funari, S. S.; Nunes, S. P.; Peinemann, K-V. *Macromolecules*, 43, **2010**, 326-333.

14. Lin, H.; Van Wagner, E.; Freeman, B. D.; Toy, L.G.; Gupta, R. P.; *Science*, 311, 2006, 639.

15. Robeson, L. M. *J. Membr. Sci.*, 320, **2008**, 390-400.

16. Lin, H.; Kai, T.; Freeman, B. D.; Kalakkunnath, S.; Kalika, D. S. *Macromolecules*, 38, **2005**, 8381-8393.

17. Lin, H.; Van Wagner, E.; Swinnea, J. S.; Freeman, B. D.; Pas, S. J.; Hill, A. J.; Kalakkunnath, S.; Kalika, D. S. *J. Membr. Sci.*, 276, **2006**, 145-161.

18. Yagci, Y.; Jockusch, S.; Turro, N. J.; *Macromolecules*, 43, **2010**, 6245.

19. Fouassier, J. P.; *An Introduction to the Basic Principles in UV Curing*, in: Fouassier, J. P. and Rabed, J. F. (Eds.), Radiation Curing in Polymer Science and Technology – Volume I, Elsevier Applied Science, New York, **1993**, pp. 49-117.

20. Hoyle, C.E.; *Photocurable Coatings*, in: C.E. Hoyle, J.F. Kinstle (Eds.), Radiation Curing of Polymeric Materials, ACS, Washington D.C., **1990**, pp. 1-16.

21. Hoyle, C. E.; Bowman, C. N. Angew. Chem. Int. Ed., 49, **2010**, 1540-1573.

22. Lee, T. Y.; Roper, T.; Hoyle, C. E. *J. Polym. Sci., Part A: Polym. Chem.*, 42, **2004**, 5301-5338.

23. Hoyle, C. E.; Lowe, A. B.; Bowman, C. N. *Chem. Soc. Rev.*, 39, **2010**, 1355-1387.

24. Kwisnek, L.; Nazarenko, S.; Hoyle, C. E.; *Macromolecules*, 42, **2009**, 7031-7041.

25. Kwisnek, L.; Kaushik, M.; Hoyle, C. E.; Nazarenko, S.; *Macromolecules*, 43, **2010**, 3859-3867.

26. Kwisnek, L.; Heinz, S.; Wiggins, J. S.; Nazarenko, S. *J. Membr. Sci.* **2011**, *369*, 429–437.

27. Good, B. T.; Reddy, S.; Davis, R. H.; Bowman, C. N. *Sensors and Actuators B*, 120, **2007**, 473-480.

28. Sperling, L. H., *Introduction to Physical Polymer Science: Fourth Edition*, Wiley, Hoboken, **2006**.

29. Erman, B., Mark, J. E., *Structures and Properties of Rubberlike Networks*, Oxford University Press, New York, **1997**.

30. Treloar L.R.G., *The Physics of Rubber Elasticity*, Clarendon Press, Oxford, **1975**.

31. J. E. Mark, et al (Eds.), *Physical Properties of Polymers, 2nd ed.*, ACS, Washington, D.C., 1993.

32. Okay, O.; Bowman, C. N.; *Macromol. Theory Simul.*, **2005**, 14, 267-277.

33. Okay, O.; Reddy, S. K.; Bowman, C. N.; *Macromolecules*, **2005**, 38, 4501-4511.